FABRICATION OF SPECTRALLY SELECTIVE SOLAR POWER ABSORBER MATERIAL VIA POWDER METALLURGY PROCESS

MOHD ZAKUAN BIN ZABRI

FACULTY OF ENGINEERING
UNIVERSITY OF MALAYA
KUALA LUMPUR

2019

FABRICATION OF SPECTRALLY SELECTIVE SOLAR POWER ABSORBER MATERIAL VIA POWDER METALLURGY PROCESS

MOHD ZAKUAN BIN ZABRI

DISSERTATION SUBMITTED IN FULFILMENT OF THE REQUIREMENETS FOR THE DEGREE OF MASTER OF ENGINEERING SCIENCE

FACULTY OF ENGINEERING
UNIVERSITY OF MALAYA
KUALA LUMPUR

2019

UNIVERSITY OF MALAYA
ORIGINAL LITERARY WORK DECLARATION

Name of Candidate: Mohd Zakuan Bin Zabri

Matric No: KGA150061

Name of Degree: Master of Engineering Science

Title of Project Paper/Research Report/Dissertation/Thesis (“this Work”):

Fabrication of spectrally selective solar power absorber material via powder metallurgy process

Field of Study: Materials Engineering

I do solemnly and sincerely declare that:

(1) I am the sole author/writer of this Work;
(2) This Work is original;
(3) Any use of any work in which copyright exists was done by way of fair dealing and for permitted purposes and any excerpt or extract from, or reference to or reproduction of any copyright work has been disclosed expressly and sufficiently and the title of the Work and its authorship have been acknowledged in this Work;
(4) I do not have any actual knowledge nor do I ought reasonably to know that the making of this work constitutes an infringement of any copyright work;
(5) I hereby assign all and every rights in the copyright to this Work to the University of Malaya (“UM”), who henceforth shall be owner of the copyright in this Work and that any reproduction or use in any form or by any means whatsoever is prohibited without the written consent of UM having been first had and obtained;
(6) I am fully aware that if in the course of making this Work I have infringed any copyright whether intentionally or otherwise, I may be subject to legal action or any other action as may be determined by UM.

Candidate’s Signature Date:

Subscribed and solemnly declared before,

Witness’s Signature Date:

Name:

Designation:

FABRICATION OF SPECTRALLY SELECTIVE SOLAR POWER ABSORBER MATERIAL VIA POWDER METALLURGY PROCESS

ABSTRACT

In recent years, studies on the effects of nanofiller materials addition in metal matrix composites have been progressing in order to develop new materials for various applications. In this research work, aluminum-based composites reinforced with carbon nanofillers, i.e., multi-walled carbon nanotubes (MWCNTs) and graphene nanoplatelets (GNPs) that are distributed in the matrix of aluminum (Al) nanocomposites have been investigated to determine the optical properties, i.e., spectral selectivity behavior of Al nanocomposite materials. Over the years, most of the researchers have been investigating the effects of nanofillers on thermal, electrical, and mechanical properties of metal-based composites. However, none of the studies concentrated on the optical properties of Al nanocomposites, especially with MWCNTs and GNPs. Thus, the focus of this research is more toward the effects of both MWCNT and GNP nanofillers on the optical properties of Al nanocomposites. Al matrix composites were filled with different compositions of nanofillers, i.e., functionalized and pristine carbon nanofillers (5 to 15 wt. %) and fabricated using powder metallurgy (PM) process. Samples morphology, optical, and microhardness properties were measured for different compositions of Al-MWCNT-GNP nanocomposites. Dispersion of carbon nanofillers and spectral selectivity behavior of Al nanocomposites were enhanced with the addition of functionalized nanofillers (MWCNTCOOH-GNPCOOH). X-ray diffraction (XRD) analysis confirmed the existence of functionalized and pristine MWCNT-GNP nanofillers without the presence of aluminum carbide (Al_4C_3). Micro-Vickers hardness values of Al nanocomposites added with MWCNTCOOH-GNPCOOH were higher compared to the samples added with MWCNT-GNP/MWCNT/GNP. Light absorption was enhanced in the ultraviolet-visible-near-infrared (UV-Vis-NIR) region (from 200 to 2,500 nm) whereas reflectance was improved in the near-infrared-far-infrared (NIR-FIR) region (from 3,000 to 14,000 nm) with the addition of MWCNTCOOH-GNPCOOH nanofillers. The highest selectivity ratio obtained was 14.60 for Al nanocomposites with the addition of 2.5 wt. % MWCNTCOOH and 2.5 wt. % GNPCOOH.

Keywords: Aluminum nanocomposites; Multi-walled carbon nanotubes; Graphene nanoplatelets; Spectral selectivity; Solar absorbers.

PEMBUATAN BAHAN PENYERAP SPEKTRA KUASA SURIA TERPILIH MELALUI PROSES METALURGI SERBUK

ABSTRAK

Sejak kebelakangan ini, kajian mengenai kesan bahan tambahan melibatkan pengisian partikel nano dalam komposit matrik logam telah berkembang dalam usaha untuk membangunkan bahan-bahan baru untuk pelbagai aplikasi. Dalam penyelidikan ini, komposit berasaskan aluminium (Al) diperkukuhkan dengan kehadiran partikel nano karbon iaitu tiub nano karbon berbilang dinding (MWCNTs) dan platelet nano grafin (GNPs) yang disebarkan di dalam matriks komposit nano Al telah dikaji untuk meningkatkan sifat-sifat optikal seperti tingkah laku selektiviti spektrum bahan komposit nano Al. Kebanyakan daripada penyelidik telah menyiasat kesan pengisian partikel nano ke atas sifat mekanik, haba, dan elektrik bagi komposit berasaskan logam. Walau bagaimanapun, tiada kajian yang memberi tumpuan kepada ciri-ciri optik komposit nano Al terutamanya dengan kombinasi MWCNTs dan GNPs setakat ini berdasarkan penelitian terhadap kajian-kajian yang lepas. Oleh itu, fokus kajian ini akan lebih ke arah kesan campuran kedua-dua pengisian partikel nano karbon MWCNT dan GNP terhadap sifat morfologi, optikal, dan mekanik matriks komposit Al. Matriks komposit Al telah dicampurkan dengan komposisi partikel nano karbon yang berbeza, iaitu partikel nano karbon yang telah diubah suai fungsinya dan partikel nano karbon yang asal (5 sehingga 15% berat komposisi) dan dibuat menggunakan proses metalurgi serbuk (PM). Morfologi, sifat optikal, dan sifat kekerasan mikro bagi sampel yang dihasilkan diukur berdasarkan komposisi komposit Al-MWCNT/GNP yang berlainan. Analisis pembelauan sinar-X (XRD) mengesahkan kewujudan isian nano karbon yang telah diubah suai fungsinya dan isian nano karbon yang asal MWCNT/GNP tanpa kehadiran aluminium karbida (Al_4C_3). Penyebaran partikel nano karbon dan tindak balas pilihan spektrum bertambah baik dengan penggunaan MWCNT-GNP yang telah diubah suai fungsinya

(MWCNTCOOH-GNPCOOH). Nilai kekerasan mikro-Vickers bagi komposit nano Al yang ditambah dengan MWCNTCOOH-GNPCOOH juga lebih tinggi berbanding dengan komposit nano Al yang ditambah dengan MWCNT-GNP/MWCNT/GNP yang asli. Penyerapan cahaya berjaya dipertingkatkan dalam lingkungan ultra lembayung-cahaya nampak-inframerah dekat (UV-Vis-NIR) (dari 200 hingga 2,500 nm) manakala kadar pantulan menjadi lebih tinggi dalam lingkungan inframerah dekat-inframerah jauh (NIR-FIR) (dari 3,000 hingga 14,000 nm) dengan penambahan isian nano MWCNTCOOH-GNPCOOH. Nisbah pemilihan spektrum tertinggi yang berjaya diperoleh ialah 14.60 untuk partikel nano komposit Al dengan tambahan 2.5 peratus berat komposisi MWCNTCOOH dan 2.5 peratus berat komposisi GNPCOOH.

Kata kunci: Komposit nano aluminium; Tiub nano karbon berbilang dinding; Platelet nano grafin; Selektiviti spektrum; Penyerap solar.

ACKNOWLEDGEMENTS

I would like to take this opportunity to express my gratitude and appreciation to everyone who have contributed directly and indirectly throughout the thesis writing process until the end of this work. Without the help from all these people, it is definitely hard to complete the thesis.

Thank you so much to my supervisor as well as my mentor, Dr. Shaifulazuar bin Rozali for his time and effort spent in assisting me, discussing all the problems together with the alternative solutions, refining all my writings and above all, his concern towards my research progress. Not just that, I would like to thank my co-supervisor, Dr. Afifah binti Yahaya for her effort in helping to assist a few parts of my work, especially in optical characterization.

Besides that, I would like to thank my beloved wife, Siti Shafiah binti Shazali who managed to act as my backbone in completing my Master's project. I am deeply impressed with her effort in providing necessary suggestions and handful help whenever a problem arises. I would also wish to extend my warmest thanks to the Department of Mechanical Engineering staff especially Mr. Said, Mr. Khlaid, Mr. Shukri, Mr. Zaman, Mr. Dzahir, and Ms. Shafini for their direct and indirect help that has made this work successful. Moreover, I am thankful to the Faculty of Science UM, Institute of Science UiTM, and Faculty of Science UiTM for providing me with characterization equipment.

Last but not least, I would like to acknowledge my parents for their unrelenting advice, concern, and faith throughout my study. Thank you for not giving up and making me into someone valuable to the society.

TABLE OF CONTENTS

LIST OF FIGURES

LIST OF TABLES

LIST OF SYMBOLS AND ABBREVIATIONS

Symbols

α	Absorption
T	Transmittance
ε	Emittance
R	Reflectance
Hv	Hardness value
α/ε	Spectral selectivity ratio

Abbreviations

Al	Aluminum
BPR	Ball-to-powder ratio
FESEM	Field emission scanning electron microscopy
FTIR	Fourier transform infrared spectroscopy
GNP	Graphene nanoplatelet
MWCNT	Multi-walled carbon nanotube
RPM	Rotation per minute
UV-VIS	Ultraviolet-visible spectrophotometry
wt. %	Weight percentage
XRD	X-Ray diffraction

CHAPTER 1: INTRODUCTION

1.1 Research background

The conversion of sunlight into electricity can be done either directly using photovoltaic (PV) technology or indirectly using concentrated solar thermal (CST) and concentrated solar power (CSP) systems. Photovoltaic technology converts light into electric current using PV effect. However, CST and CSP systems use concentrated sunlight to produce heat. This heat can be directly used such as in CST water heater or for power production using CSP technology.

PV technology produces direct current (DC) power that fluctuates with sunlight intensity. One of the disadvantages of PV technology is its relatively low-efficiency level (between 12% and 25%) compared to other renewable energy systems such as CSP. Thus, for megawatt-scale electricity production, relatively large areas are required for deployment. Moreover, the efficiency of PV panels degrades over time by approximately 20% over 25 years.

On the other hand, both CST and CSP systems use lenses or mirrors to focus a large area of sunlight into a small beam. Then, the concentrated sunlight is converted into heat by using a solar absorber. The main concept of solar thermal energy utilization is to convert sunlight into heat without re-emitting thermal energy. The heat collected from the solar absorber will be used to heat water or molten salt to generate steam and finally rotate a turbine. The efficiency of CSP system ranged from 20% to 35% according to the existing plant operation and it can be improved with the development of an excellent solar absorber material together with a good heat storage system.

An important characteristic that can be evaluated for a solar absorber material is spectral selectivity. An ideal solar absorber material should possess high solar absorptance (α) greater than 90% in the solar wavelength range of 0.3 to 2 µm and low thermal emittance (ε) less than 10% in the near-infrared (NIR) and far-infrared (FIR) wavelength range of 2.5 to 25 µm (Vince et al., 2003). Thus, the absorber needs to be spectrally selective.

Generally, black chrome (Anandan et al., 2002), black nickel (John, 1997), black cobalt (Abdel Hamid et al., 2008), black brass (Richharia, 1996), copper oxide (Richharia et al., 1991), and composites such as ceramic-metal composite (cermet) are commercially used as selective solar absorbers. Commercial selective surfaces for a solar thermal system currently are prepared through sputtering, electrodeposition, chemical vapor deposition, and anodization methods (Barshilia, Selvakumar, et al., 2008a; S. Kumar et al., 1983; Maruyama, 1998; Tharamani & Mayanna, 2007). These methods require expensive equipment and complex procedures, whereas some of them have high material consumption to fabricate selective absorbers (Katumba et al., 2008). Hence, the production of an excellent selective solar absorber through a cheaper process is required for the realization of an efficient solar thermal collector with cost-effective process.

1.2 Problem statement

Recently, transition metals such as nitride/oxide and oxynitride-based coatings have been used as common high-temperature solar selective coatings for solar thermal power generation applications (Barshilia, Selvakumar, et al., 2008a, 2008b; Barshilia et al., 2006; N Selvakumar et al., 2010). Hafnium oxide-based multilayer absorber coating (i.e., HfOx/Mo/HfO_2) has been developed for high-temperature applications. The coating is thermally stable in air up to 400 °C. However, the coating starts to degrade at higher temperature, because of the oxidation of Mo metal particles and its subsequent reaction with hafnium oxide (HfO_2) (N Selvakumar et al., 2010).

In addition, metal-dielectric composites for coatings, such as nickel-pigmented aluminum oxide (Al_2O_3) have also been widely investigated by both theoretical and experimental approaches (Sathiaraj et al., 1991; Tesfamichael & Roos, 1998). However, such metal-dielectric absorbers suffer from degradation over a long period caused by the oxidation of metal nanoparticles, especially at high temperature and in high-humidity environment.

There are several problems in solar selective coatings such as oxidation of the coating, interdiffusion between layers, and delamination of the coating. The usage of titanium (Ti) or Al is proven to oxidize layer by layer inside the coating with the presence of oxygen (X. Wang et al., 2014). Besides, interdiffusion between the layers can also occur due to thermal stress relaxation, thus causing the original coating consisting of Ti or Al to be damaged. Thia oxidation effect can be mitigated by restraining the oxygen to a very small quantity inside a vacuum case (X. J. Wang et al., 2014). Commercial coatings such as Pyromark 2500 that is used as absorber coatings for many central receiver projects have also faced delamination issue when tested with thicker coating and exposed to air at high temperature (above 750 °C) (Coventry & Burge, 2017). These above problems will degrade performance.

In order to overcome the challenges of using coating as solar absorber, in this project, we investigate the development of bulk materials. This could eliminate serious solar selective coatings issues at high temperature and in humid environment. Metals and their composites as solar absorber materials are the potential candidates in this study. Thus, a study to produce new composites from Aluminum (Al) as the matrix and nanofiller materials such as multi-walled carbon nanotube (MWCNT) and graphene nanoplatelet (GNP) is carried out. Al is chosen due to its capability to be fitted with a variety of technical applications. Al possesses the capability to be machined or processed at a lower working temperature compared to steel, which helps manufacturers to reduce their production and fabrication costs. Apart from that, Al also has excellent corrosion resistance in most of the service environments due to its naturally thin invisible oxide skin formation that protects Al from further oxidation. Al is excellent enough to be used even in industrial atmospheres that generally corrode other metals (Davis, 1999) (tjong et.al, 2016).

The fabrication of solar absorber materials is carried out using powder metallurgy process. The aim is to produce inexpensive solar absorber materials with less-complex fabrication process such as in the current situation. Powder metallurgy is commonly an inexpensive, simple, and fast production process. The process includes mechanical mixing (e.g., ball milling) and sintering. Furthermore, it is easier to create a solar absorber that is optically and thermally efficient by using powder metallurgy process. An ideal solar absorber required the following properties; 1) can achieve high solar absorption (low reflectance) in the ultraviolet-visible-near-infrared (UV-Vis-NIR) solar spectrum (0.2µm to 2.5µm); and 2) lower thermal emittance (higher reflectance) in the infrared (IR) wavelength region (2.5µm-14µm). Powder metallurgy process allows for fine control of the creation of uniform and controlled porosity which is crucial toward fulfilling parts of an ideal solar absorber criteria. For the purpose of the thesis, the micrograph, optical absorbance and emmitance will be specifically discussed according to the optical performance of the formulation in the ground.

1.3 Research objectives

This research aims for the following objectives:

1. To fabricate Al nanocomposites together with both pristine and functionalized MWCNTs and GNPs through powder metallurgy process.
2. To characterize the surface morphology, mechanical, and optical properties of the samples.
3. To investigate the suitable type and amount of nanofillers that give high solar absorptance (α) (in the solar wavelength range from 0.3 to 2.5 µm) and low thermal emittance (ε) (in near-infrared (NIR) and far-infrared (FIR) wavelength range from 2.5 to 14 µm).

1.4 Chapter outline

This thesis reports the study of solar power absorber materials fabricated using powder metallurgy process. The procedures involved the selection of the base and filler materials for potential solar absorber materials, functionalization of MWCNT and GNP nanoparticles, and fabrication of samples. In addition, this thesis also focuses on the potential of all prepared Al nanocomposites with functionalized MWCNTs and/or GNPs toward optical properties of a spectrally selective solar absorber.

Chapter 1 provides the general introduction about this study. It gives an overview on solar absorber materials. This chapter also explains the problem statements and the targeted objectives to be achieved at the end of the study. The literature review about Al, MWCNTs, GNPs, and their properties is discussed in Chapter 2. The fundamentals behind the powder metallurgy process of the composites and solar absorbers are also included in this chapter.

In Chapter 3, the details on the methodology for the fabrication of Al nanocomposites are explained. Furthermore, this chapter gives an introduction regarding material selection, equipment used, material synthesis, and finally powder metallurgy process. Furthermore, the procedures related to the experimental setup are described in detail.

Meanwhile, the details regarding the results and discussion for each characterization test are explained in Chapter 4. This chapter also discusses the performance of Al-MWCNTs and/or GNPs nanocomposite materials based on different variations and test setups as mentioned previously. Lastly, in Chapter 5, all of the outcomes in this study that are discussed in previous chapters are summarized as a conclusion. The possibilities and recommendations for future works are also explained in this chapter.

CHAPTER 2: LITERATURE REVIEW

2.1 Introduction to metal matrix composites

It is hard to gain a single homogeneous material that possesses all the desired properties. One of the feasible strategies to gain all the desirable properties on a single material is through the addition of several materials together to form a composite that has a variety of properties in which a single material cannot achieve. A composite material is a material that contains both combination of matrix as the main element together with one or more physically distinct and distributed elements, known as fillers or reinforcements. The matrix is commonly added with the filler in order to obtain the desirable properties such as thermal and electrical conductivity, toughness, strength, wear resistivity, and optical properties. Composite materials can be seen in most of the human creation from as big as reinforced concrete in the construction industry to nanocoating for corrosion protection. Knowledge and fundamentals of composite material have become an important part of our day-to-day life (Agarwal et al., 2016).

Metal matrix composites (MMCs) is one of the newer material developments that involves the combination of particulates, reinforcements, and fibers in a ductile metal such as nickel, copper, aluminum, titanium, magnesium, iron, or alloy matrix to form composites with good strength and excellent elastic modulus. The combination of particulates, reinforcements, and fibers in a ductile metal is expected to overcome the drawback of metals and alloys in providing both strength and stiffness to the structure (Bakshi et al., 2010; Borkar et al., 2015; S. F. Li et al., 2013; Munir et al., 2015; Nardone & Prewo, 1986; Rashad, Pan, Asif, et al., 2015; Tjong & Lau, 1999). Besides that, MMCs materials also possess high resistance to wear, good strength, and relatively good heat conduction, which is practical for automotive application such as discs of car brakes

MMCs especially composites materials that associated with copper basis also possess good electrical conductivity which is good for electrical appliances. (Kaczmar et al., 2000). For space application, the application of B/Al tubular struts as the frame and rib truss members in the mid-fuselage section, and as the landing gear drag link of the Space Shuttle Orbiter proved the first successful application of continuous-fiber reinforced MMCs. The usage of B/Al tubes provided 45% weight savings over the baseline aluminum design (Rawal, 2001).

MMCs with particulates as well as fiber reinforcements own excellent mechanical and physical properties such high fatigue strength, high service temperature capabilities, excellent temperature stability, and high thermal conductivity, which make MMCs suitable for thermal management and storage devices, structural and infrastructure applications, industrial (transportation and chemical), recreational, as well as aerospace and automotive usages (Agarwal et al., 2016; Y. F. Liu et al., 2013; Tjong, 2013; Tjong & Ma, 2000; Wejrzanowski et al., 2016; Wu et al., 2012).

However, at present, MMCs are still facing challenges due to its limited commercial applications, due to its poor wettability properties, especially with the reinforcement of carbon after molten or sintering process of the metal, escalating production setup cost, metal corrosion issues, and formation of interfacial reaction products (Hihara & Latanision, 1994; Landry et al., 1998; S. H. Li & Chao, 2004). Therefore this work aims to overcome the current weaknesses of MMCs using powder metallurgy processes.

2.2 Aluminum and its properties

Previous research related to solar collector absorber materials has been done mainly on a single solar thermal absorber material with a flat absorber setup, namely stainless steel, mild steel, and copper (Akpinar & Koçyiğit, 2010) (Bouadila et al., 2013) (Alvarez et al., 2004). Even though copper is preferred due to its high thermal conductivity, it is not cost-effective compared to other inexpensive materials, such as aluminum (Al) with just a slight trade-off in its performance. This is supported by the research done by Shariah *et al*. who discovered that copper is 3% higher in terms of performance compared to Al (Shariah et al., 1999). Despite this small percentage difference, the relatively high cost of using copper against Al means that Al is a better material, which is suitable for most heating applications in terms of economic and performance considerations.

Al is a silvery, light, non-magnetic, and ductile material, and has good malleability and formability. Al has a density of 2.70 g/cm^3 and a Young's modulus of 70 GPa, i.e., a ratio of steel to Al of 1 to 3. Besides being the third most abundant elements in the Earth's crust and the most abundant metal (Exley, 2013), Al is the best choice of element to be used in many fields such as automobile, aerospace, constructions, and packaging due to its unique properties (Zehn et al., 1997). Al possesses the capability to be machined or processed at a lower working temperature compared to steel, which helps manufacturers to reduce their production and fabrication costs. Apart from that, Al also has excellent corrosion resistance in most of the service environments due to its naturally thin invisible oxide skin formation that protects Al from further oxidation. Al is excellent enough to be used even in industrial atmospheres that generally corrode other metals (Davis, 1999).

Al is one of the common lightweight materials that have excellent thermal conductivity. However, for the manufacturing of specific applications, thermal conductivity of Al as the only advantage is inadequate. One method to enhance the thermal conductivity of Al while maintaining their lightweight is through the fabrication of MMCs using materials with extremely high thermal conductivity as the reinforcement while Al still remains as the matrix (Jeon et al., 2014).

Al is commonly used in metal-carbon nanotube composites with a variety of technical applications. Mixed results can be observed by researchers with some of them reporting little or no increase in mechanical strength while others have seen significant improvements in strength (Kuzumaki et al., 1998). The factors that can be concluded on the differences include fabrication method, interfacial reactions that occurred, and the quality of dispersion itself (Bartolucci et al., 2011).

Although commercially pure (CP) Al (99.99%) has a good combination of excellent strength-to-weight ratio, high corrosion resistance, good thermal conductivity, and excellent malleability and formability, it is often lacking in some aspects. Those are the reasons why Al needs to be treated in certain conditions with other alloying elements to produce a comparable material with excellent properties to fit in many engineering fields. The most common elements used are magnesium, manganese, copper, zinc, and silicon. Each element gives different impact on the properties of Al alloy based on their effect and suitability (Rana et al., 2012).

2.3 Processing routes for aluminum composites

There are several processing methods that can be used for Al composites processing. Figure 2.1 shows the processing routes for Al composites through electrochemical deposition, melting and solidification, powder metallurgy, thermal spray, and others.

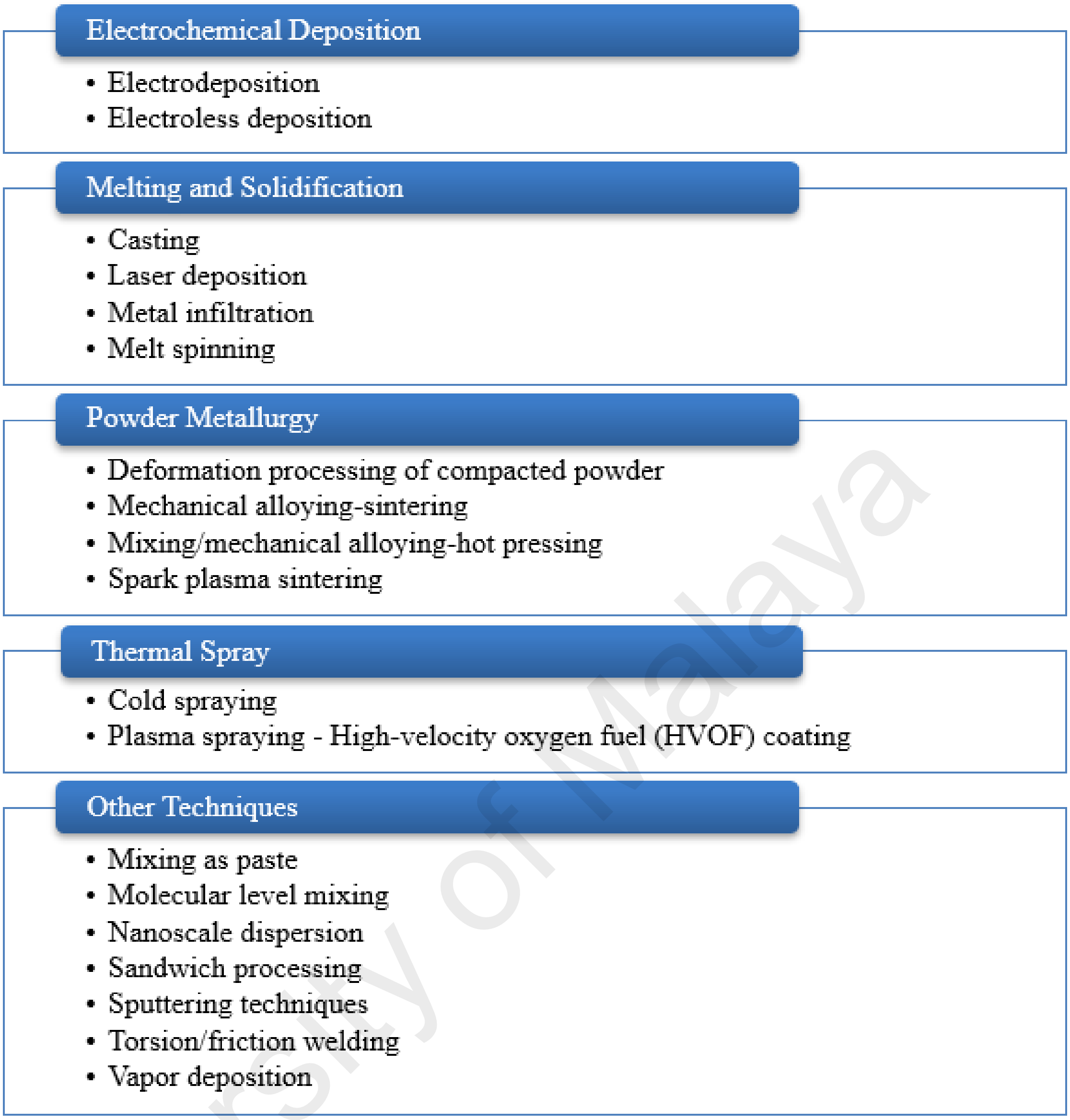

Figure 2.1: Possible processing routes for Al-based composites (Agarwal et al., 2016)

2.4 Carbon nanotubes

Two decades ago, Sumio Iijima discovered a new material known as carbon nanotubes (CNTs). Due to their unique atomic arrangement and attractive properties, such as low density, high tensile strength, excellent electrical and thermal conductivity, high aspect ratio, and high elastic modulus, CNTs have drawn researchers' attention as reinforcements in various kinds of ceramic, metallic, and polymer matrices (Cho et al., 2010; Chu et al., 2013; Guiderdoni et al., 2011; Harris, 2004; Kwon et al., 2009; Q. Q. Li et al., 2009; Uddin et al., 2010). Generally, CNTs can be divided into three types, which are multi-walled CNT (MWCNT), double-walled CNT (DWCNT), and single-walled CNT (SWCNT). Each type of CNT is determined by the number of graphene layers wrapped into a seamless cylinder. The diameter of SWCNT ranging from 1–2 nm whereas the diameter of DWCNT and MWCNT ranging from 4–20 nm (Tjong, 2013). SWCNT can be further categorized into zigzag, chiral, and armchair structures, depending on the hexagonal arrangement around the circumference (Harris, 2004), as shown in Figure 2.2.

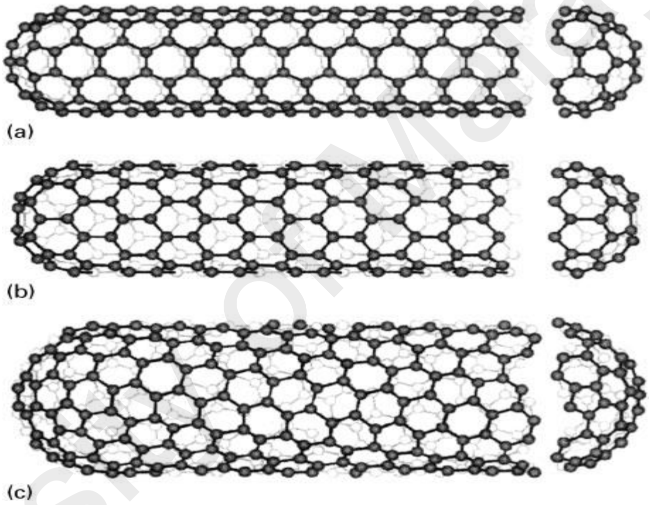

Figure 2.2: Categories of CNT structure: (a) armchair, (b) zigzag, and (c) chiral (Harris, 2004)

There are several methods of synthesizing CNTs such as laser ablation, chemical vapor deposition, and electric arc discharge processes. Laser ablation process is the process of producing CNTs through the use of a high-energy laser beam that produces carbon vapor species from a graphite, followed by the condensation of the species. Laser ablation method is much simpler and can produce fine quality of CNTs due to the full process control over the desired parameters. However, the laser source cost is highly expensive, which limits its potential applications. By using laser ablation technique, pulse laser beams such as UV excimer, Nd:YAG, and CO_2 laser are capable to be used to synthesize CNTs (Tjong, 2009). The yield and diameter of SWCNTs obtained from laser ablation technique are mainly controlled using several processing parameters, such as laser properties (e.g., wavelength, energy, repetition rate, and pulse duration), chamber pressure, furnace temperature, and composition of the target material.

Another main process is electric arc discharge. For this process, two graphite electrodes create an electric direct current arc (between two graphite electrodes) under inert environment and large current setting, which stimulate carbon atom vaporization into a plasma. Carbon vapor is then condensed and deposited on the cathode to form CNT. Electric arc discharge is one of the easiest and low-cost techniques to synthesize CNT. The quality of CNT synthesized by this technique depends on the processing states, such as reaction chamber pressure, plasma temperature, uniformity of plasma arc, the gap between electrodes, and efficient cooling of the cathode (Tjong, 2009).

CNT can also be produced through chemical vapor deposition (CVD) where hydrogen gases are decomposed over metal nanoparticle catalysts such as nickel (Ni), copper (Cu), cobalt (Co), iron (Fe), and rare earth nanoparticles. This process takes place in a vertical or horizontal furnace at a very high temperature as shown in Figure 2.3. CNTs are then nucleated and grow on the metallic catalyst in a vertical furnace before they are gathered at the bottom of the furnace. Catalysts (Ni, Cu, Co, Fe, and rare earth nanoparticles) are suspended by high space velocity and upward gas flow in a fluidized bed reactor furnace, which is suitable for the production of CNTs in a large scale. Nucleation and growth of CNT using CVD process rely on several processing criteria, such as flow rate, type of hydrocarbon gas precursor, type and size of nanoparticles, and synthesis temperature (Ando et al., 2004; Tjong, 2013). CVD is the most common method for the large-scale production of CNTs compared to other available processing methods of synthesizing CNT (Dasgupta et al., 2008; Szabó et al., 2010; Tjong, 2013). Figure 2.3

shows the illustration of CVD method through (a) a horizontal furnace, (b) a vertical furnace, and (c) a fluidized bed reactor.

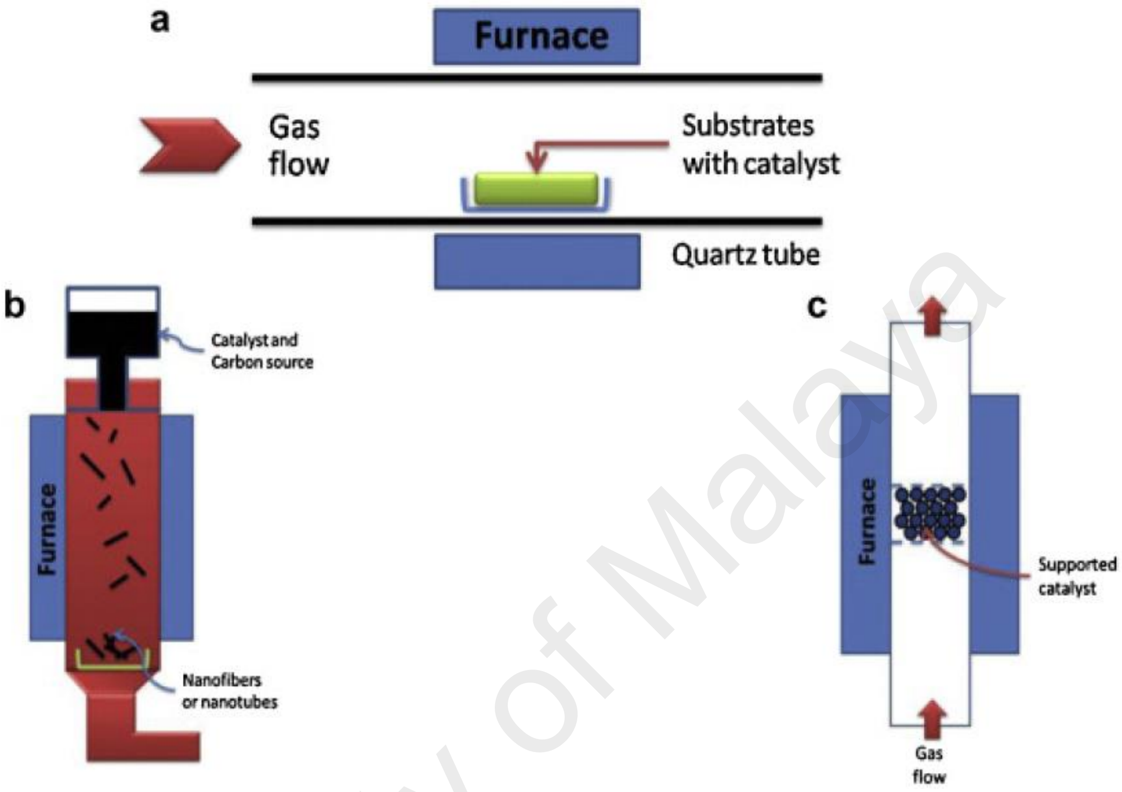

Figure 2.3: Schematic demonstration of CVD method in (a) a horizontal furnace, (b) a vertical furnace, and (c) a fluidized bed reactor (Szabó et al., 2010) (Tjong, 2013)

Previous researchers have studied the thermal properties of CNT. Thermal characteristics of CNT are mainly influenced by the conduction of phonon. Several factors are considered, such as the number of phonon active modes, inelastic umklapp scattering, and length of phonons free path. The presence of impurities, lengths, and diameters of nanotubes also contributes to the variation of the thermal conductivity of CNTs (Han & Fina, 2011; Tjong, 2013). CNTs possess high thermal conductivity (6600 W/mK) provided by MD simulations (Berber et al., 2000), whereas experimentally-recorded thermal conductivity values ranging from 1,750 up to 5,800 W/mK (Berber et al., 2000; Heremans & Beetz Jr, 1985; Hone et al., 1999). Table 2.1 shows the mechanical and thermal conductivity of carbon-based materials.

Table 2.1: Carbon nanotubes and graphene properties (Tjong, 2013)

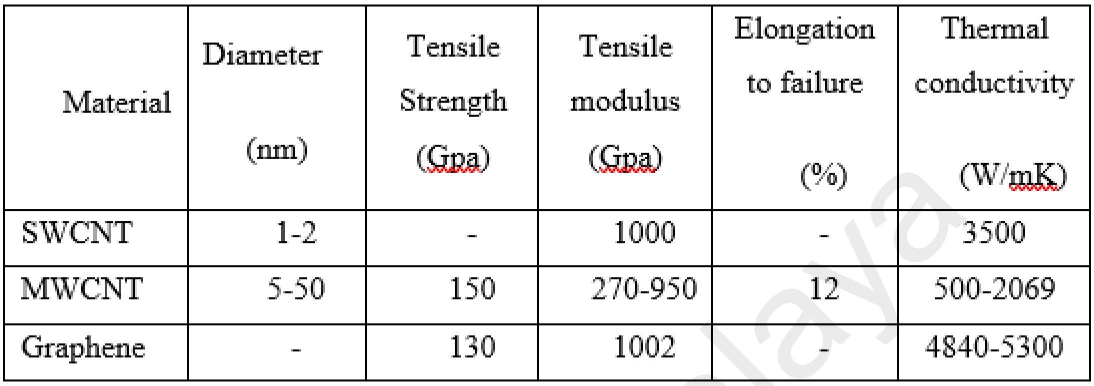

Material	Diameter (nm)	Tensile Strength (Gpa)	Tensile modulus (Gpa)	Elongation to failure (%)	Thermal conductivity (W/mK)
SWCNT	1-2	-	1000	-	3500
MWCNT	5-50	150	270-950	12	500-2069
Graphene	-	130	1002	-	4840-5300

For macroelectronic applications, multipurpose and multifunctional circuits and transistors become viable with the presence of CNTs, which exhibit excellent properties in terms of their transparency, flexibility, reliability, printability, and electrical performance (Q. Cao et al., 2008; Sun et al., 2013; C. Wang et al., 2013; C. Wang et al., 2009; J. Zhang et al., 2011). CNT-based thin-film transistor (TFT) exhibits excellent flexibility and transparency, which are crucial for the development of flexible and transparent electronics. Besides, CNT thin films are capable of being deposited at room temperature, which makes them suitable for flexible electronics on polymeric substrates.

2.5 Graphene

Graphene is a form of carbon that has been recently found and consists of only one plain layer of atoms stacking in a honeycomb lattice, which provides a number of intrinsic properties (Balandin et al., 2008). Graphene has attracted a favorable amount of interest because of its intrinsic properties such as high electrical and thermal conductivity, as well as excellent mechanical strength and Young’s modulus, and high optical transmittance that is usable for optical applications. Fabrication methods have been proposed and improvements are still ongoing in order to produce single and multilayer graphene and graphene oxide in small amounts, with the intention to search for the technique that is able to produce graphene in bulk quantities for the implementation in composite applications (Bartolucci et al., 2011).

Graphene can be synthesized through several methods such as mechanical exfoliation, plasma enhanced chemical vapor deposition (PECVD), chemical vapor deposition (CVD), chemical reduction of graphene oxide (GO), plasma unzipping of CNT through chemical reaction, and rubbing MWCNT bulk samples on glass microblades (W. W. Liu et al., 2014). Mechanical exfoliation using monocrystalline graphitic films is the first successful attempt by Novoselov *et al*. in 2004 to prepare graphene (Novoselov et al., 2004). However, the graphene produced through mechanical exfoliation is too little, which is not feasible for the large-scale production of graphene.

Graphene is also feasible to be synthesized successfully by chemical reduction of GO. This method is usually performed by using chemical reducers such as hydrazine, sodium borohydride ($NaBH_4$) (D. Li & Kaner, 2008), and hydroquinone with vigorous stirring at 80–100 °C. The conductance and structure of GO are capable to be restored at low temperature under hydrazine reduction. However, high structural defect and the presence of an oxygenic group were discovered on graphene as demonstrated in Raman spectra, which need to be reduced through additional processes such as solvothermal technique (H. Wang et al., 2009) developed by Dai *et al*. in order to obtain GO in an effective manner.

The growth of CVD has been one of the common methods for mass production of mono- or few-layer graphene films. Both CNT and graphene can be produced by using CVD method. The major difference between CNT and graphene synthesized by similar

CVD method is the presence of the catalyst that decomposes the carbon source into carbon atoms. In both productions, catalyst nanoparticles are prepared and used to produce CNT whereas a foil is used to produce graphene. As a result, the formation of CNT according to the spherical shape of catalyst nanoparticles takes place whereas a sheet of graphene is produced based on the shape of one piece of foil (Eizenberg & Blakely, 1979; Shelton et al., 1974; Somani et al., 2006).

Graphene is also feasible to be synthesized at a lower reaction temperature by using PECVD compared to CVD to reduce the production cost. The use of a direct current (DC) discharge PECVD in the fabrication of nanostructured graphite-like graphite can lead to the higher amount of graphite. The first production of mono- and few-layers of graphene by radio-frequency PECVD on several categories of substrates was reported, which used a gas mixture of methane (CH_4) and hydrogen (H_2) at 900 W and at the reaction temperature of 680 °C (Reina et al., 2008; J. Wang et al., 2004). Several advantages of PECVD compared to CVD include deposition time of less than 5 min, and also the capability of PECVD to retain a lower growth temperature of 650 °C. PECVD has additional high-density reactive gas atoms and radicals, which can achieve low temperature and faster synthesis of carbon (Nandamuri et al., 2010; Zhu et al., 2007).

The structure of graphene can also be unzipped into CNT by using chemical reaction (Higginbotham et al., 2010; Kosynkin et al., 2009; Z. Zhang et al., 2009). Aside from using chemical reaction, plasma processing is also viable to unzip CNT. CNT needs to be coated by polymers (PMMA) prior to plasma processing in order to establish a process that is compatible with silicon technology (Jiao et al., 2009). Moreover, graphene sheets can be mechanically made by rubbing MWCNT bulk samples on glass microblades (J. Chen et al., 2012). This process promotes an effective and convenient technique to produce graphene sheets. In addition, this method permits the production of graphene sheets on any substrate through a simpler rubbing technique.

Previous researchers discovered several intrinsic properties of graphene. Balandin *et al*. reported that the thermal conductivity of a single-layer graphene at room temperature could reach up to 5,300 W/mK. Due to its excellent thermal conductivity, graphene is strongly recommended in thermal management applications, especially for heat dissipation, electronics, optoelectronics, photonics, and bioengineering applications (Balandin et al., 2008).

The mechanical properties of free-standing monolayer graphene membranes are evaluated based on several criteria such as nanoindentation depth, besides measuring both breaking strength and Young’s modulus. The breaking strength and Young’s modulus recorded the values of 42 N/m and 1.0 TPa, respectively, which suggests single-layer graphene membranes as the strongest material ever measured (Lee et al., 2008).

The excellent optical properties of graphene are determined through light absorbance measurement. White light absorbance of a suspended single-layer graphene measured 2.3% absorbance with negligible reflectance less than 0.1%, and this absorbance increased linearly with the layer numbers from 1 to 5 (Nair et al., 2008). The measured values and the observed linearity are in accordance with the theoretical and actual results acquired with a non-interacting massless Dirac fermion model.

Besides, graphene also possesses superior electronic properties where graphene charge carriers are able to behave as massless relativistic particles or the Dirac fermions (Novoselov et al., 2004). It has been proven that graphene is a carbon entity with zero-gap two-dimensional (2D) semi-metal with a tiny overlap between valence and conductance bands, and charge carriers move with little scattering under ambient conditions. When the gate voltage is applied, strong ambipolar electric field effect is exhibited with the room-temperature mobilities of nearly 10,000 $cm^2/V^{-1}s^{-1}$ and the concentration of charge carriers up to 10^{13} cm^{-2} take place (Novoselov et al., 2004).

2.6 Metal-carbon nanotube-graphene nanoplatelet nanocomposites

Graphene nanoplatelet (GNP) and CNT are parts of carbon-based nanomaterials known for their distinction in physical and mechanical properties, such as high mechanical strength, and high electrical, optical, and thermal conductivity, which make them as a perfect selection for both functional devices and structural engineering applications (Tjong, 2013). GNP and CNT are considered as the most effective reinforcing materials in MMCs for improving their physical and mechanical properties due to their large aspect ratios (i.e., length-to-diameter or length-to-thickness ratio) (Harris, 2004). In addition, the potential of graphene-CNT as a part of reinforcement in composites has also stimulated a huge amount of attention, especially in MMCs in order to fulfill the increasing domestic and global demand for stronger, lighter, and stiffer structural materials from the field of transportation, military, and aerospace applications (Z. Li et al., 2015). However, metal-CNT/GNP nanocomposites received less attention due to the difficulties and challenges involved in metal-CNT/GNP nanocomposites processing (T. Borkar & S. Harimkar, 2011; Tjong, 2013), which include:

(a) Agglomeration of embedded CNT and graphene inside the metal matrix,

(b) Poor wettability between CNT/graphene and metal matrix due to the surface tension issues, and

(c) Difficulties in retaining structural and chemical stability of CNT and graphene.

At present, more attempts have been made on attaining homogeneous dispersion of CNT and graphene into the metal matrix by using different types of processing methods (A. M. K. Esawi et al., 2009; Kwon et al., 2009; Laha et al., 2004; Tjong, 2009). The processing techniques of metal-CNT/GNP composites, strengthening mechanisms, and physical and mechanical properties of metal-CNT/GNP composites are discussed in their research works.

2.7 Processing of metal-CNT/GNP nanocomposites

Even though CNT/GNP is well known for its superior properties in terms of electrical, mechanical, thermal, and optical properties, the processing of CNT/GNP with other materials such as metal matrix is difficult to be executed due to the extreme preparation criteria such as high pressure and high temperature (Tjong, 2013). Some of the main difficulties related within the preparation steps of metal matrix-CNT/GNP composites are as follows (Bakshi et al., 2010; Tjong, 2013):

i. Obtaining homogeneous dispersion of carbon-based reinforcing materials (CNT/GNP) into the metal matrix,
ii. Strong interfacial bonding between CNT/GNP and the metal matrix, and
iii. The ability to retain structural and chemical stability of carbon-based materials (CNT/GNP).

Several techniques are available for the fabrication of metal matrix-CNT/GNP nanocomposites. The processing techniques available include electrodeposition, thermal spray, melting and solidification, and powder metallurgy. Every processing route mentioned can be further subcategorized. For example, the melting and solidification route includes all metal infiltration, casting, laser deposition, and melt spinning. It is similar for electrochemical deposition, powder metallurgy, and other novel techniques. Based on available processing routes, powder metallurgy is the preferred processing technique. The advantages of powder metallurgy process are (Bakshi et al., 2010) (Tjong, 2013) :

i. Ease of the process;
ii. Possibility for large scale bulk production; and
iii. Flexible and almost near to the net shape dimension

However, the most favorable factor that powder metallurgy process can offer are the degree of controllability on the porosity, mixture homogeneity and overall morphology which would be probably hard for other technique to achieve such as by using casting method. This can be explained in terms of required formation energy for a specific nanoparticles formulation which can then be tuned as a function of the process parameters such as Ball to Powder ratio (BPR), Rotation per minute (RPM) and duration of milling process. On the other hand, casting method might be a rival in term of 1) Its better matrix-particles bonding; 2) easier control of matrix structure; and 3) Its simplicity, but it is extremely difficult for the mechanical stirring method to distribute and disperse nano-scale particles uniformly in metal melts due to their large surface-to-volume ratio and their low wettability in metal melts (Koli et al., 2013). Figure 2.4 presents previous powder metallurgy processing routes applied by researchers.

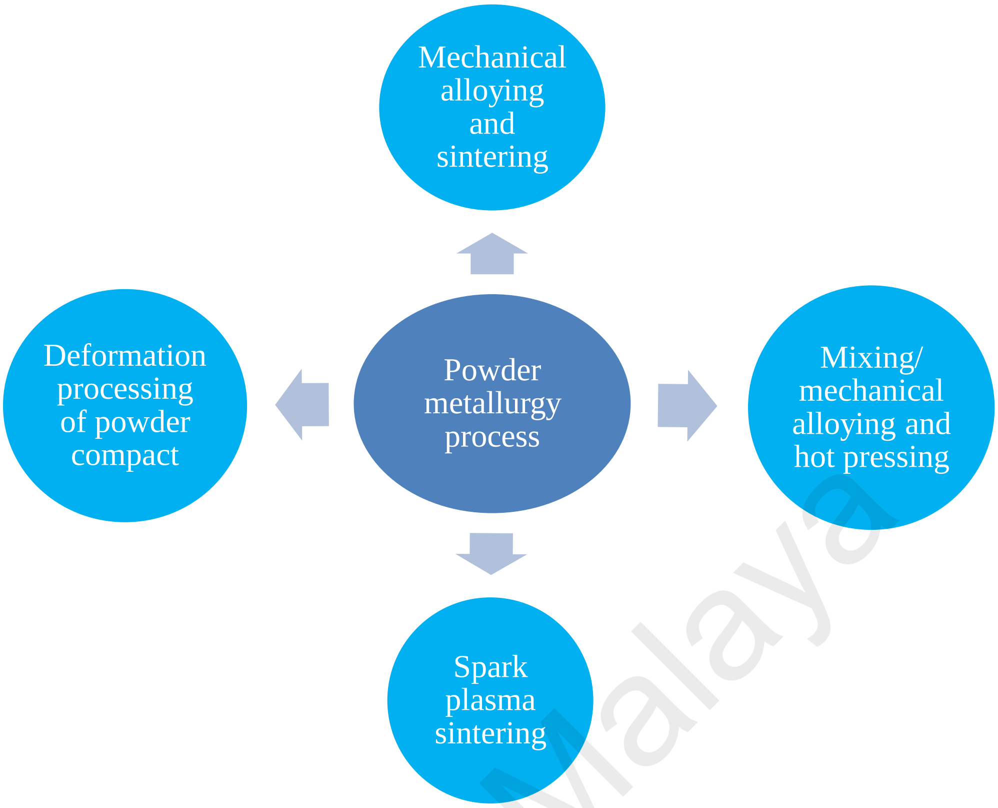

Figure 2.4: Previous powder metallurgy processing routes used by researchers in metal matrix-CNT composites (Bakshi et al., 2010)

2.8 Powder metallurgy process

Powder metallurgy process is one of the popular processing methods for the fabrication of metal-CNT/GNP nanocomposites due to its flexibility, near-net shape, and simplicity (Bakshi et al., 2010; Tjong, 2013). Most metal-CNT/GNP composites such as copper, aluminum, tungsten-copper, magnesium, silver, and nickel are produced using this method (Bakshi et al., 2010). Powder metallurgy method is more convenient compared to liquid metal processing as any composition of material can be processed besides promoting minimum waste of materials due to the less end product chipping, which requires extra machining process (Agarwal et al., 2016). One of the most important steps in powder metallurgy is to get nanofillers to homogenously disperse in the starting metal powder, which has a considerable effect on the final distribution of nanofillers in metal composites (Jiang et al., 2012). There are several basic processing steps involved in powder metallurgy process. These include:

i. Mixing/grinding/mechanical alloying of CNT/GNP with metal powder, and
ii. Consolidation by compaction and sintering, spark plasma sintering (SPS), and cold or hot isostatic pressing.

Some of the researchers even added an additional step of post-sintering deformation such as friction stir processing, hot rolling, hot forging, hot extrusion, and equal channel angular pressing (ECAP). These additional steps help to increase the densification of composites. Even though powder metallurgy is the most simplest and convenient method, the expensive raw material powder becomes the major stumbling block for the execution of powder metallurgy process.

There are four types of process selection that can be applied under the category of powder metallurgy. The first one is mechanical alloying with sintering. Mechanical alloying is based on the processing of solid powder materials at room temperature in order to achieve uniform dispersion of CNT/GNP-MMC. In order to promote and enhance interfacial bonding, both CNT and GNP are coated with nickel through electroless deposition, mixed with metal powder, and followed by compaction and sintering of metal-CNT/GNP composites (Bakshi et al., 2010). In order to avoid agglomeration of CNT/GNP due to poor van der Waals forces, effective techniques such as wet/slurry mixing can be applied. Wet mixing technique can be applied by dispersing both metal powder and CNT/GNP nanofillers inside certain organic solvents (e.g., acetone, ethanol, and methanol). This composite powder mixture is then left to dry before proceeding with mechanical alloying and sintering processes (Tjong, 2013). Previous researchers successfully achieved a homogeneous dispersion of CNT/GNP into the metal matrix through wet mixing process. Yang *et al*. managed to obtain a homogenous dispersion of CNT into Mg-metal matrix (Yang & Schaller, 2004) whereas Wang *et al*. successfully achieved a uniform dispersion of GNP by preparing Al with 0.3 wt. % GNP composite using wet mixing process (J. Wang et al., 2012).

The second method is through the combination of mixing-sintering-hot pressing. The combination of mixing together with sintering and hot pressing has shown considerable enhancement in mechanical properties (e.g., hardness, bend strength, and compressive strength) for both Mg-CNT and Fe_3 Al-CNT due to the homogeneous distribution of CNTs in the metal matrix, as well as grain refinement. The interlocking of CNT initiates grain growth inhibition, which leads to grain refinement (Tjong, 2013). The dispersion of CNT/GNP in the starting composite powder is one of the crucial factors that lead to their successful dispersion into the metal matrix because subsequent compaction, sintering, and hot pressing do not enhance carbonaceous material dispersion. However, matrix material, types of nanotubes, nanotube content, functionalization of nanotubes, and milling time could contribute to the homogeneous dispersion of CNT into the metal matrix processed *via* mechanical alloying (Tjong, 2013). Al-CNT nanocomposites fabricated using mechanical alloying followed by sintering and hot pressing showed improvement in mechanical properties. (A. Esawi et al., 2010; Jafari et al., 2012; Kondoh et al., 2009; Z. Liu et al., 2012; Singhal et al., 2012; Stein et al., 2012).

The third method is spark plasma sintering (SPS). The method is a newer processing tool to produce metal-CNT/GNP nanocomposites. In SPS process, spark is discharged in a gap or at the contact point between the particles of powder and creates a local high-temperature state. Surface melting of powder particles starts during local high-temperature state, which produced a fully-dense nanocomposite at the end of the process. SPS introduces high-speed powder sintering technology that enables processing of the materials and simultaneously utilizes uniaxial force and ON-OFF DC pulse. Consolidation of nanopowders is possible in SPS without excessive grain growth due to lower sintering time and high heating rate. Kim *et al*. was the first researcher that addressed the fabrication of Cu-CNT composites processed *via* SPS and managed to show the uniform dispersion of CNTs with improved density (K. Kim et al., 2008; K. T. Kim et al., 2011). Hong's group also fabricated Al-Cu-CNT and Cu-GNP composites processed *via* SPS, which showed significant improvement in their mechanical properties (Hwang et al., 2013; Jeong et al., 2007). The main reasons in mechanical properties enhancement are uniform dispersion of CNTs into the metal matrix and strong metal-CNT interfacial bonding.

The last method is deformation processing of powder compact. Al-CNT and Cu-CNT composites produced through this method shows enhancement in terms of density and also dispersion of CNT into the metal matrix. Significant wear resistance and strength enhancement are observed in rolled Cu-CNT composites compared to Cu-CNT composites processed *via* extrusion method. Cu-CNT composites processed *via* ECAP shows a uniform dispersion of CNTs into the metal matrix with an increasing number of passes (T. Borkar & S. P. Harimkar, 2011).

Homogenous dispersion of CNT/GNP into the metal matrix, and interfacial bonding between CNT/GNP and the metal matrix are the two major aspects related to the fabrication of metal-CNT/GNP composites. Proper mixing process together with shorter sintering time can effectively overcome these issues. The introduction of mechanical alloying or ball milling can significantly help to homogenize uniform dispersion of CNT/GNP into the metal matrix. The selection of SPS looks promising for the consolidation of metal-CNT/GNP nanocomposites with uniform dispersion of CNT/GNP into the metal matrix, together with excellent interfacial bonding between CNT/GNP and the metal matrix.

2.9 Solar absorbers

2.9.1 Introduction to solar absorbers

Solar absorbers can be defined as absorbers made from materials that are able to absorb, store, and transfer the thermal energy obtained from solar radiation to heat transfer media such as water and air. The capabilities of solar absorbers depend on the material and corresponding thermophysical properties (Razak et al., 2016).

Ideally, a good solar absorber has a surface that can absorb high incoming solar radiation (i.e., solar absorptance (α)) without major loss of thermal energy through re-radiation from heated surface (i.e., low emittance (ε)). The division of solar absorptance with emittance is called spectral selectivity. With the development of solar thermal technology in the last few decades, various materials, design methods, and manufacturing techniques have been employed to improve the spectral selectivity of solar absorbers.

Figure 2.5 shows the spectral selectivity performance of an ideal solar absorber. A low reflectance ($\rho \approx 0$) at wavelengths (λ) ≤ 3 μm and a high reflectance ($\rho \approx 1$) at $\lambda \geq 3$ μm characterize spectrally selective surfaces (C. E. Kennedy, 2002).

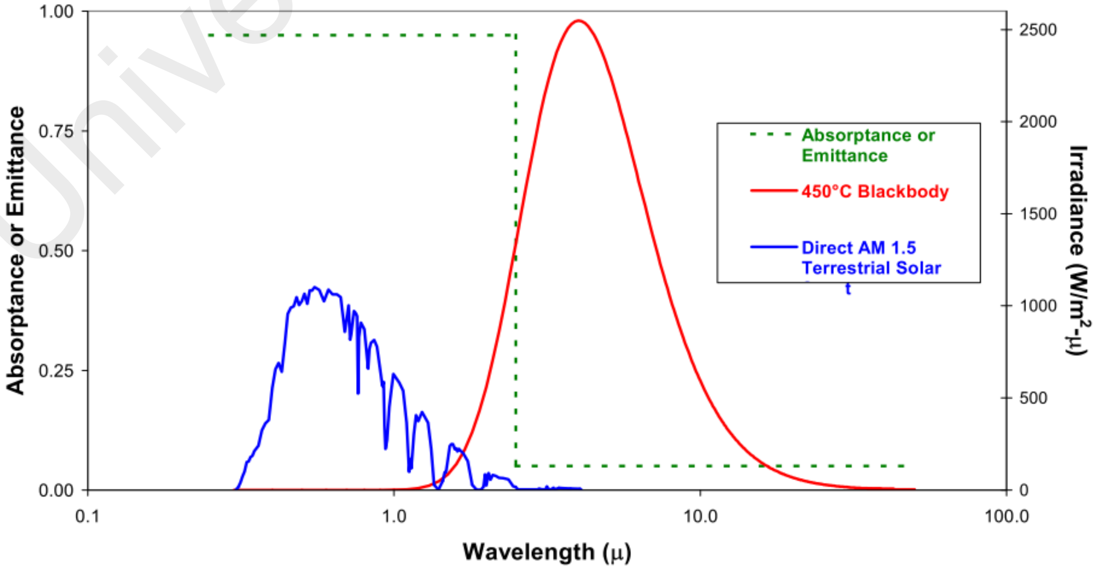

Figure 2.5: Spectral selectivity performance of an ideal selective solar absorber.

However, there is no natural material that can meet those criteria mentioned above. As such, there is a need to fine-tune the optical and structural properties of a surface through the combination of materials, modification of the surface, or synthesis of multilayer solar absorber materials to achieve the desired wavelength selectivity (Barshilia, Selvakumar, Rajam, Rao, et al., 2008).

2.9.2 Spectrally selective solar absorbers

Solar thermal absorbers absorb and convert solar radiation into heat in solar thermal collectors. For a solar absorber to be optically and thermally efficient, it has to be spectrally selective, which means it can achieve high solar absorption in the ultraviolet-visible-near-infrared (UV-Vis-NIR) solar spectrum and lower thermal emittance in the infrared (IR) wavelength region. Photothermal conversion efficiency has been greatly improved from the original solar absorbers that used non-selective black paint surface (Orel et al., 1990) (El Nady et al., 2016) to those using highly selective surfaces such as black chromium (Shanker & Holloway, 1985) (Axelbaum & Brandt, 1987), black nickel (Srinivasan et al., 1984) (Lira-Cantu et al., 2005), and cermet (Zheng et al., 2015) (Rebouta et al., 2015). Among the designed methods, surface texturing, tandem structure, and quantum size effects have been used (Yianoulis et al., 2012). Solar absorbers that are commonly available exist in the form of tandem type and consist of an IR reflective metal plate with an excellent thermal conductivity material such as aluminum (Boström et al., 2003) (Konttinen et al., 2005) (Tinchev et al., 2010) or copper (Kunič et al., 2009). On top of the metal plate, an absorbing layer is coated or fabricated with various methods of thin-film deposition such as chemical vapor deposition, electroplating, sputtering, anodization spray pyrolysis, and sol-gel to produce a spectrally selective surface (Hollands et al., 2001) (Boström et al., 2003). This absorbing layer should absorb the radiation in the UV-Vis-NIR solar spectrum and should be transparent to longer wavelength radiation.

2.9.3 Optical characterization of solar absorbers

Generally, when the radiation beam hits the surface of a solar absorber, a part of the radiation is reflected at the surface and there is some radiation that is absorbed in the absorber and transmitted throughout the absorber. The addition of reflectance, absorptance, and transmittance equals to 1, which can be shown in Equation (1):

$$R(\lambda) + A(\lambda) + T(\lambda) = 1 \qquad \text{Eq. (2.1)}$$

Where:

R (λ) = Spectral reflectance

A(λ) = Spectral absorbance, and

T(λ) = Transmittance

According to Kirchhoff's law, for a blackbody in thermodynamic equilibrium, the absorbed energy is equal to the emitted thermal radiation, which is characterized by the emittance (λ):

$$\varepsilon(\lambda) = A(\lambda) \qquad \text{Eq. (2.2)}$$

For solar absorbers that have opaque characteristic such as metal substrate, the transmittance is equal to zero as the light cannot pass through the opaque sample. By substituting Equation (1) in Equation (2), Equation (3) is obtained:

$$A(\lambda) = 1 - \varepsilon\ (\lambda) \qquad \text{Eq. (2.3)}$$

2.9.4 Spectral selectivity

An effective solar absorber should have high solar absorptance and low thermal emittance. This is translated into low reflectance in the wavelength range of 0.3–2.5 µm and high reflectance in the infrared region of 2.0–50.0 µm. Consequently, the transition from low to high reflectance should be located between 2.0 and 2.5 µm for optimized solar absorbers. This optical property of solar absorbers is named spectral selectivity. An ideal solar absorber should have solar absorptance of 1 and thermal emittance of 0. The reflectance of an ideal solar absorber is illustrated in Figure 2.6.

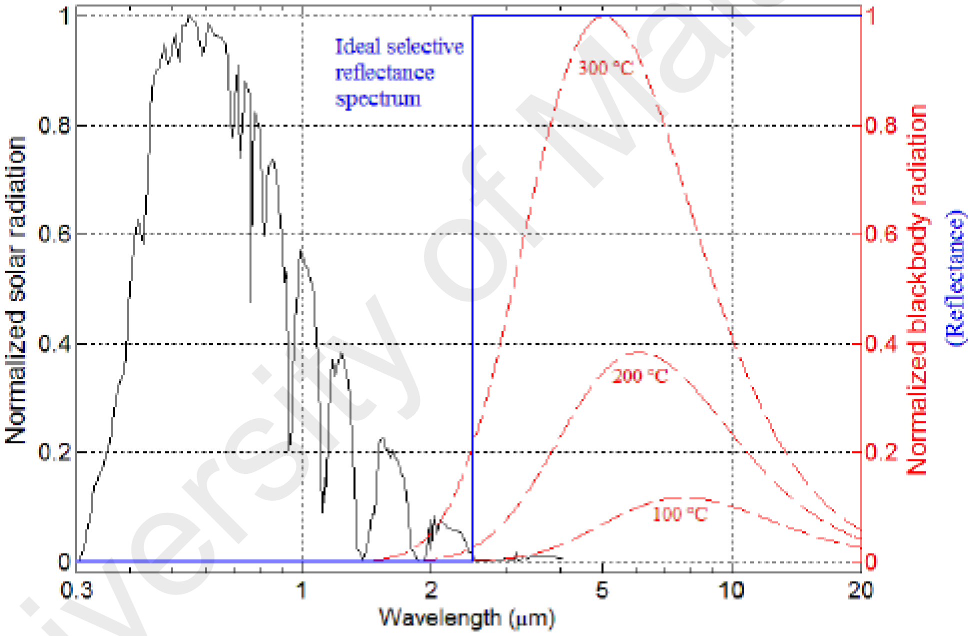

Figure 2.6: The normalized solar irradiation, blackbody radiation spectra at 100 °C, 200 °C, 300 °C, dashed curves together with indicated ideal selective reflectance spectrum.

There are several ways to evaluate spectral selectivity. One of the most frequently used methods is to calculate the ratio of solar absorptance to thermal emittance (α/ε), which is used in this study.

2.9.5 Different designs of spectral selective surface

To obtain a solar absorber with excellent spectral selectivity, various methods and materials have been applied for the fabrication of solar absorbers. Technically, the methods of obtaining spectral selectivity can be classified into three categories, namely intrinsic selectivity, textured surfaces, and tandem structures.

2.9.5.1 Intrinsic selectivity

An intrinsic solar absorber can be defined as a single material that comes with intrinsic optical properties that can absorb in the solar spectrum and reflect in the FIR region. An intrinsic solar absorber is more structurally stable over long-term operation. On the other hand, it is less optically effective than other types of spectral selective absorbers due to either low solar absorptance or high thermal emittance, i.e., low spectral selectivity. Intrinsic solar selective materials can be found through transition metals and semiconductors. These selective materials are also suitable to be used as components in other types of spectrally selective absorbers (C. E. Kennedy, 2002).

2.9.5.2 Textured surfaces

Enhancement of solar absorption can also be realized with the introduction of textured surfaces. The concept behind a textured surface is the effect of optical trapping. When incident radiation strikes on these rough or textured surfaces, the radiation with shorter wavelength is either immediately absorbed or scattered by the surface. The scattering leads to multiple reflections that can result in increased absorption. Simultaneously, the radiation with longer wavelength passes through the rough or textured surface and is not absorbed, instead reflected to the surroundings *via* multiple reflections. This type of selective absorber is less sensitive to environmental effects such as oxidation or thermal shocks and therefore has a long lifetime (Yianoulis et al., 2012).

2.9.5.3 Tandem solar absorbers

Tandem solar absorbers are known as absorbers that are constructed with one or multiple layers of solar absorbing thin films coated on top of an infrared reflective metal substrate. Various methods are used to design and coat the top absorbing layers in order to absorb solar radiation whereas the metal substrate reflects infrared light to reduce heat loss. Black chromium (Harding, 1976) (Eugénio et al., 2011) (Survilienė et al., 2014), cermet (a composite made of ceramic and metal, for example copper oxide) (Karlsson & Roos, 1984) (Xiao et al., 2011) (S. K. Kumar et al., 2013), cobalt oxide (Maruyama & Nakai, 1991) (Barrera et al., 1996) (Choudhury & Sehgal, 1982), metal/oxides composites (Boström et al., 2003) (Ienei et al., 2010), and spinels (KalužA et al., 2001) are among the most used materials for a single absorbing layer. There are also reports on using aligned CNTs grown on metal substrates (A. Cao et al., 2002) (N. Selvakumar et al., 2014). As mentioned above, highly reflective metals such as aluminum and copper are commonly used as substrates. With these materials, solar absorptance of > 0.80 and thermal emittance of < 0.2 can readily be achieved.

2.9.6 Current development on bulk solar absorber

One of the most promising way of generating the energy other than using Photovoltaic System is through the introduction of concentrating solar power to a central tower where solar radiation receiver as the most critical part located (Behar et al., 2013). In general, there are several criteria that need to be satisfied (Bogaerts & Lampert, 1983) (Lampert, 1987) (C. E. Kennedy, 2002) such as, good thermal properties, to properly transfer the thermal energy to the exchange medium, high solar absorbance, to efficiently absorb sunlight, and a low thermal emittance, to limit thermal re-radiation losses. Thus, the main difficulties in establishing an excellent thermal plant is the development of novel receiver materials which are stable at very high temperatures and able to exhibit all the favorable optical and thermal properties mentioned above. Based on the current research works, it can be seen that transition metal nitrides, carbides and borides have been attracting researchers interest due to their inherent spectral selectivity. Among these materials, titanium carbide could be a good candidate because it is spectrally selective and it has good mechanical properties. However, it also has a low resistance to oxidation (Aréna et al., 2019). Previous studies showed that the combination of SiC and TiC Sciti et. al reported the suitability of borides as material for bulk solar absorber. Investigated borides clearly shows the metal-like optical behavior through step-like reflectance curves with low reflectance in the UV-VIS and high reflectance values in the medium infrared. (Sciti et al., 2013). Sani et. al on the other hand reported that intrinsic radiative properties of carbides as material for bulk solar absorber could affect optical spectra. Sani et. al also reported that surface roughness could affect the optical spectrum and surface roughness is mainly related to the surface porosity. Lower roughness of bulk samples surface can lead to higher reflectance (E. Sani et al., 2014). Arena et. al reported that SiC-TiC nanocomposites could be a good candidate for bulk solar application due to its oxidation resistant besides achieve high solar absorptance of 0.76 and lower emittance of 0.44 (Aréna et al., 2019).

CHAPTER 3: METHODOLOGY

3.1 Introduction

This chapter is divided into several main sections:

i. Material selection,
ii. Required equipment,
iii. Material synthesis, and
iv. Powder metallurgy process.

In this research, aluminum (Al), multi-walled carbon nanotubes (MWCNTs), and graphene nanoplatelets (GNPs) are used as the main materials for the fabrication of a solar absorber sample. The utilization of modified MWCNTs and GNPs through chemical functionalization is used as the comparison in terms of the properties with pristine MWCNT and GNP. Furthermore, all the equipment used for characterizing the samples in terms of its surface morphology and intrinsic properties such as X-ray diffraction (XRD), field emission scanning electron microscopy (FESEM), Fourier transform infrared spectroscopy (FTIR), ultraviolet-visible/near-infrared (UV-Vis-NIR), and Vickers microhardness test are explained in detail. Figure 3.1 shows the flow chart of the experimental process throughout the research.

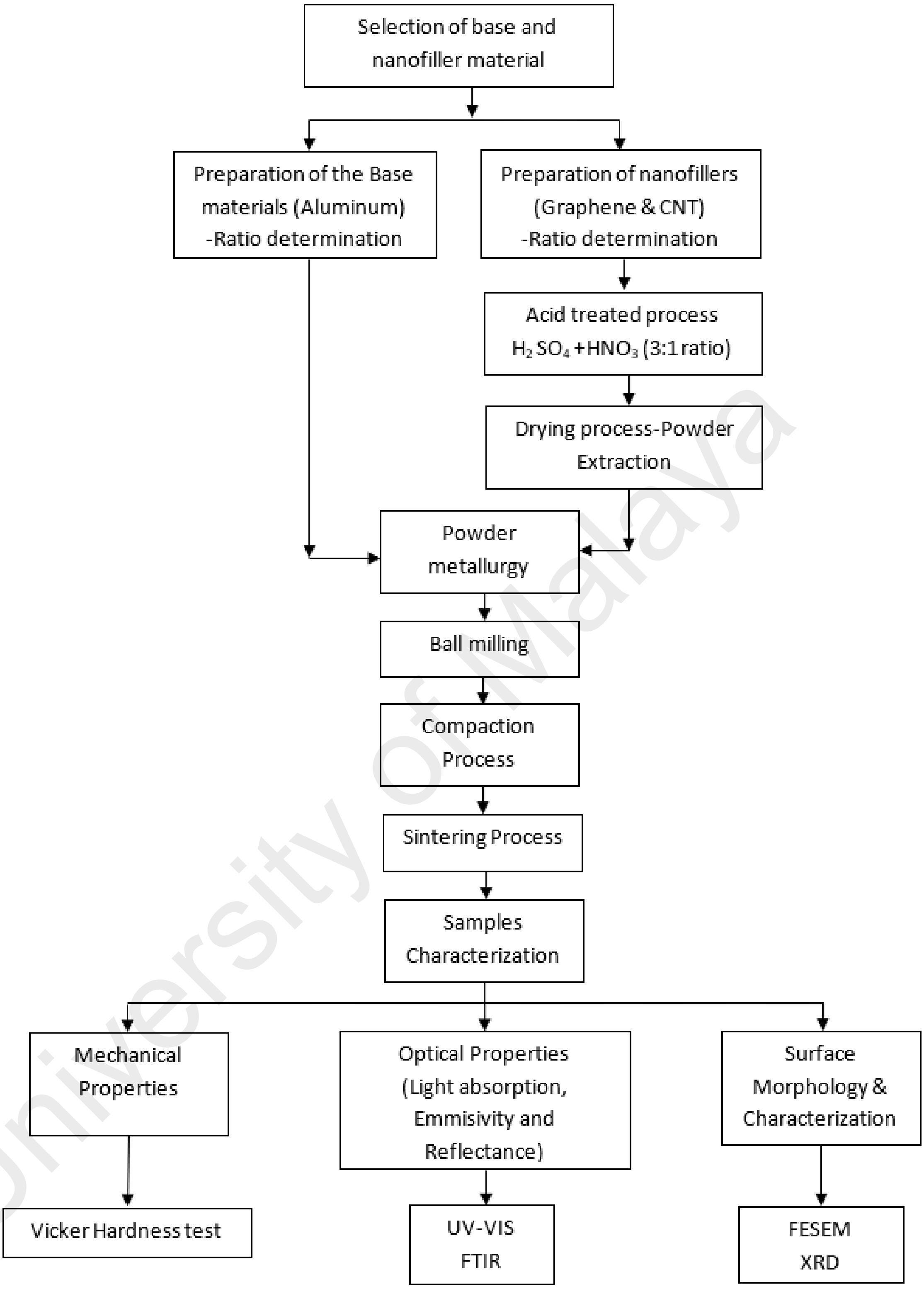

Figure 3.1: Flow chart of the processes involved throughout the research

3.2 Material selection

The materials used for sample fabrication are MWCNT, GNP, and Al powders. All the materials chosen for this research are in powder form because powder metallurgy is selected as the main process. The usage of two and more powders inside the sample fabrication is made easier with the introduction of powder metallurgy process. In the existing literature, researchers (Hernandez-Pinilla et al., 2016) (Raccurt et al., 2015) (Cuevas et al., 2016) (Gao et al., 2016) are inclined toward coating process in order to produce solar absorber samples instead of making bulk samples through powder metallurgy. However, there are several disadvantages of coating. Some of the critical disadvantages are higher cost and delamination problems (Boubault et al., 2014). Most of the researchers are aware of the delamination of solar absorber coating, especially under high operating temperature (Boubault et al., 2014; Z. Chen & Boström, 2016). Moreover, the preparation of coating will involve the use of high technology and expertise which in return will cause higher production cost. Based on these two critical issues, powder metallurgy route is selected for sample fabrication in this research. Powder metallurgy process is selected due to its simplicity, cost economics for the manufacturing of aluminum MMCs, achievement to near end shape dimension and last but not least better controlled on the mixture homogeneity (Koli et al., 2013). Figure 3.2 shows the materials involved in the research work.

Figure 3.2: The materials used for this research (From left: X-GnP C-300, aluminum 99% purity-200 mesh, and MWCNT)

3.3 Equipment for sample preparation and characterization

A number of equipment is required in order to support the fabrication process, characterization, and performance evaluation. Table 3.1 presents the equipment used in this research.

Table 3.1: List of the instruments involved for sample fabrication and analysis

INSTRUMENTS	FUNCTION OF EQUIPMENT
Scanning Electron Microscope (SEM)	A FESEM machine is used to investigate the morphology, surface topography, microstructure, and the distribution of fillers in the sample.
X-Ray Diffractometer	An XRD machine is used to check the composition of the sample and for the detection of aluminum carbide (Al_4C_3) contamination.
Vickers Hardness Tester	A Vickers hardness tester is used to check the mechanical properties of samples through the depth of indentation.
High-Temperature Furnace	A furnace is used to sinter the green compacted Al nanocomposites pallet into solid hardened pallet before proceeding to the characterization and analysis of the pallet.
Centrifuge	A centrifuge is used for the separation of functionalized MWCNTs and GNPs from the

	diluted solution after chemical functionalization process.
Ball-Milling Machine	A ball-milling machine is used to crush bigger Al nanoparticles into refine powder and to simultaneously promote homogenous mixing of carbon nanofillers with Al nanocomposite powder.
Compacting Machine	A compacting machine is used for the preparation of samples by compacting Al nanocomposites powder into a pallet prior to sintering process.
UV-Vis Spectrophotometer	A UV-Vis-NIR spectrophotometer is used to obtain and analyze the UV-visible light spectrum of absorption and reflectance of samples from 200 to 2,500 nm (lower limit).
Fourier Transform Infrared Spectrometer	A Fourier transform infrared spectrometer is used for two types of characterizations. The first one is to check the presence of carboxylic acid (COOH) attachment on the surface of functionalized GNPs and MWCNTs. The second purpose is to obtain and analyze the infrared spectrum of absorption and reflectance of samples from 3,000 to 14,000 nm (upper limit).

3.4 Material synthesis

3.4.1 Synthesis of functionalized MWCNTCOOH and GNPCOOH

Figure 3.6 illustrates the flow chart of converting both pristine MWCNT and GNP into functionalized MWCNT (MWCNTCOOH) and functionalized GNP (GNPCOOH), respectively. In order to obtain better dispersion of MWCNT and GNP in Al-based nanocomposites, 0.5 g of the as-received powder of both MWCNT and GNP were treated with 20 ml of mixture of concentrated sulfuric acid (96% H_2SO_4) and nitric acid (65% HNO_3) with the volume ratio of 3:1. The mixture was stirred using a hot plate and a magnetic stirrer at 75 °C for 2 h and a condenser was used to minimize mixture losses through evaporation. After both stirring and heating were completed, the mixture was left cooled to room temperature before diluted with the solution consisting of 150 ml of distilled water and 50 ml of acetone. Hettich Rotofix 32A benchtop centrifuge was used to filter both MWCNTCOOH and GNPCOOH at 6,000 rpm for 15 min for three times and then the filtered solid was washed with distilled water. The filtered solid was dried in a drying oven (Binder ED series) for 24 h at 80 °C. Film-like dried solids were obtained for MWCNTCOOH and GNPCOOH.

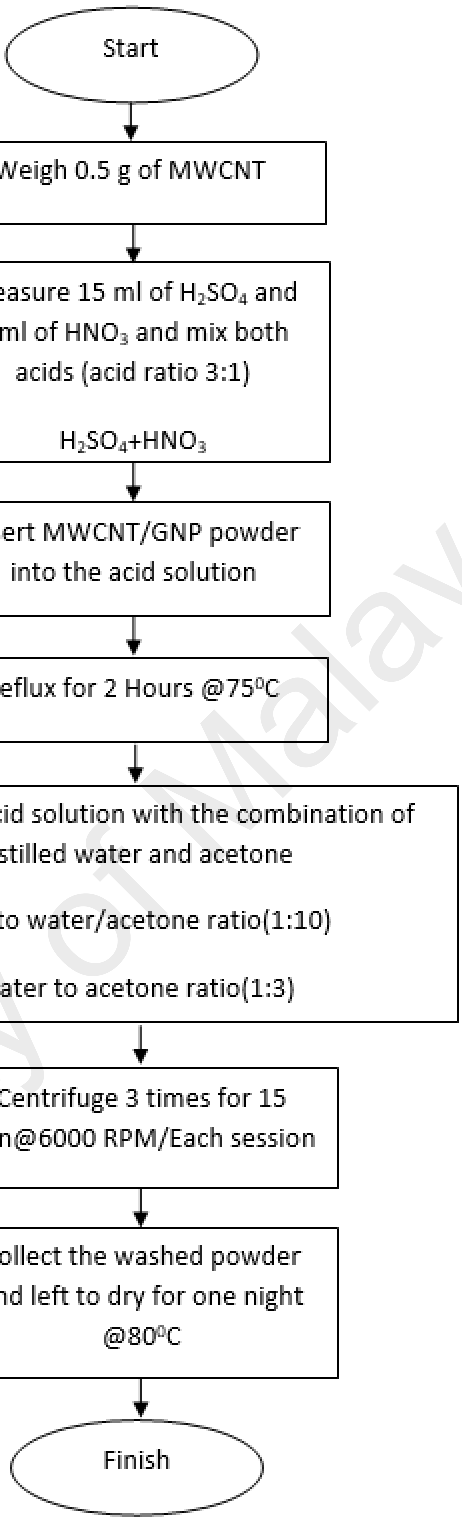

Figure 3.3: Flow chart of synthesizing MWCNTCOOH/GNPCOOH from pristine MWCNT/GNP

3.5 Powder metallurgy process

3.5.1 Composition of Al nanocomposites

The preparation of Al nanocomposites is made based on nanofillers that can give optimized dispersion, hardness, and optical properties for Al nanocomposites. In order to achieve the objective, Al nanocomposites with different types of nanofillers were set up. Tables 3.2, 3.3, 3.4, and 3.5 list down the compositions of Al nanocomposites in this study.

Table 3.2: Composition of Al-pristine MWCNT nanocomposites

No.	Al (wt. %)	Pristine MWCNT (wt. %)
1.	100	0
2.	95	5
3.	90	10
4.	85	15

Table 3.3: Composition of Al-pristine GNP nanocomposites

No.	Al (wt. %)	Pristine GNP (wt. %)
1.	100	0
2.	95	5
3.	90	10
4.	85	15

Table 3.4: Composition of Al-pristine MWCNT-GNP nanocomposites

No.	Al (wt. %)	Pristine MWCNT (wt. %)	Pristine GNP (wt. %)
1.	100	0	0
2.	95	2.5	2.5
3.	90	5	5
4.	85	7.5	7.5

Table 3.5: Composition of Al-functionalized MWCNTCOOH-GNPCOOH nanocomposites

No.	Al (wt. %)	MWCNTCOOH (wt. %)	GNPCOOH (wt. %)
1.	100	0	0
2.	95	2.5	2.5
3.	90	5	5
4.	85	7.5	7.5

Since MWCNT and GNP are generally known for their difficulty to disperse well in metal composites (Bartolucci et al., 2011; Jiang et al., 2012), thus MWCNT and GNP are subjected to treatment by attaching carboxylic functional group (-COOH) onto their surface. The effect of functionalized nanofiller addition on dispersion, hardness, and spectral selectivity improvement is investigated.

3.5.2 Blending/mixing process

The details of methods for mixing and blending, ball-to-powder ratio (BPR), the type and amount of process control agent (PCA) used, ball milling time and speed, and duration of powder drying are described as follows:

a) Method of blending

Previous research works done by Li Zan *et al*. and Novak *et al*. recommended the addition of pure ethanol during milling process to distribute the reinforcement in Al nanoparticles uniformly (Z. Li et al., 2015; Novak et al., 2014). By following those precedence research works, in this study, the process suggested is slurry blending process. Slurry blending process is recommended in order to facilitate the ball milling process for uniform nanofiller dispersion and reducing the damage of MWCNT and GNP nanofillers throughout the milling process.

b) Ball-to-powder ratio

According to Toozandehjani *et al*., a suitable BPR that can be used is 8:1 (Toozandehjani et al., 2017). Another research work conducted by Ostovan *et al*. also introduced a similar BPR of 8:1 in their study. Ostovan et. al find that uniform dispersion of CNTs at BPR ratio of 8:1 at longer milling time along with grain refining enhances the elastic modulus and hardness of nanocomposite specimens. While, the presence of CNT clusters at shorter aging time contributes to the lower values of hardness and Young's modulus. (Ostovan et al., 2016). In addition, another research work conducted by Mallikarjuna *et al*. suggested the optimal usage of 8:1 for BPR during blending process. The nanocomposite powder (MWCNTs and SiC) are successfully flattened in shape and embedded inside the copper particles due to sufficient cold welding between individual flattened copper particles. (Mallikarjuna et al., 2016). Liu *et al*. also selected BPR of 8:1 for its research on effect of ball-milling time on Al-CNT (Z. Liu et al., 2012). .Some researchers such as Munir *et al*. introduced a BPR of 5:1 in their study (Munir et al., 2016). Meanwhile, another research work conducted by D. H. Nam *et al*. suggested the optimal usage of 10:1 for BPR during blending process (Nam, 2012). Rikhtegar F. *et al*. in their study also suggested the usage of BPR of 10:1. According to Yadav *et al*., empirically, ball mass-to-powder ratios of 5 to 10 are typically used and effective (Yadav et al., 2012). After referring to the literature, the BPR of 8:1 was used and fixed for all powder milling processes after considering the suitable BPR employed by previous researchers. The powder was milled inside a stainless steel milling jar coated with zirconia internally together with the help of zirconia balls. 5-mm zirconia balls were used to promote mixing of slurry, besides minimizing the damage of MWCNT and GNP nanofillers during the milling process.

c) Addition of process control agent

In this research, a PCA was used to create slurry-based milling process. 8 ml of ethanol was added to 4 g of powder prior to milling in order to reduce the effect of cold welding and prevent agglomeration during milling process.

d) Ball-milling time and speed

Ball-milling time was fixed at 4 h, excluding the total break time of 35 min (5-min break between 30 min of milling session) whereas milling speed was fixed at 300 rpm throughout the milling process. The rotation of milling was set to alternate rotation mode (clockwise-anticlockwise rotation) for every 30 min of milling process. The variable rotation mode was used to promote homogeneous mixing of the nanocomposites. The interval break was also introduced to reduce the heat generated on the slurry nanocomposites due to continuous milling process.

e) Drying of milled powder

Milled powder was dried inside an oven for one night at 80 °C to ensure that the powder had fully dried prior to compacting process.

3.5.3 Compacting process

After blending and mixing processes, the dried powder was weighed before being compacted. 2.5 g of the ball-milled powder mix was compacted in a 20-mm diameter of hardened stainless steel die using a hand-press compacting machine (Specac Atlas) at the pressure of 9.61 tons (~300 MPa) with 20 min of holding time. Figure 3.7 shows the tablet compacting machine used for compacting process.

Figure 3.4: Hand press compacting machine used for compacting Al nanocomposites powder

3.5.4 Sintering process

All sintering processes were conducted in a tube furnace with continuous flow of argon gas (100 ml/min). This method is very effective in preserving a controlled inert atmosphere inside the tube furnace, which can avoid oxidation of the samples during sintering process. A green sample with 20 mm diameter and 3 mm thickness was subjected to sintering in an argon atmosphere for 6 h at 625 °C (heating rate: 5 °C/min). Figure 3.8 shows the tube furnace used for sintering process.

Figure 3.5: Carbolite tube furnace used for sintering Al nanocomposites

Table 3.6 lists the parameters involved during sintering process. All Al nanocomposite samples prepared for this research were subjected to similar parameter settings.

Table 3.6: Setting parameters for sintering process

No.	Parameters	Value
1.	Sintering temperature (°C)	625
2.	Soaking time (h)	6
3.	Heating rate (°C/min)	5
4.	Environment control	High-purity argon gas flow (99.999%)

CHAPTER 4: RESULTS AND DISCUSSIONS

4.1 Morphologies of raw material for research

4.1.1 Aluminum powder

Figure 4.1 presents the image of the as-received Al powder (Brand: Acros Organics, purity: 99%, average particle size: 74 μm) purchased from Fisher Scientific (M) Sdn. Bhd., Malaysia, obtained from FESEM.

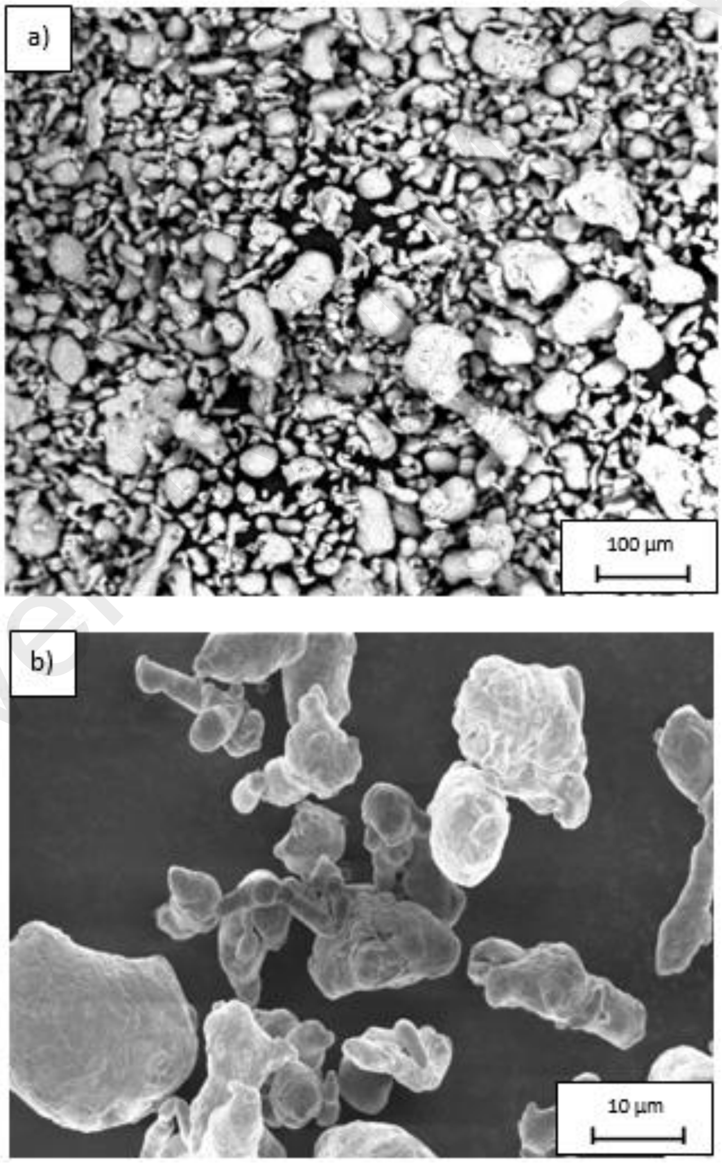

Figure 4.1: FESEM images of pure Al used for the research: (a) 300× magnification and (b) 1,000× magnification

4.1.2 Multi-walled carbon nanotubes

Figure 4.2 shows the FESEM image of pristine MWCNTs taken at 20,000× magnification. The MWCNT used for this research was purchased from Nanostructured & Amorphous Materials, Inc., Houston, USA, and this MWCNT consists of 95%+ purity with an outside diameter of 20–30 nm, an inside diameter of 5–10 nm, and a length of 10–30 µm. The specific surface area of the MWCNT is approximately 110 m^2/g and the density is approximately 2.1 g/cm^3. The melting point of the MWCNT is 3,652–3,697 °C and it is insoluble in water.

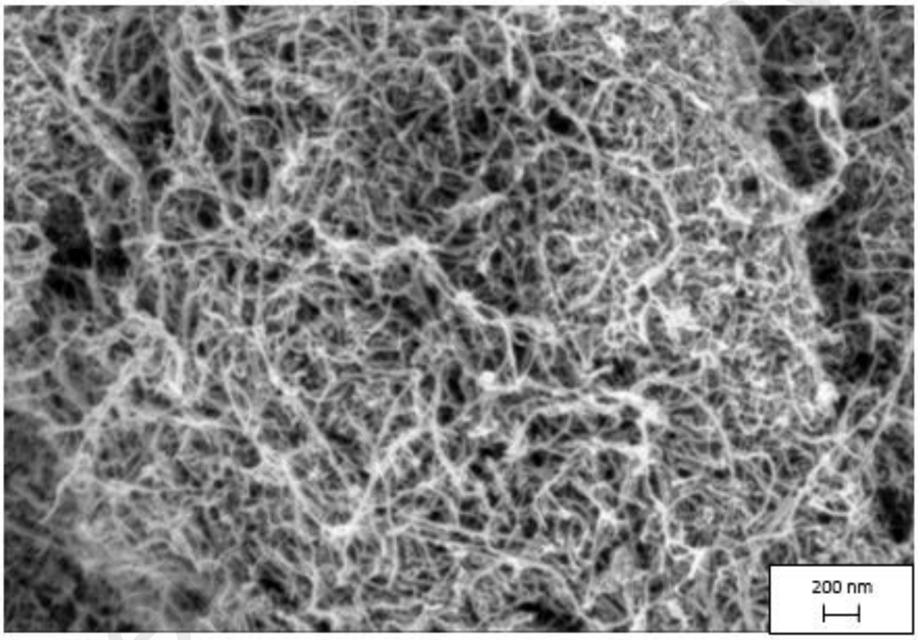

Figure 4.2: FESEM images of pristine MWCNT used for this research

4.1.3 Graphene nanoplatelets

The FESEM image of GNP taken at 20,000× magnification as shown in Figure 4.3 was purchased from XG Science, Inc. GNP is a unique nanoparticle consisting of short stacks of graphene sheets with a platelet shape. The bulk density of this GNP is 0.2–0.4 g/cm^3. The size of the GNP in this research is 300 m^2/g (GNP C-300). The thickness of the GNPs ranging from 1 to 20 nm and the width ranging from 1 to 50 μm.

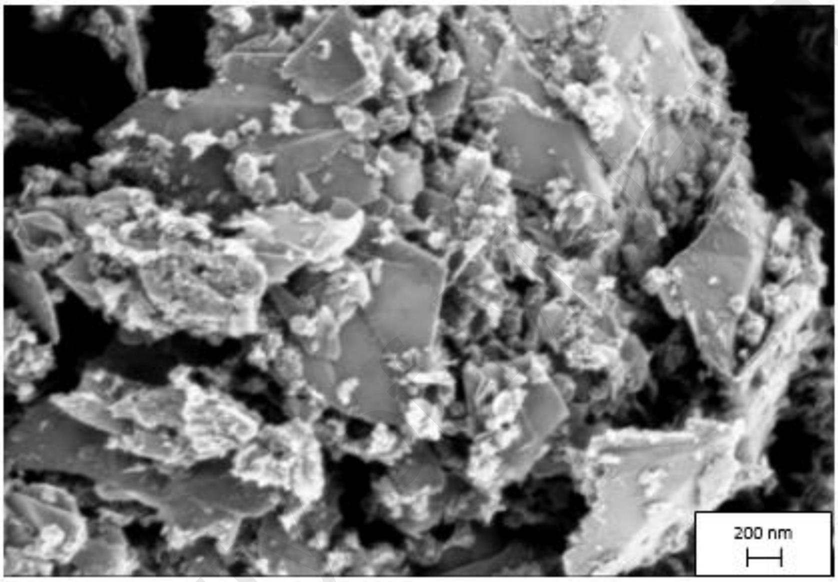

Figure 4.3: FESEM image of pristine GNP used in this research

4.2 Functionalization of MWCNTs and GNPs

4.2.1 Morphologies of functionalized MWCNTs and GNPs

Functionalization process affects the structure of MWCNTs and GNPs. An observation under FESEM was carried out for both pristine and functionalized MWCNTs and GNPs. Figures 4.4(a) and (b) represent the morphologies of pristine MWCNTs (purity: 95%, outer diameter: 30–50 nm, length: 10–20 μm) and MWCNTCOOH, respectively. As shown in Figure 4.4(a), the morphology of pristine MWCNTs is curly and intertwined with each other. The diameter of pristine MWCNTs is still maintained in a uniform shape without any deformity on its structure. After the chemical treatment using a combination of H_2SO_4/HNO_3, the diameter of MWCNTCOOH becomes a little smaller, which is due to the oxidation of the outer layer of MWCNTs by a strong acid combination, which can be seen in Figure 4.4(b).

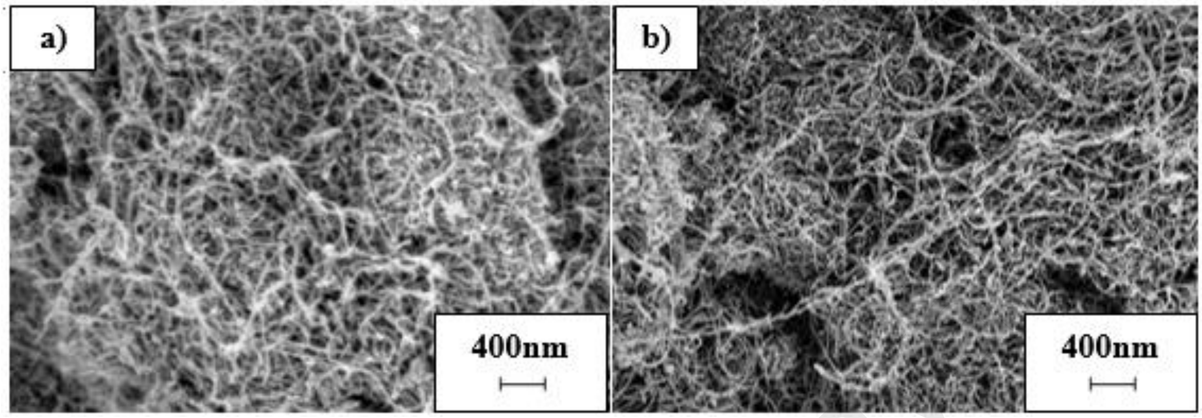

Figure 4.4: FESEM images of a) pristine MWCNTs and b) functionalized MWCNTs

Meanwhile, Figures 4.5(a) and (b) illustrate the morphology of pristine GNPs (average thickness: 2 nm, width: 1–2 μm, surface area: 300 m^2/g) and functionalized GNPs after the chemical treatment process, respectively. The morphology of pristine GNPs shows several layers of plane surface stacking onto each other, as shown in Figure 4.5(a). After the chemical treatment using a combination of H_2SO_4/HNO_3, the plane surface of GNPCOOH becomes a little smaller due to the oxidation of the outer layer of GNPs by a strong acid combination, which can be seen in Figure 4.5(b).

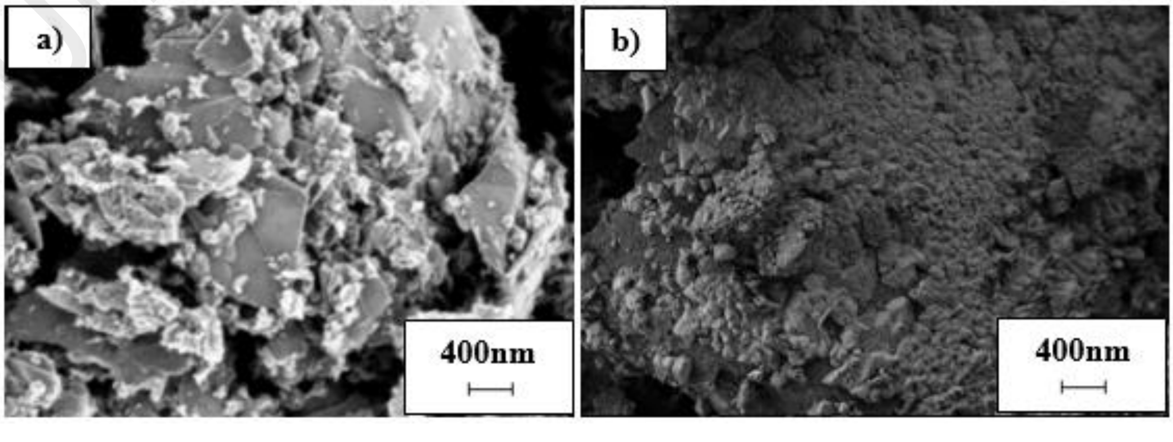

Figure 4.5: FESEM images of a) pristine GNPs and b) functionalized GNPs

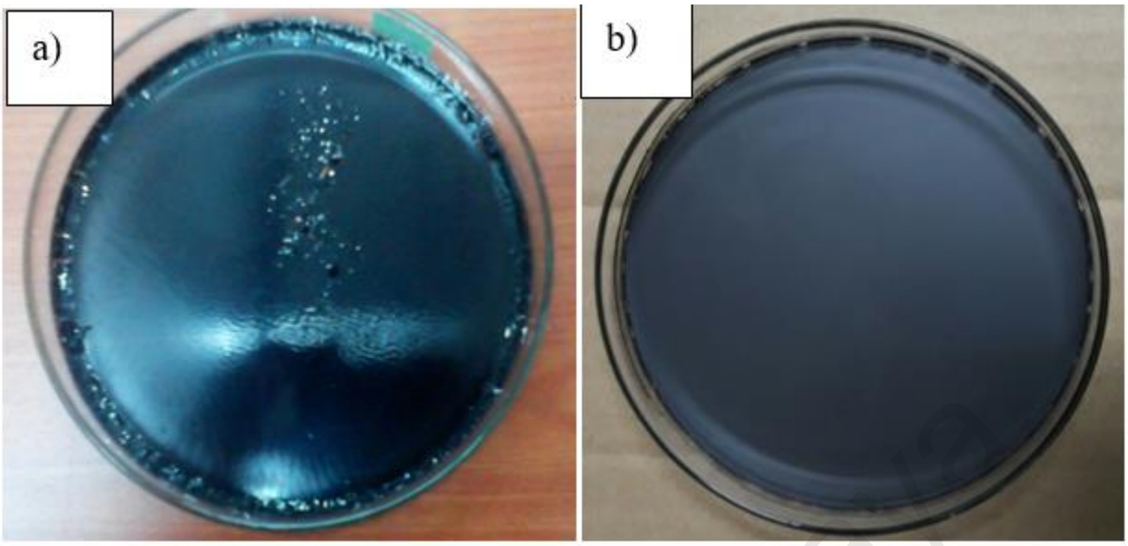

Figure 4.6: Physical appearance of dried (a) functionalized MWCNTs and (b) functionalized GNPs

The dispersion test in aqueous media was also carried out in order to support the evidence of functionalized MWCNTs and GNPs for a clearer comparison before and after chemical treatment process. The functionalized MWCNTs and GNPs in Figure 4.6 in thin-film form were scrapped into powder and then dispersed in distilled water to observe the ability of the modified carbon nanofillers to remain stable in the solution. The photographs were taken for all samples after 24 h, which can be seen in Figures 4.7(a) and (b). It can be observed that the pristine MWCNTs and GNPs samples could not remain stable even within 24 h provided with sediments could be observed at the bottom of the tubes. Meanwhile, functionalized MWCNTS and GNPS samples are able to stand longer with great stability compared to pristine samples, as shown in Figure 4.7.

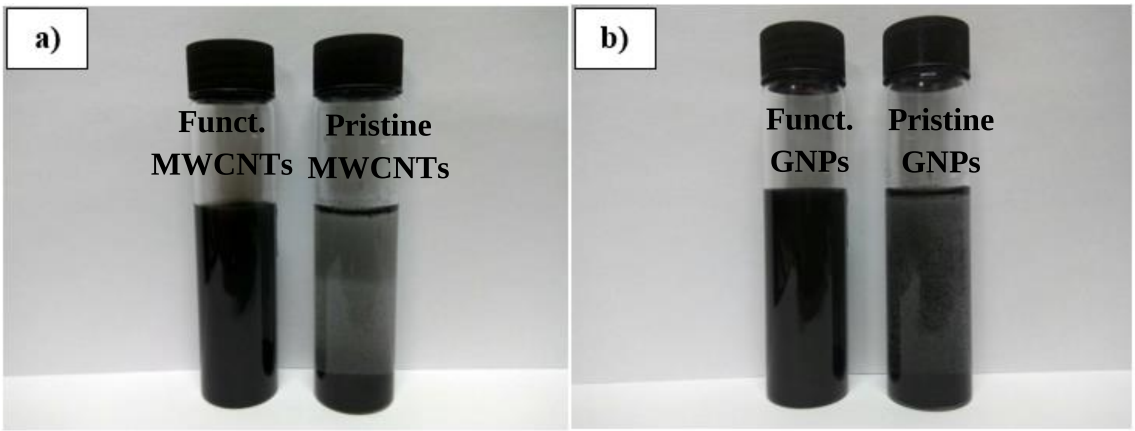

Figure 4.7: Dispersion test of (a) functionalized MWCNTs (left) and pristine MWCNTs (right) and (b) functionalized GNPs (left) and pristine GNPs (right) (Note: All results were taken after 24 h)

4.2.2 FTIR spectroscopy analysis of MWCNT, MWCNTCOOH, GNP, and GNPCOOH powders

FTIR spectroscopy was used to confirm the attachment of -COOH functional group onto the surface of pristine MWCNTs and GNPs after functionalization process. The attachment of the functional group will improve the dispersibility of MWCNTs and GNPs in solvents and aqueous media, particularly water and ethanol. Figure 4.8 shows the FTIR spectra of pristine and functionalized MWCNTs whereas Figure 4.9 shows the FTIR spectra of pristine and functionalized GNPs. It can be observed from the FTIR spectra for MWCNTCOOH and GNPCOOH that there are two distinctive peaks (O–H and C=O) due to the attachment of -COOH functional group onto the surface of MWCNTs and GNPs. A new peak appears at 3436.29 cm^{-1} for MWCNTs after functionalization (Figure 4.8), whereas the peak at 3435.04 cm^{-1} broadens for GNPs after functionalization (Figure 4.9), which may be due to the presence of the hydroxyl group (O–H) stretching from the carboxyl groups (O=C−OH and C−OH) (Amiri et al., 2013; Atieh et al., 2010; Gorji et al., 2015). In addition, the presence of a new peak at 2925.24 cm^{-1} (Atieh et al., 2010) for the functionalized MWCNTs and the presence of a new peak at 2926.57 cm^{-1} (Atieh et al., 2010) and 1383.90 cm^{-1} (Z. Li et al., 2015) for the functionalized GNPs are due to hydroxyl (O–H) stretching. Furthermore, a new peak appears at 1635.10 cm^{-1} (Tan et al., 2015) and 1698.04 cm^{-1} (Gorji et al., 2015) for the functionalized MWCNTs, whereas a new peak appears at 1634.94 cm^{-1} (Solangi et al., 2016) and 1697.71 cm^{-1} (Gorji et al., 2015) for the functionalized GNPs, which are attributed to the stretching mode of carboxylic groups. These results confirm the successful attachment of the carboxylic group (O=C−OH) onto the surface of MWCNTs and GNPs.

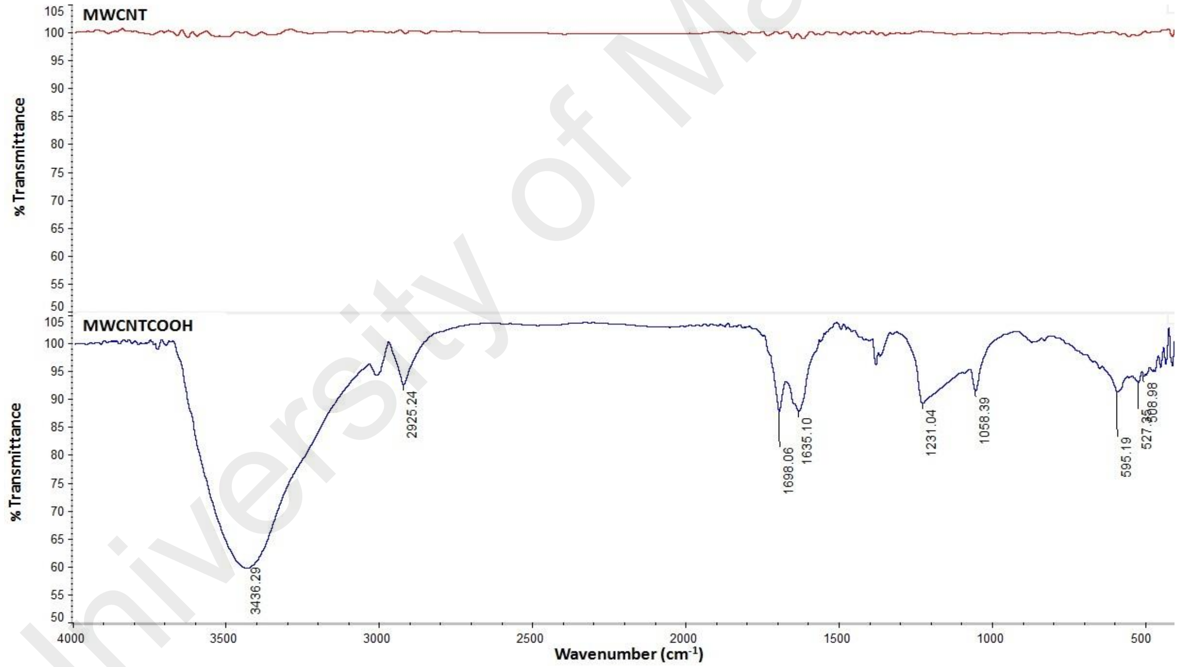

Figure 4.8: FTIR spectra of pristine MWCNTs (MWCNT) and functionalized MWCNTs (MWCNTCOOH)

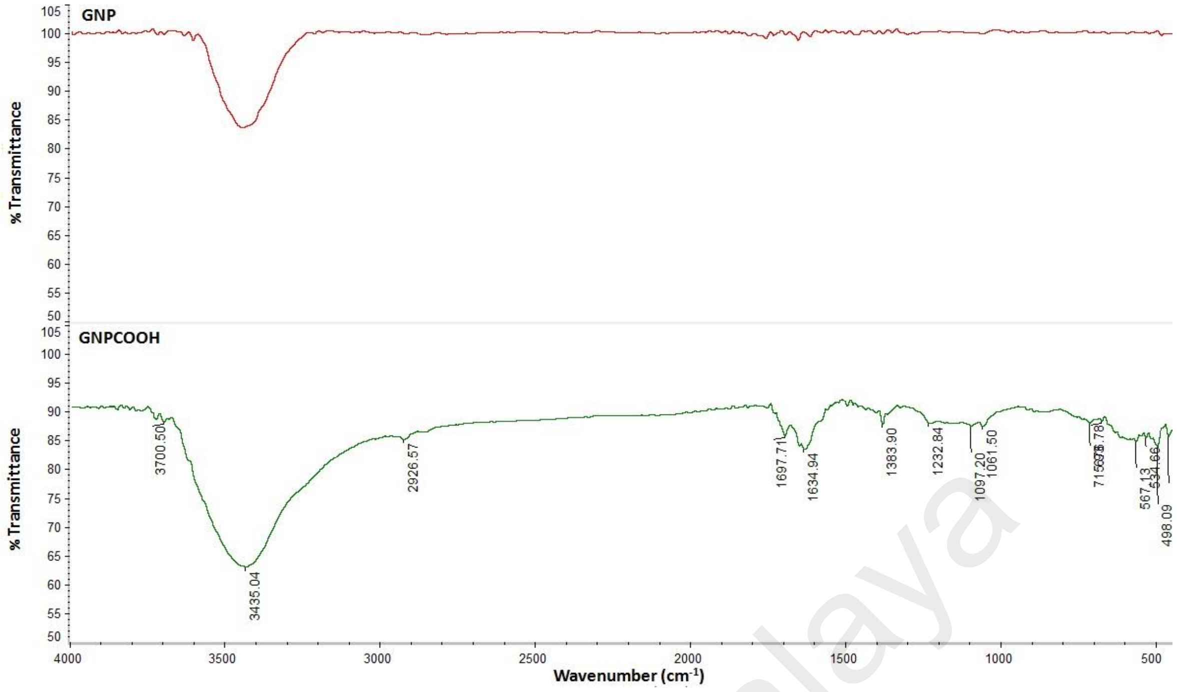

Figure 4.9: FTIR spectra of pristine GNPs (GNP) and functionalized GNPs (GNPCOOH)

4.3 X-Ray diffraction characterization

Figure 4.10 shows the X-ray diffractograms of pure Al sample, Al nanocomposite with 7.5 wt. % MWCNTCOOH and 7.5 wt. % GNPCOOH, and Al nanocomposite with 7.5 wt. % MWCNT and 7.5 wt. % GNP. It can be seen that there are four main peaks at 38.57° (111), 44.82° (200), 65.19° (220), and 78.73° (311) for the pure Al sample, which represent the spectrum of Al. In contrast, a new peak is present at 26.6653° for both Al nanocomposites with pristine and functionalized carbon nanofillers. This peak indicates the presence of carbon, which is due to the addition of pristine and functionalized MWCNTs and GNPs (Bartolucci et al., 2011; Latief & Sherif, 2012). It can be observed that there is no visible reflection peak from Al_4C_3 for both nanocomposites. The peaks of Al_4C_3 (which are normally present at 31.8°, 55.0°, and 72.5°) are absent from the X-ray diffractograms (Bartolucci et al., 2011), indicating that there is no appreciable reaction between carbon nanofillers and Al during the blending and sintering processes. It is also evident that there are no significant changes in the intensity between Al nanocomposites with pristine and functionalized carbon nanofillers, which indicates that the chemical treatment does not affect the original structure and integrity of pristine GNPs and MWCNTs.

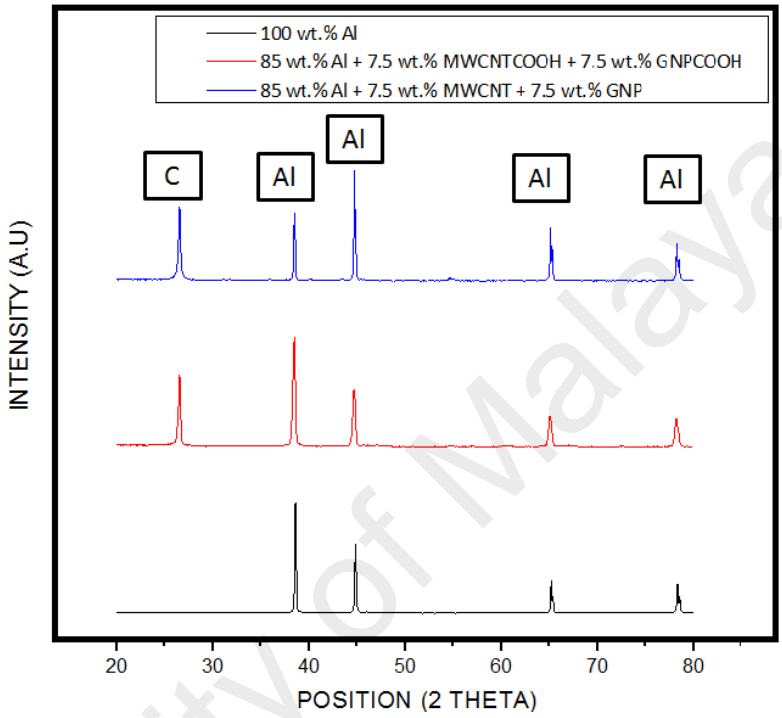

Figure 4.10: XRD patterns (diffractograms) of pure Al sample, Al nanocomposite with 7.5 wt. % MWCNTCOOH and 7.5 wt. % GNPCOOH, and Al nanocomposite with 7.5 wt. % MWCNT and 7.5 wt. % GNP (Note that a.u. represents arbitrary units)

4.4 Surface morphologies of Al nanocomposites

4.4.1 Pure Al

The pure Al sample (100 wt. % Al) was fabricated as a basis for comparison with Al nanocomposites containing different concentrations of carbon nanofillers. Figure 4.11 shows the FESEM image of the pure Al sample that has been compacted and sintered into a pellet. It can be observed that there are micropores (indicated by the black holes) in between Al particles (indicated by the white color) due to the conventional sintering process adopted in this study. However, micropores could serve as light-trapping sites, which enhance light absorption. The presence of micropores also allows carbon nanofillers to occupy these voids. The addition of carbon nanofillers such as MWCNTs and GNPs will further enhance the light absorption capability of Al nanocomposite.

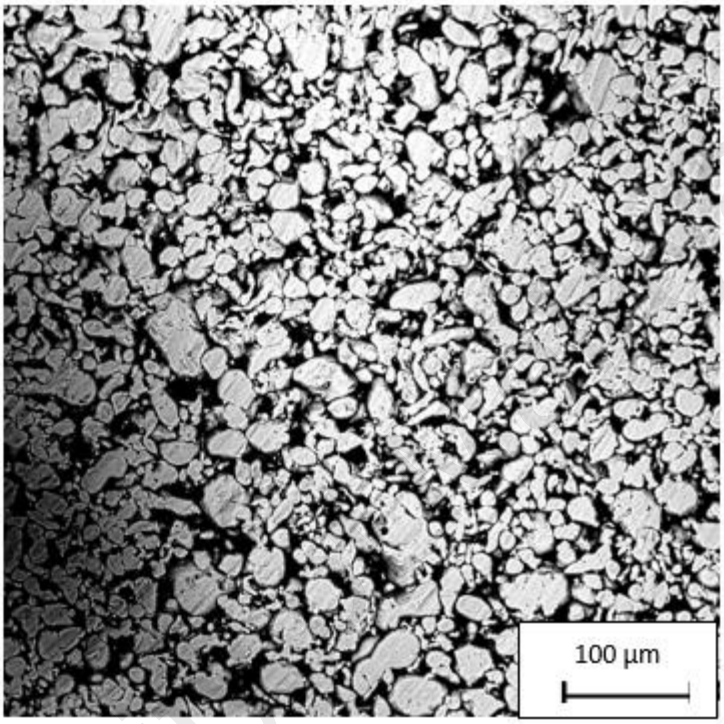

Figure 4.11: FESEM image of pure Al sample (100 wt. % Al)

4.4.2 Al-MWCNT nanocomposites

Figure 4.12 presents the surface morphologies of Al nanocomposites with different concentrations of pristine MWCNT. It can be observed from Figures 4.12(a) to (c) that pristine MWCNTs are unable to disperse homogenously in each Al nanocomposite with 5.0, 10.0, and 15.0 wt. % MWCNT. It is evident from the images that not all carbon nanofillers (observed as black regions) dispersed and embedded throughout Al surface. A clear image of Al (as indicated by the white color) suggests that pristine MWCNTs does not mix well with Al nanocomposites. Previous studies also obtained similar findings, where it is hard to achieve a uniform dispersion of MWCNT in various metal matrices (Agarwal et al., 2016; Poirier et al., 2009) since MWCNT tends to self-assemble into clusters even though after various attempts made to disperse them (Islam et al., 2003; X. Wang et al., 2004).

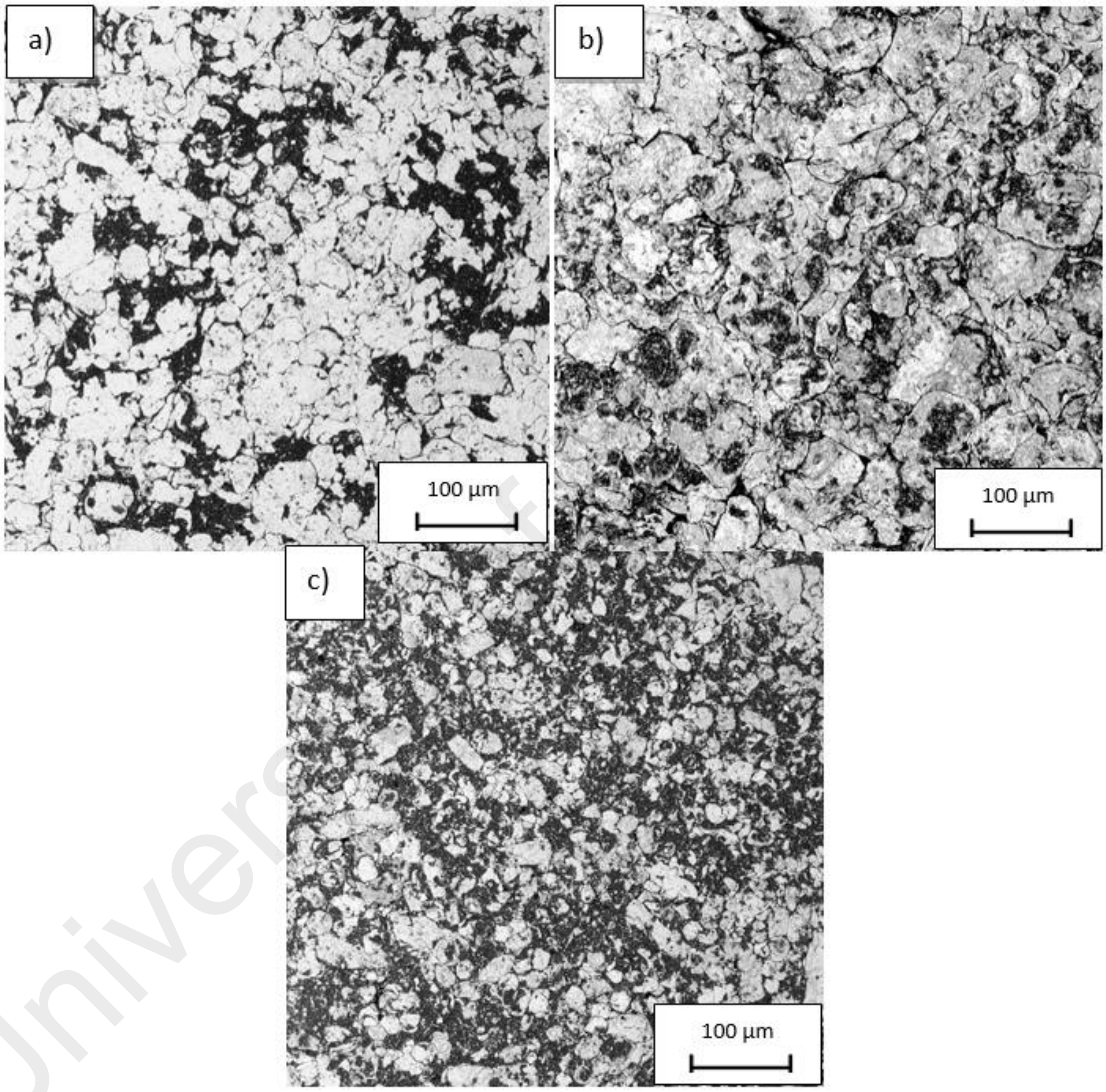

Figure 4.12: SEM images of Al-pristine MWCNT nanocomposites with the addition of a) 5, b) 10, and c) 15 wt. % nanofillers

4.4.3 Al-GNP nanocomposites

Figure 4.13 shows the surface morphologies of Al nanocomposites with different concentrations of pristine GNP. The observation throughout Figures 4.13(a) to (c) suggest that pristine GNPs are also unable to disperse homogenously in Al nanocomposites with 5.0, 10.0 and 15.0 wt. % GNP. However, there is a slight improvement for carbon nanofiller dispersion as the Al surface (as indicated by the white color) is reduced and replaced by black pristine GNPs nanofiller. Previous studies also observed a similar observation that GNPs dispersed much easier compared to MWCNTs due to the open surface area structure (H. G. P. Kumar & Xavior, 2014) (Rashad, Pan, Tang, et al., 2015).

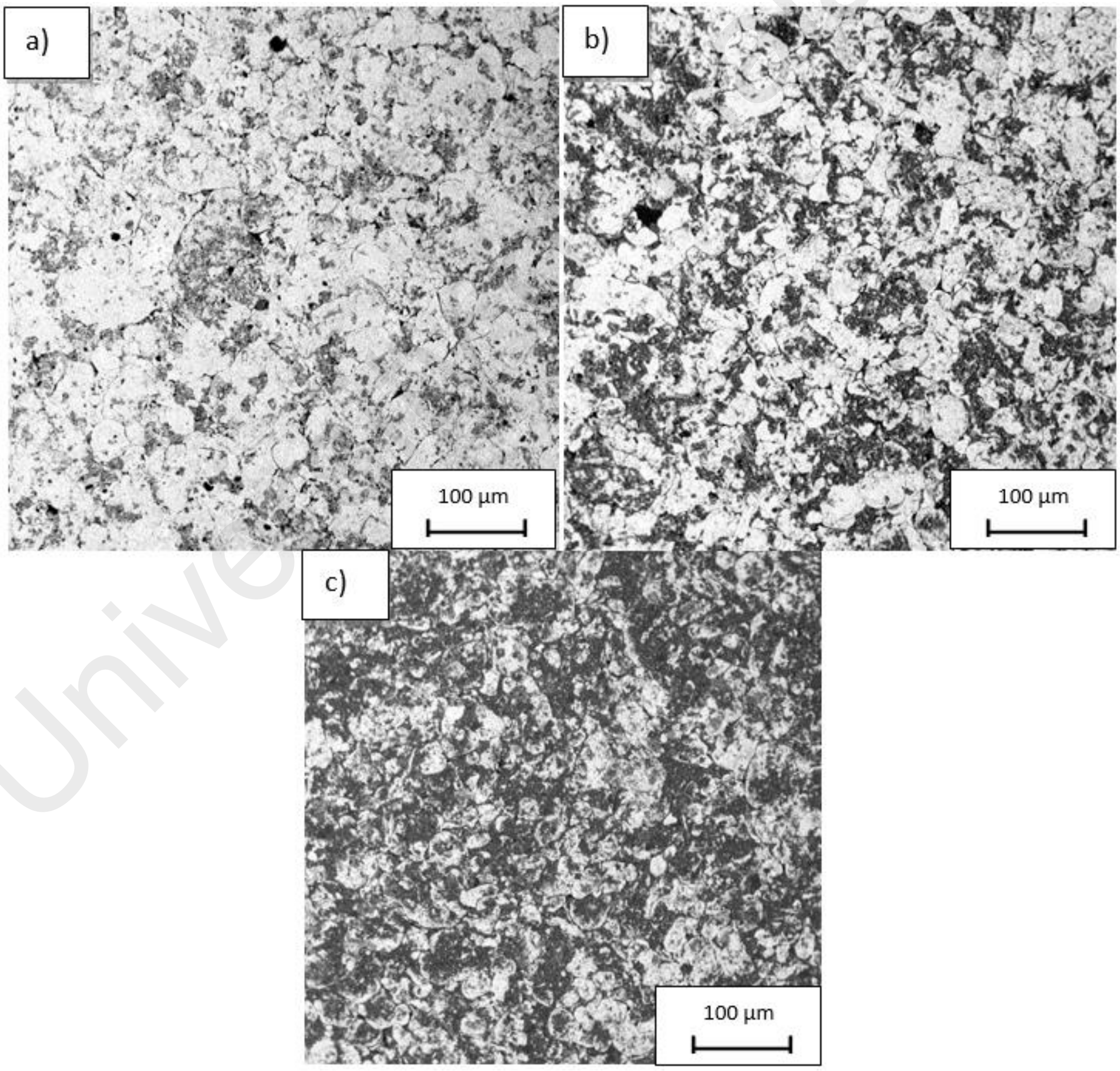

Figure 4.13: SEM images of Al-pristine GNP nanocomposites with the addition of a) 5, b) 10, and c) 15 wt. % nanofillers

4.4.4 Al-MWCNT-GNP nanocomposites

Figure 4.14 presents the surface morphologies of Al nanocomposites with different concentrations of pristine MWCNTs and pristine GNPs. It can be observed from Figures 4.14(a) and (b) that pristine MWCNTs and GNPs are dispersed homogeneously in Al nanocomposite with 2.5 wt. % MWCNT and 2.5 wt. % GNP, and Al nanocomposite with 5.0 wt. % MWCNT and 5.0 wt. % GNP. It is evident from the images that the micropores are completely filled with carbon nanofillers (as indicated by the black particles) whereas others are embedded within the Al surface. It is apparent from Figure 4.14(c) that that there is agglomeration of carbon nanofillers in Al nanocomposite with 7.5 wt. % MWCNT and 7.5 wt. % GNP. This indicates that excessive amounts of carbon nanofillers result in the stacking of nanofillers, culminating in agglomeration. Interestingly, the dispersion of carbon nanofillers is better in Al nanocomposite with 5 wt. % MWCNT and 5 wt. % GNP compared to other Al nanocomposite samples.

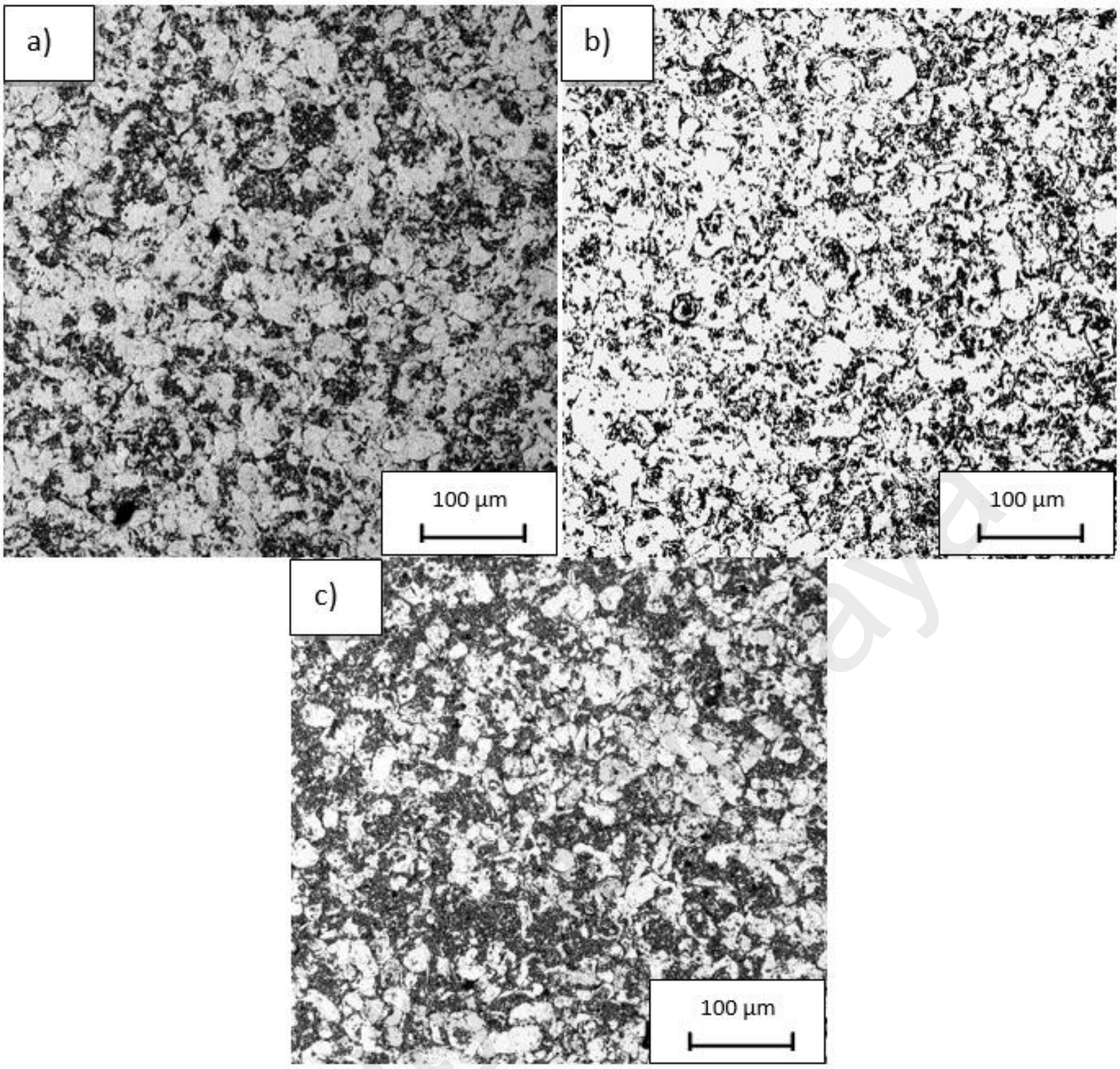

Figure 4.14: FESEM images of Al nanocomposites with (a) 2.5 wt. % MWCNT and 2.5 wt. % GNP, (b) 5 wt. % MWCNT and 5 wt. % GNP, and (c) 7.5 wt. % MWCNT and 7.5 wt. % GNP

4.4.5 Al-MWCNTCOOH-GNPCOOH nanocomposites

Figure 4.15 shows the surface morphologies of Al nanocomposites with different concentrations of functionalized MWCNTs and functionalized GNPs. It can be observed that MWCNTCOOH and GNPCOOH are dispersed homogeneously in all of the samples fabricated in this study. In general, functionalized carbon nanofillers have better dispersibility in the Al matrix compared to pristine carbon nanofillers. This effect is even more apparent for Al nanocomposite with 7.5 wt. % MWCNT and 7.5 wt. % GNP (Figure 4.15(c)) and Al nanocomposite with 7.5 wt. % MWCNTCOOH and 7.5 wt. % GNPCOOH (Figure 4.15(c)). The results indicate that the -COOH functional group improves the dispersibility of MWCNTs and GNPs in the Al matrix. In this study, it is found that the optimum concentration of carbon nanofillers is 2.5 wt. % MWCNTCOOH and 2.5 wt. % GNPCOOH since it is evident from the surface morphology of this sample that the functionalized carbon nanofillers (indicated by the black spots) are dispersed uniformly throughout the Al surface (indicated by the white areas). It is expected that the homogeneity of the mixture could enhance the optical properties on both lower (0.2 µm-2.5 µm) and higher wavelength region (2.5 µm-14 µm) which will increase the spectral selectivity ratio. The optical properties will be discussed in the next section.

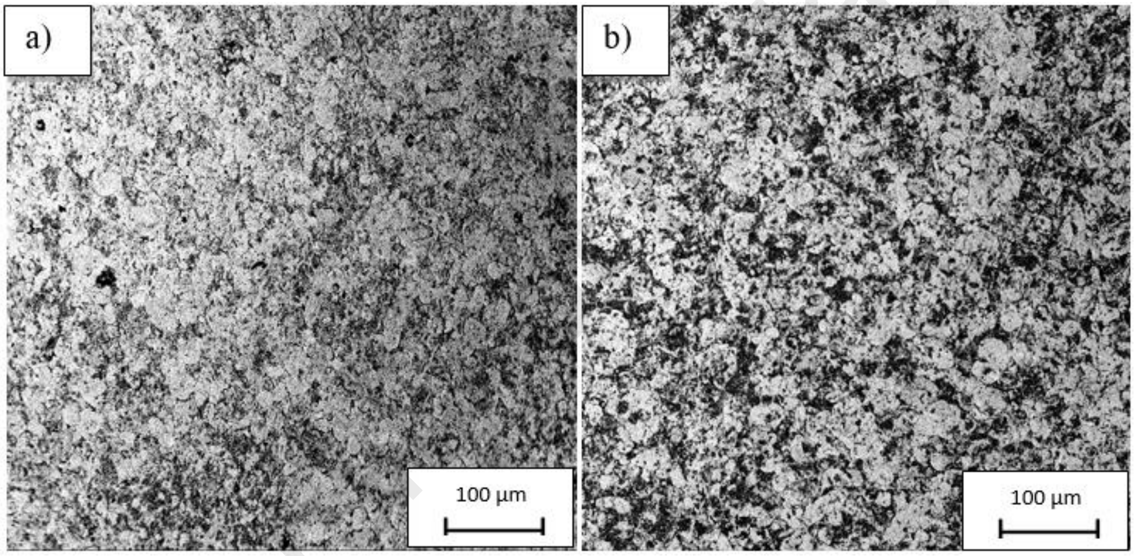

Figure 4.15: FESEM images of Al nanocomposites with (a) 2.5 wt. % MWCNTCOOH and 2.5 wt. % GNPCOOH, (b) 5 wt. % MWCNTCOOH and 5 wt. % GNPCOOH, and (c) 7.5 wt. % MWCNTCOOH and 7.5 wt. % GNPCOOH

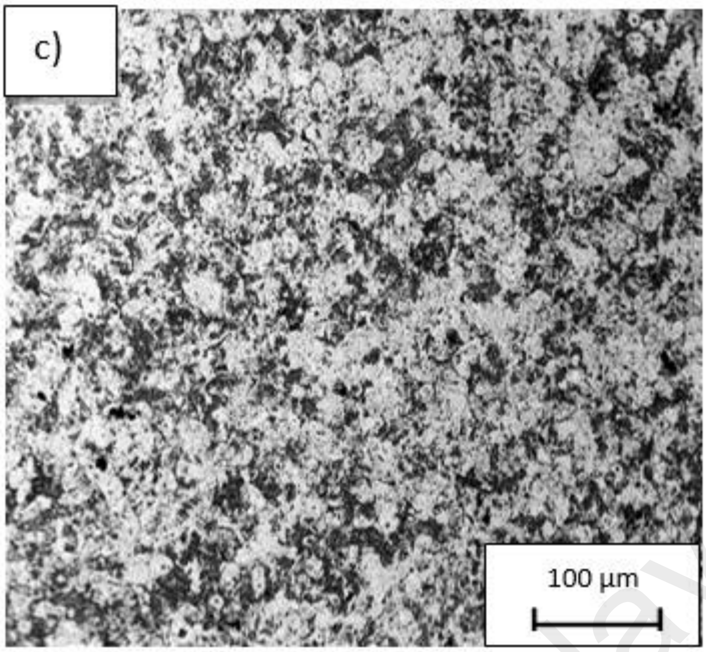

Figure 4.15: FESEM images of Al nanocomposites with (a) 2.5 wt. % MWCNTCOOH and 2.5 wt. % GNPCOOH, (b) 5 wt. % MWCNTCOOH and 5 wt. % GNPCOOH, and (c) 7.5 wt. % MWCNTCOOH and 7.5 wt. % GNPCOOH (Cont.)

4.5 Vickers microhardness analysis

Figure 4.16 shows the variation of Vickers hardness values of Al with pristine and functionalized MWCNT-GNP nanocomposites with varying amounts of weight percentage of nanofillers. It is important to point out that Al nanocomposites with the addition of 10 wt. % functionalized MWCNT and GNP nanocomposites (Al-MWCNTCOOH-GNPCOOH nanocomposites) possess the highest microhardness value (44.9 Hv) whereas Al nanocomposites with the addition of 5 wt. % pristine MWCNT nanofiller (AL-MWCNT nanocomposites) secures the lowest spot in terms of microhardness value (26.7 Hv).

Microhardness values are influenced by the distribution of nanofillers, which in this research can be divided into two: pristine MWCNT and/or GNP (denoted as MWCNT and/or GNP) and functionalized MWCNT and/or GNP (denoted as MWCNTCOOH and/or GNPCOOH). SEM images in Figures 4.15(a) and 4.12(a) show the evidence of how hardness value is improved due to the incorporation of effective and ineffective nanofiller distribution. The use of suitable nanofillers as shown in Figure 4.15(a), i.e., functionalized MWCNT and GNP (MWCNTCOOH and GNPCOOH) nanofillers can spread uniformly throughout Al nanocomposites, which can increase the microhardness value of Al nanocomposites. The easier way to evaluate the effective distribution of nanofillers on the surface of Al nanocomposites is through the uniform spread of nanofillers denoted by tiny black color spots.

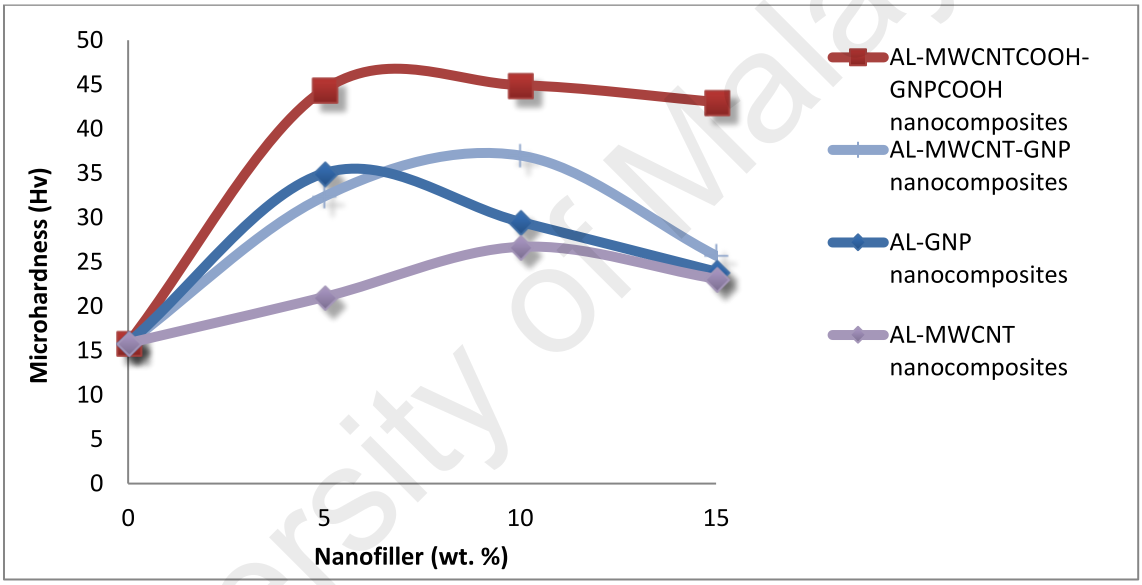

Figure 4.16: The variation of Vickers hardness values of Al with pristine and functionalized MWCNTs-GNPs nanocomposites with varying amounts of weight percentage of nanofillers

Another factor that can affect the microhardness values is the amount of nanofillers (wt. %) introduced to Al nanocomposites. For example, Al nanocomposites with the addition of 5 wt. % GNP nanofiller outperforms Al nanocomposites with the addition of 10 wt. % GNP nanofiller. SEM images in Figures 4.13 (a) and (b) show that the addition of excessive amounts of pristine GNP nanofiller caused pristine GNP nanofiller to agglomerate and stack onto each other. As a result, the interfacial strength between GNP nanofillers and Al matrices becomes weaker and the hardness of Al-GNP nanocomposites is reduced.

A considerable enhancement of hardness at a specific weight percentage (wt. %) of nanofillers can be observed by the addition of pristine MWCNT and GNP in Al nanocomposites (Al-MWCNT-GNP nanocomposites). The hardness value of Al-MWCNT-GNP increases linearly up to 10 wt. %. However, the hardness value of Al-MWCNT-GNP nanocomposites eventually drops by 2/3 as the addition of pristine MWCNTs and GNPs increased to 15 wt. %.

Opposite findings were recorded for the addition of MWCNTCOOH and GNPCOOH in Al nanocomposites. The hardness value of Al nanocomposites with the addition of 5 wt. % MWCNTCOOH and GNPCOOH increases 1/3 more than Al nanocomposites with the addition of 5 wt. % pristine MWCNTs and GNPs. Besides, the hardness value of Al nanocomposites with the addition of 15 wt. % MWCNTCOOH and GNPCOOH drops slightly compared to Al nanocomposites with the addition of similar wt. % of MWCNT and GNP, which shows a significant drop in the hardness value. Thus, based on this result, it can be shown that the mechanical properties of Al nanocomposites are improved with the addition of functionalized MWCNTs and GNPs nanofillers. Al nanocomposites with functionalized MWCNTs and GNPs are homogeneously distributed even at 15 wt. % whereas pristine MWCNTs and GNPs with a similar weight percentage already shows a small sign of agglomeration formation.

In general, the optimum microhardness values obtained from this research are low compared to other research works. Yan *et al*. reported that Al nanocomposites with 0.4 wt. % CNTs could reach up to 79 Hv by milling and hot extrusion process at 390 °C, with an extrusion ratio of 40:1 (Yan & Qiu, 2016). Latief *et al*. stated that Al nanocomposites added with 5 wt. % xGnP could reach 67 Hv by producing the sample through green compaction at 500 Mpa and sintered at 600 °C for 5 h (Latief & Sherif, 2012). The differences between this study and other works are the presence of porosity from the lower pressure applied for cold compaction process, which is 300 MPa. Moreover, compaction at lower pressure can be done using a hand pressing machine, which is simple and has low fabrication cost. The presence of porosity is expected to improve sunlight absorption through light trapping and multiple reflection effects. As a result, a better optical performance material can be produced by taking advantage from the presence of the porosity on the surface of Al nanocomposites itself which is expected to increase light trapping capability. Even though the performance of Al nanocomposites produced in this study is still acceptable to be experimentally tested and analyzed, it still allows much room for future improvement in term of post treatment such as Hot Isostatic Pressing which will enhance the strength of the material itself.

4.6 Optical property characterization

4.6.1 UV-Vis-NIR spectroscopy analysis of pure Al sample, Al-MWCNT nanocomposites, Al-GNP nanocomposites, Al-MWCNT-GNP nanocomposites, and Al-MWCNTCOOH-GNPCOOH nanocomposites

Light reflectance (*R*) within a wavelength range of 200–2,500 nm was measured using a UV-Vis-NIR spectrophotometer. Figures 4.17, 4.18, 4.19, and 4.20 show UV-Vis-NIR reflectance spectra of Al nanocomposites with different concentrations of pristine and/or functionalized carbon nanofillers. In general, there is a decrease in the reflectance with an increase in the concentration of carbon nanofillers. The reason that attribute to the decrease in the light reflectance may come from the types of nanofillers used and the dispersion of nanofillers itself on the surface of the samples. Black color that coming from carbon nanofiller worked well as light trapping media (Mizuno et al., 2009). Whenever there is an increase in nanofiller amount, the reflectance value will be lower for UV-VIS wavelength region. Based on the observation from both FESEM results (Figures 4.12 to 4.15) and UV-VIS results (Figures 4.17 to 4.20), it can also be observed that the reflectance is less than 40% for Al-GNP, Al-MWCNT-GNP, and Al-MWCNTCOOH-GNPCOOH nanocomposites, which is lower compared to the pure Al sample. This shows that the presence of suitable carbon nanofillers improves the light absorption capability of Al nanocomposites (Guler et al., 2015; Olek, 2006). However, Al-MWCNT nanocomposites failed to achieve the desired reflectance as obtained by the other three combinations of nanofillers in this study. Higher reflectance recorded in Figure 4.20 might be influenced by the non-homogeneous dispersion of MWCNT nanofillers in Al nanocomposites as MWCNT is known for its difficulties in dispersion and fabrication of metal composites (Bartolucci et al., 2011). The evidence of non-homogeneous dispersion of MWCNT nanofillers can be seen through the SEM image in Figure 4.12.

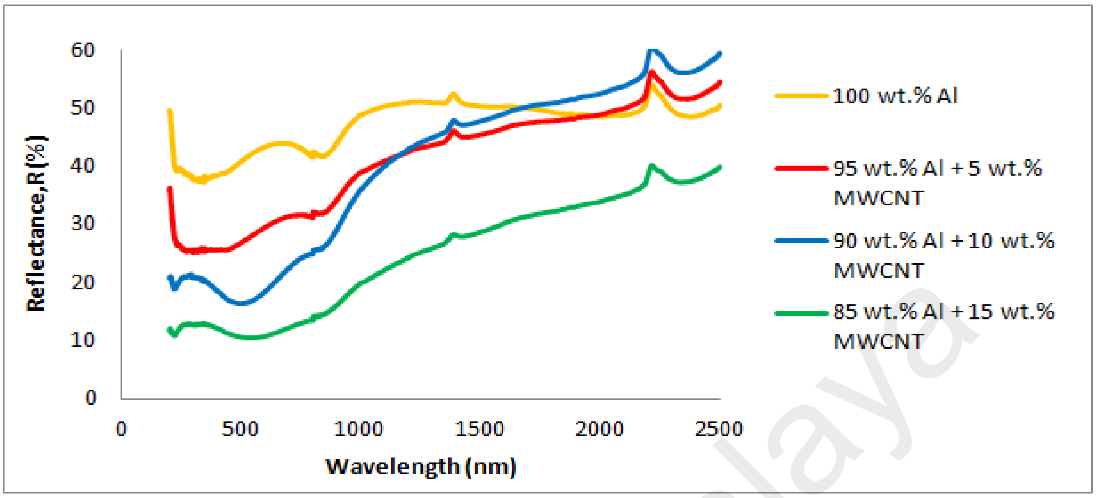

Figure 4.17: UV-Vis-NIR reflectance spectra of pure Al sample and Al-MWCNT nanocomposites within a wavelength range of 200–2,500 nm

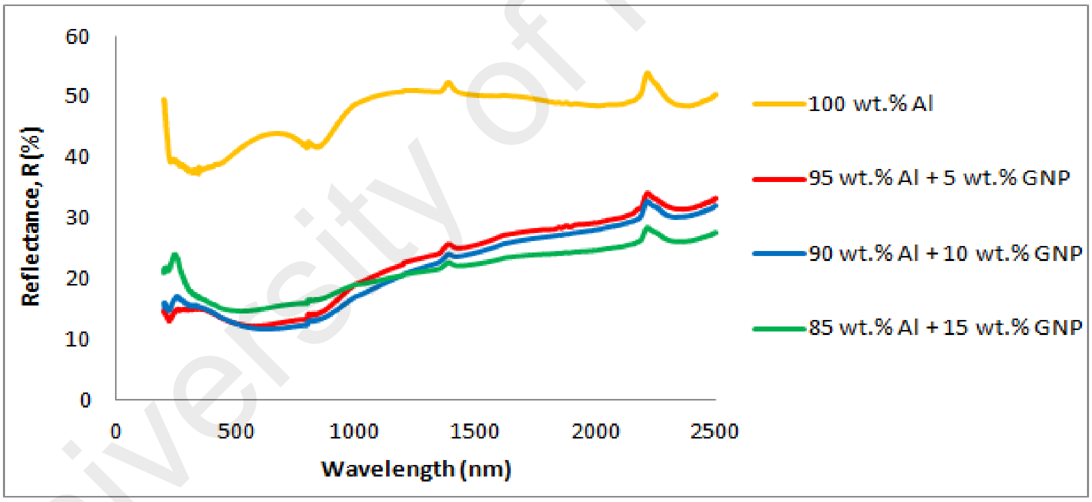

Figure 4.18: UV-Vis-NIR reflectance spectra of pure Al sample and Al-GNP nanocomposites within a wavelength range of 200–2,500 nm

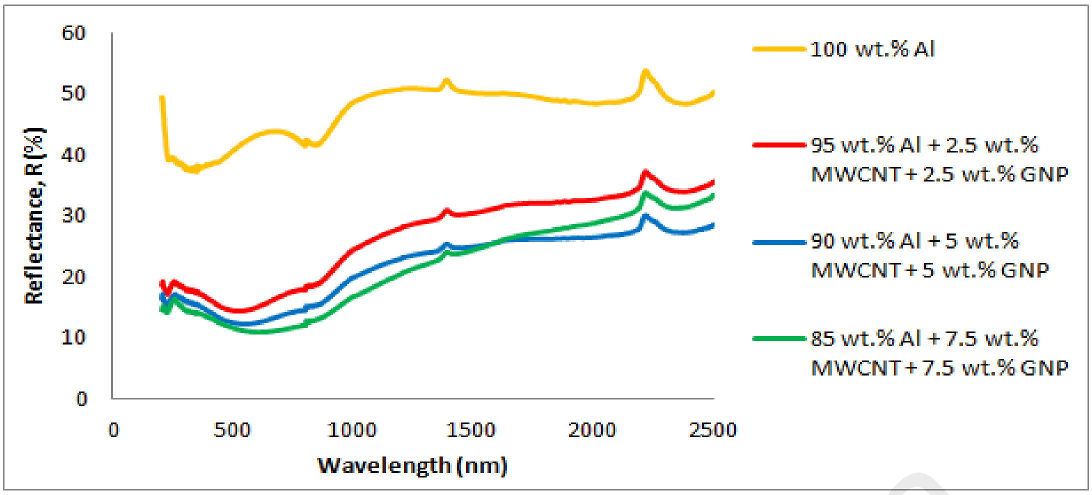

Figure 4.19: UV-Vis-NIR reflectance spectra of pure Al sample and Al-MWCNT-GNP nanocomposites within a wavelength range of 200–2,500 nm

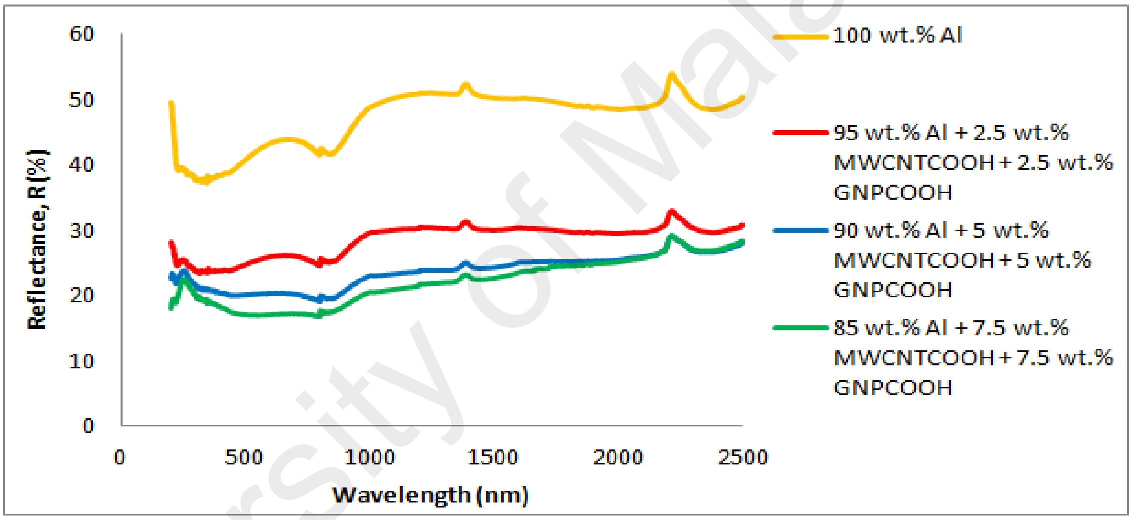

Figure 4.20: UV-Vis-NIR reflectance spectra of pure Al sample and Al-MWCNTCOOH-GNPCOOH nanocomposites within a wavelength range of 200–2,500 nm

It can be observed from Figures 4.18 and 4.19 that the reflectance is low (< 25%) within a wavelength range of 200–1,000 nm and the reflectance increase at higher wavelengths for both Al-MWCNT-GNP and Al-GNP nanocomposites, which is undesirable. However, the reflectance is reduced at higher wavelengths for Al-MWCNTCOOH-GNPCOOH nanocomposites (Figure 4.20), which indicates the advantage of incorporating functionalized carbon nanofillers into the Al matrix. The lower reflectance may be due to the more uniform dispersion of functionalized carbon nanofillers in the Al matrix, as evidenced from the FESEM images (Figure 4.15). The UV-Vis-NIR reflectance values obtained in this study are superior to those of Sani *et al*.(Elisa Sani, Mercatelli, & Meucci, 2016), who recorded a minimum reflectance of 30% at 200 nm for the hafnium carbide (HfC) sample with 20 wt. % molybdenum disilicide ($MoSi_2$) sintered using hot pressing method. The reflectance increased dramatically to 64% at 2,500 nm. The results are similar for the zirconium carbide (ZrC) sample with 20 wt. % $MoSi_2$, which shows 39% reflectance at 200 nm, and the reflectance increased to 44% at 1,000 nm and reached a maximum value of 66% at 2,500 nm (Elisa Sani, Mercatelli, & Meucci, 2016).

In order to examine the effect of attaching the -COOH functional group onto the surface of MWCNTs and GNPs, the UV-Vis-NIR reflectance spectra were grouped based on the concentration of carbon nanofillers in Al nanocomposites, as shown in Figures 4.21, 4.22, and 4.23. It can be seen that there are two distinct wavelength ranges in the UV-Vis-NIR reflectance spectra: 200–1,400 nm and 1,400–2,500 nm. In general, the reflectance is higher for Al-MWCNTCOOH-GNPCOOH nanocomposites compared to Al-MWCNT-GNP and Al-GNP nanocomposites within a wavelength range of 200–1,400 nm. Reflectance decreases with an increase in the concentration of functionalized carbon nanofillers. However, the reflectance is lower for Al-MWCNTCOOH-GNPCOOH nanocomposites compared to Al-MWCNT-GNP and Al-GNP nanocomposites within a wavelength range of 1,400-2,500 nm. In this wavelength range, the reflectance also decreases with an increase in the concentration of functionalized carbon nanofillers. It can be observed indirectly that light reflectance values obtained is related with the dipersion of nanofillers. It can be seen from both FESEM results (Figures 4.12 to 4.15) and UV-VIS results (Figures 4.21 to 4.23), lower reflectance results can be obtained if the dispersion of nanofiller is uniform. Uniform dispersion of carbon nanofillers may help in terms of light trapping capability which resulted to lower reflectance. Based on the results, it can be deduced that the -COOH functional group plays a significant role in reducing the light reflectance of Al nanocomposites, which is attributed to the dispersion of carbon nanofillers and light trapping capability inside the UV-VIS wavelength region.

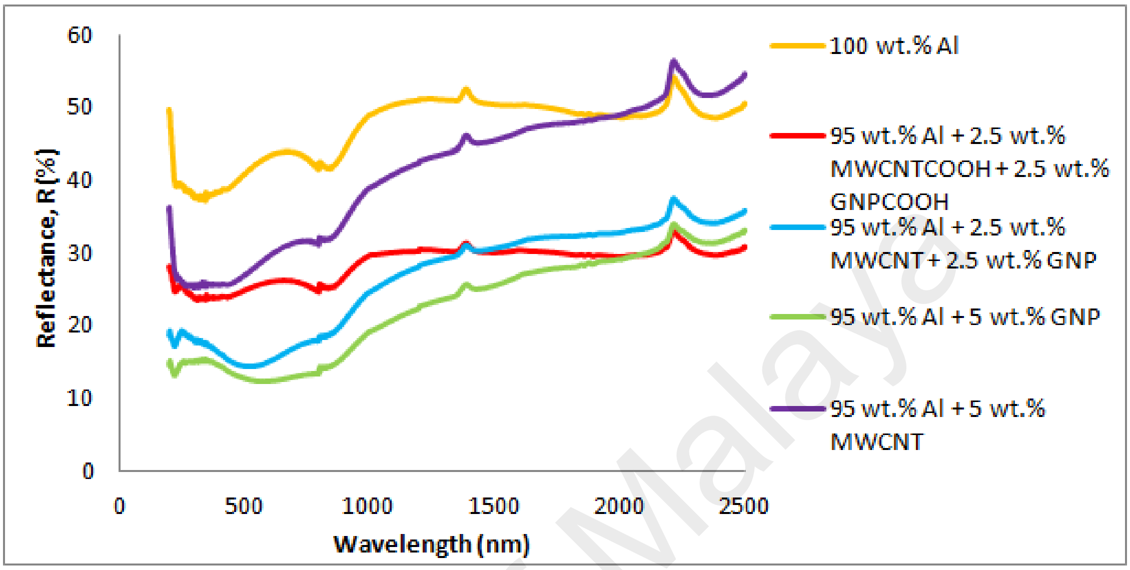

Figure 4.21: UV-Vis-NIR reflectance spectra of pure Al sample and Al nanocomposites with 5 wt. % of pristine and functionalized carbon nanofillers (MWCNTs or/and GNPs)

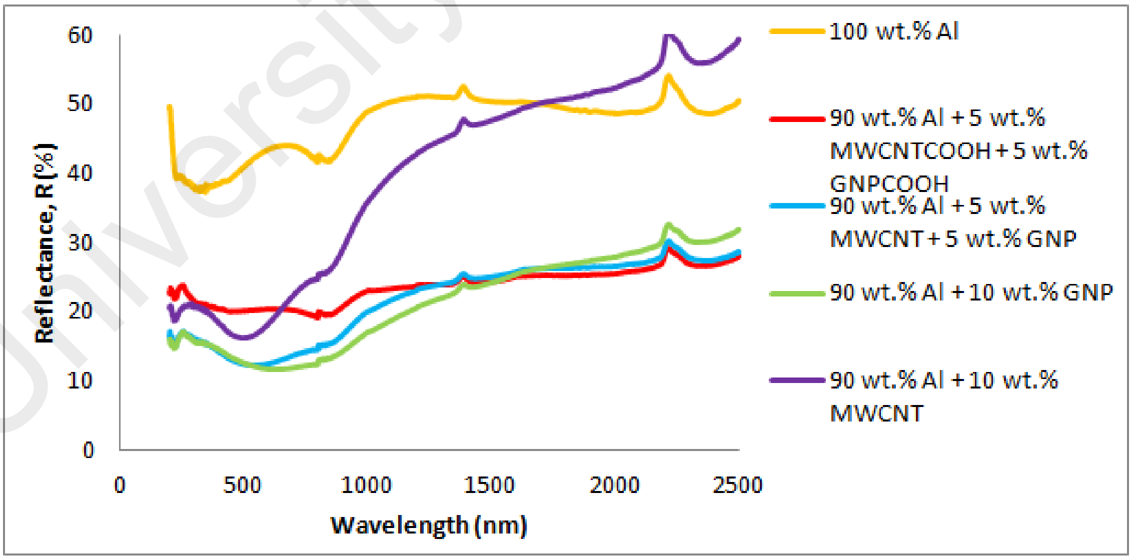

Figure 4.22: UV-Vis-NIR reflectance spectra of pure Al sample and Al nanocomposites with 10 wt. % of pristine and functionalized carbon nanofillers (MWCNTs or/and GNPs)

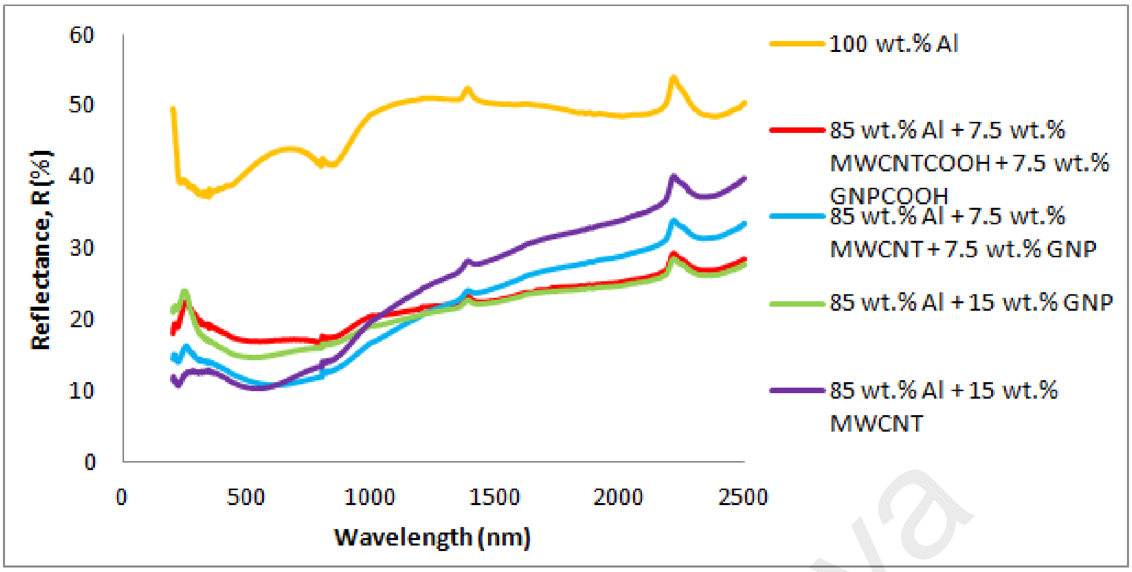

Figure 4.23: UV-Vis-NIR reflectance spectra of pure Al sample and Al nanocomposites with 15 wt. % of pristine and functionalized carbon nanofillers (MWCNTs or/and GNPs)

4.6.2 FTIR spectroscopy analysis of pure Al sample, Al-MWCNT nanocomposites, Al-GNP nanocomposites, Al-MWCNT-GNP nanocomposites, and Al-MWCNTCOOH-GNPCOOH nanocomposites

FTIR spectroscopy in this section was carried out with the aim of measuring the light reflectance of pure Al sample, Al-MWCNT nanocomposites, Al-GNP nanocomposites, Al-MWCNT-GNP nanocomposites, and Al-MWCNTCOOH-GNPCOOH nanocomposites within a wavelength range of 3,000–14,000 nm. The results obtained were converted into emittance by using the following formula:

$$\varepsilon = 1 - R - T \qquad \text{Eq. (4.1)}$$

As the samples are opaque (no light passed through samples), the transmittance is set to 0, which means that emittance can be obtained by just deducting the light reflectance values obtained from the FTIR spectrometer. The emittance values obtained are then used to classify the spectral selectivity properties, which are discussed in the next section.

The results for the light reflectance of pure Al sample, Al-MWCNT nanocomposites, Al-GNP nanocomposites, Al-MWCNT-GNP nanocomposites, and Al-MWCNTCOOH-GNPCOOH nanocomposites within a wavelength range of 3,000–14,000 nm are shown in Figures 4.24, 4.25, 4.26, and 4.27, respectively. It can be seen from Figure 4.26 that Al nanocomposite with 2.5 wt. % MWCNT and 2.5 wt. % GNP has higher reflectance compared to the pure Al sample. A similar pattern of reflectance was recorded for Al nanocomposite with 5 wt. % GNP (Figure 4.25). The reflectance decreases with an increase in the concentration of pristine carbon nanofillers in the Al matrix. In contrast, all Al-MWCNTCOOH-GNPCOOH nanocomposites have higher reflectance compared to the pure Al sample, as shown in Figure 4.27. The reflectance decreases with an increase in the concentration of functionalized carbon nanofillers; however, the reflectance is still higher for Al-MWCNTCOOH-GNPCOOH nanocomposites in the mid-infrared (MIR) and far-infrared (FIR) regions compared to the pure Al sample. Meanwhile, all Al-MWCNT nanocomposites recorded lower reflectance than the pure Al sample (Figure 4.24).

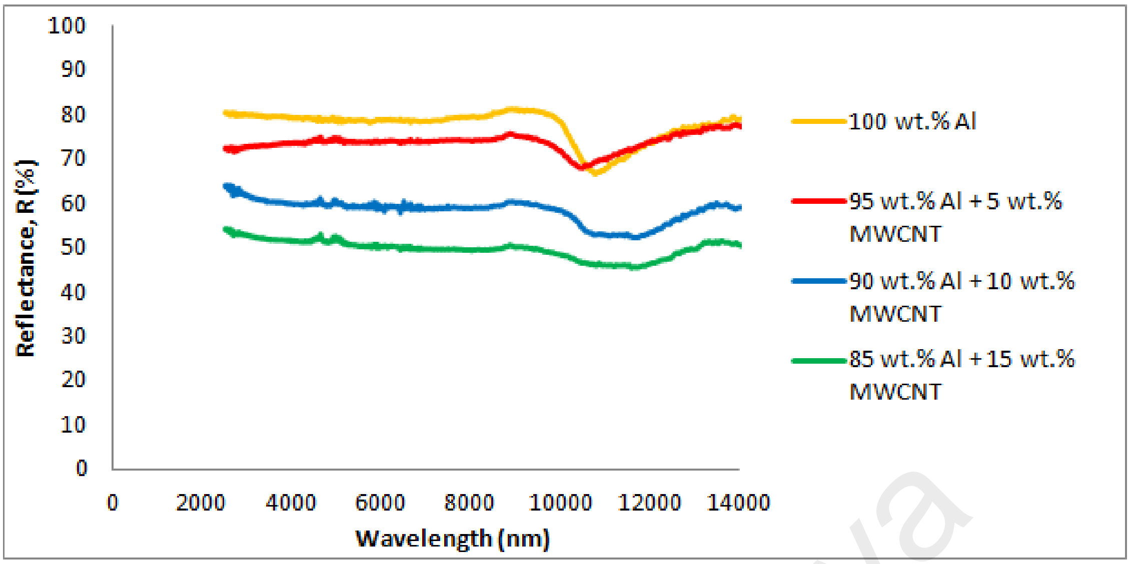

Figure 4.24: FTIR reflectance spectra of pure Al sample and Al-MWCNT nanocomposites within a wavelength range of 3,000–14,000 nm

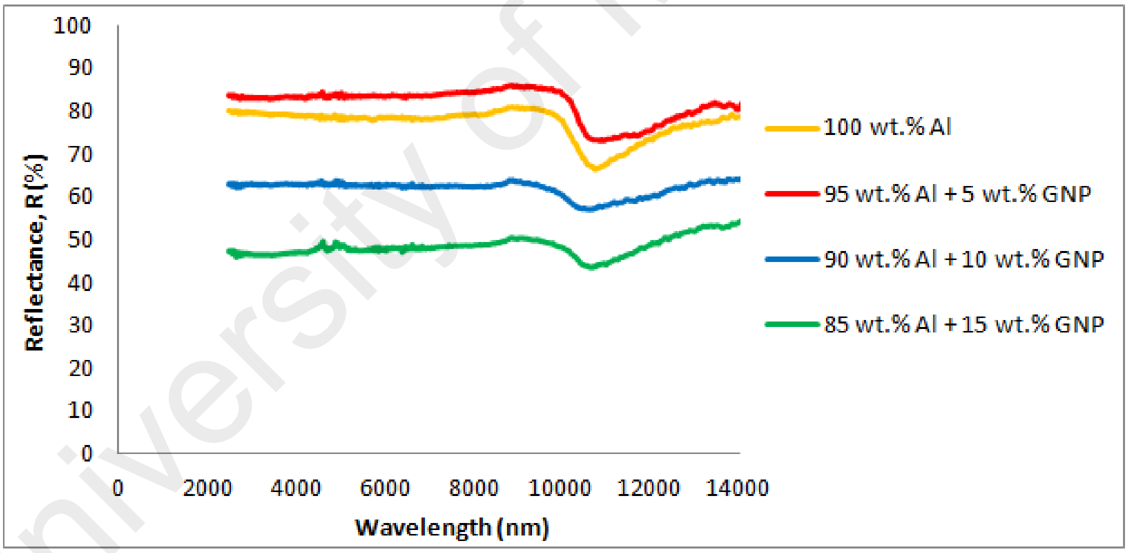

Figure 4.25: FTIR reflectance spectra of pure Al sample and Al-GNP nanocomposites within a wavelength range of 3,000-14,000 nm

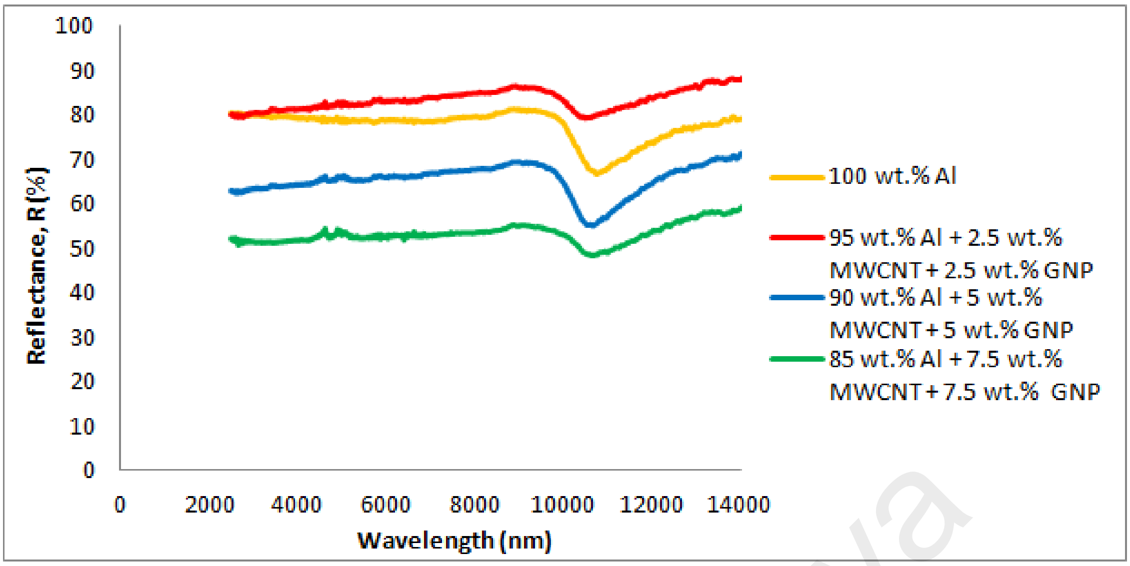

Figure 4.26: FTIR reflectance spectra of pure Al sample and Al-MWCNT-GNP nanocomposites within a wavelength range of 3,000–14,000 nm

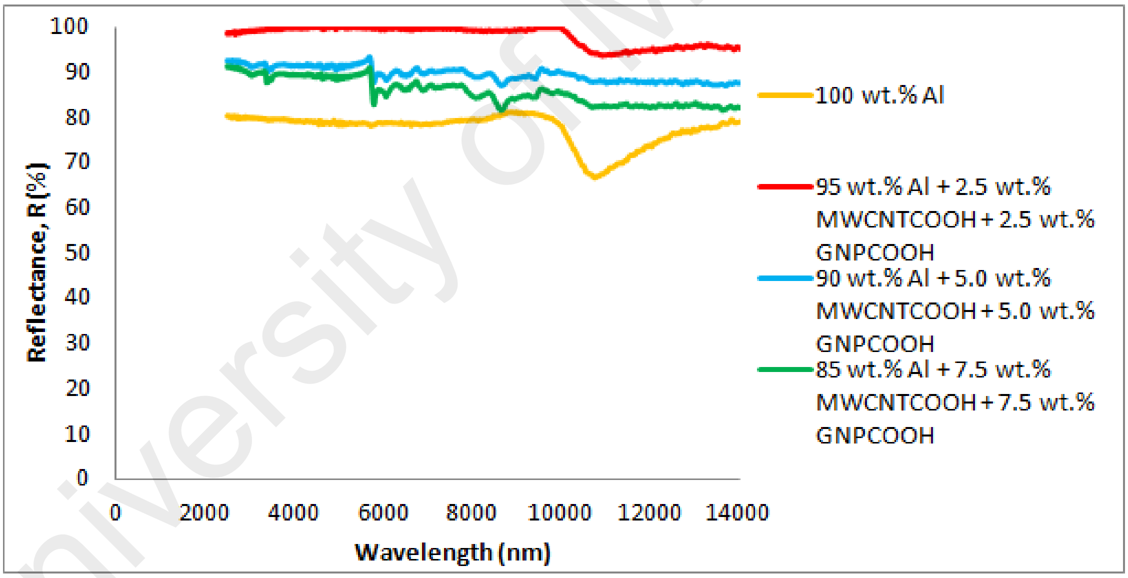

Figure 4.27: FTIR reflectance spectra of pure Al sample and Al-MWCNT-GNP nanocomposites within a wavelength range of 3,000–14,000 nm

In order to examine the effects of attaching the -COOH functional group onto the surface of MWCNTs and GNPs within MIR and FIR regions, the FTIR reflectance spectra were grouped based on the concentration of pristine and functionalized carbon nanofillers, as shown in Figures 4.28, 4.29, and 4.30. In general, it is apparent that Al-

MWCNTCOOH-GNPCOOH nanocomposites have higher reflectance compared to Al-MWCNT-GNP, Al-GNP, and Al-MWCNT nanocomposites. Even though the reflectance decreases with an increase in the concentration of functionalized carbon nanofillers, the decrease in reflectance is not as distinct as that for Al-MWCNT-GNP, Al-GNP, and Al-MWCNT nanocomposites. The results indicate that the -COOH functional group plays a vital role in retaining high reflectance in the MIR and FIR regions for Al nanocomposites.

The FTIR reflectance spectra obtained in this study are comparable to those of Sciti *et al*. (Sciti et al., 2013) and Sani *et al*. (Elisa Sani, Mercatelli, & Meucci, 2016). Sciti *et al*. (Sciti et al., 2013) found that the reflectance of hafnium diboride (HfB_2) pellet with 5 wt. % $MoSi_2$ was 88% at 3,000 nm and the reflectance increased further to 99% at 14,000 nm (Sciti et al., 2013). The results are similar to those obtained by Sani *et al*. (Elisa Sani, Mercatelli, & Meucci, 2016), who reported that the reflectance was 87% at 3,000 nm for tantalum carbide (TaC) with 10 wt. % $MoSi_2$ and the reflectance gradually increased to 99% at 14,000 nm (Elisa Sani, Mercatelli, & Meucci, 2016).

In general, the results obtained in this study are indeed encouraging because Al-MWCNT-GNP and Al-MWCNTCOOH-GNPCOOH nanocomposites have lower reflectance within the UV, Vis, and NIR regions (200–2,500 nm) and higher reflectance within the MIR and FIR regions (3,000–14,000 nm). These results conform well with the behavior of an ideal solar absorber proposed by Kennedy (C. E. Kennedy, 2002), where solar absorbers should have low reflectance within the UV, Vis, and NIR regions (200–2,500 nm) and higher reflectance within the NIR, MIR, and FIR regions (2,500–25,000 nm).

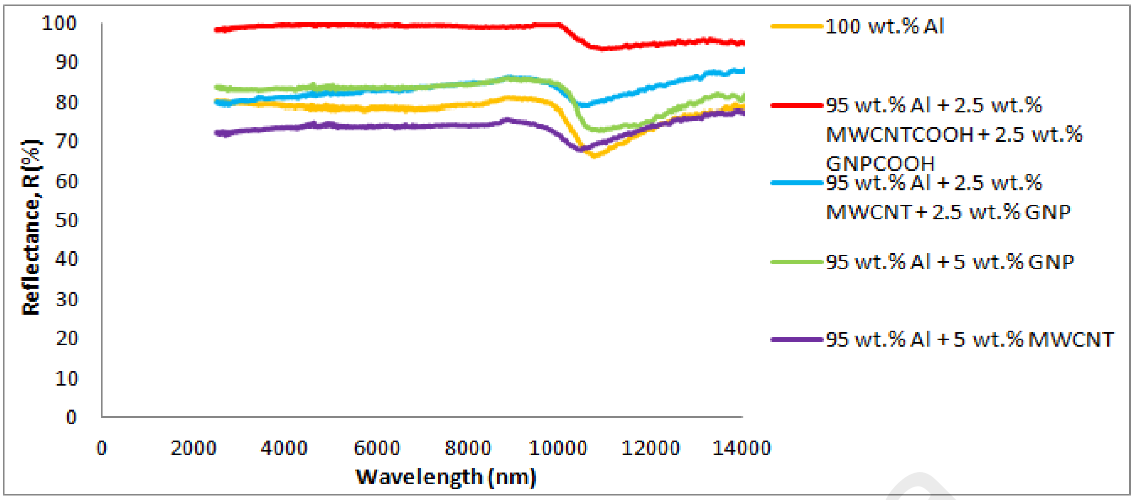

Figure 4.28: FTIR reflectance spectra of pure Al sample and Al nanocomposites with 5 wt. % of pristine and/or functionalized carbon nanofillers

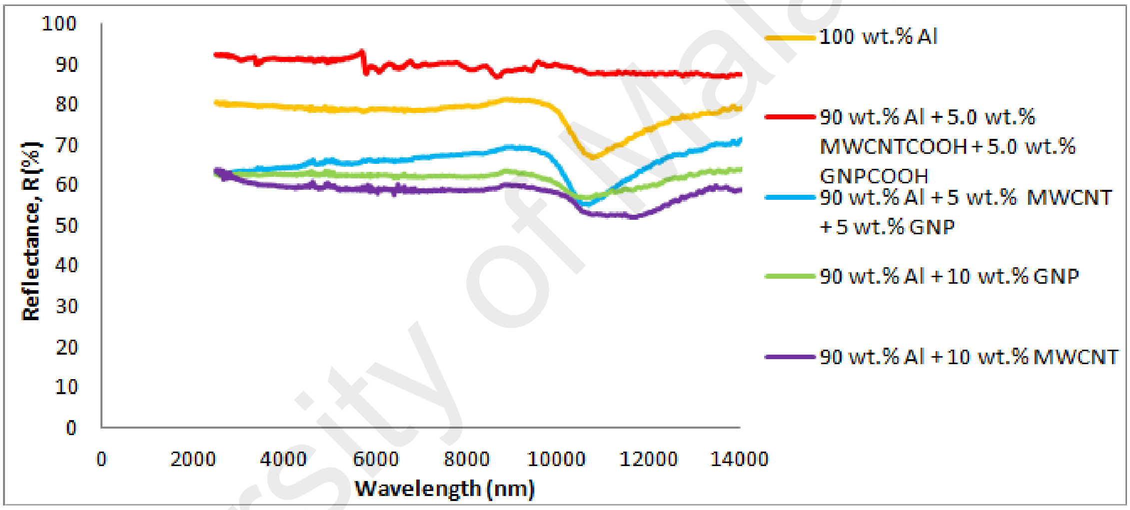

Figure 4.29: FTIR reflectance spectra of pure Al sample and Al nanocomposites with 10 wt. % of pristine and/or functionalized carbon nanofillers

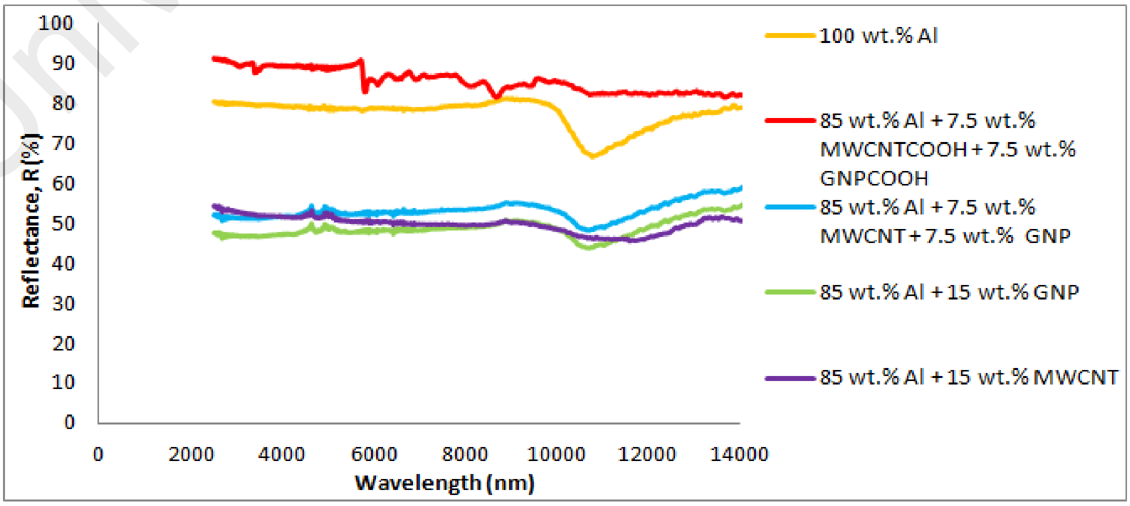

Figure 4.30: FTIR reflectance spectra of pure Al sample and Al nanocomposites with 15 wt. % of pristine and/or functionalized carbon nanofillers

4.7 Spectral selectivity behavior of pure Al sample, Al-MWCNT-GNP nanocomposites, and Al-MWCNTCOOH-GNPCOOH nanocomposites

Spectral selectivity is a key parameter used to evaluate the efficiency of solar absorbers (Burlafinger et al., 2015). The spectral selectivity behavior of a solar absorber is represented by the absorbance-to-emittance ratio. Ideally, the light absorbance (α) of a solar absorber should be high within the UV, Vis, and NIR regions (200–2,500 nm) whereas the thermal emittance (ε) should be low within the NIR, MIR, and FIR regions (2,500–25,000 nm) (C. Kennedy & Price, 2005; C. E. Kennedy, 2002).

Based on the reflectance spectra obtained from the UV-Vis-NIR spectroscopy measurements, the values of α of the pure Al sample, Al-MWCNT-GNP nanocomposites, and Al-MWCNTCOOH-GNPCOOH nanocomposites were determined from the following equation:

$$\alpha = \frac{\int_{\lambda_{min}}^{\lambda_{max}} \left(1-\rho(\lambda)\right).S(\lambda)\mathrm{d}\lambda}{\int_{\lambda_{min}}^{\lambda_{max}} S(\lambda)\mathrm{d}\lambda} \qquad \text{Eq. (4.2)}$$

Where ρ (λ) is the reflectance measured using the UV-Vis-NIR spectrophotometer, λ is the wavelength, and S (λ) is the sunlight spectrum. The limits of the definite integral are λ_{min} = 200 nm and λ_{max} = 2,500 nm.

Likewise, based on the reflectance spectra obtained from the FTIR measurements, the values of ε of the pure Al sample, Al-MWCNT-GNP nanocomposites, and Al-MWCNTCOOH-GNPCOOH nanocomposites were determined from the following equation:

$$\varepsilon(T) = \frac{\int_{\lambda_m}^{\lambda_M} (1-\rho(\lambda)).B(\lambda)\mathrm{d}\lambda}{\int_{\lambda_m}^{\lambda_M} B(\lambda)\mathrm{d}\lambda} \qquad \text{Eq. (4.3)}$$

Where ρ (λ) is the reflectance measured using the FTIR spectrometer, B (λ) is the blackbody irradiance at a particular temperature, and λ is the wavelength. The limits of the definite integral are λ_m = 3,000 nm and λ_M = 14,000 nm.

The spectral selectivity ratio (ξ) of the pure Al sample, Al-MWCNT-GNP nanocomposites, and Al-MWCNTCOOH-GNPCOOH nanocomposites was calculated by dividing α with ε, as follows:

$$\xi = \frac{\alpha}{\varepsilon} \qquad \text{Eq. (4.4)}$$

The values of α, ε, and ξ of the pure sample and Al nanocomposites are summarized in Table 4.1. In general, the addition of pristine and functionalized carbon nanofillers improves ξ of Al nanocomposites. It is evident that Al-MWCNTCOOH-GNPCOOH nanocomposites have higher ξ compared to Al-MWCNT-GNP, Al-GNP, and Al-MWCNT nanocomposites.

The highest ξ (27.41) was attained for Al nanocomposites with 2.5 wt. % MWCNTCOOH and 2.5 wt. % GNPCOOH, indicating that this is the optimum concentration of the functionalized carbon nanofillers. The value of α increases whereas the value of ε decreases with an increase in the concentration of pristine and functionalized carbon nanofillers. However, a different trend was observed for Al nanocomposites with 7.5 wt. % MWCNT and 7.5 wt. % GNP, Al nanocomposites with 15 wt. % GNP, and Al nanocomposites with 15 wt. % MWCNT since the value of ε is higher relative to that for pure Al, which results in lower ξ.

From the comparison of Aluminum with different percentage of functionalize nanofillers, the value of ξ obtained reduced from 27.41(5 wt.% funct. nanofillers) to 7.18(10 wt.% func. nanofillers) and finally 5.47(15 wt.% funct. nanofillers). The difference is due to the agglomeration which is an issue for MMCs application. Functionalization of the nanofillers in this study serve the need to promote better dispersion and cut down the agglomeration. However, after certain amount of nanofillers add up into the mixture of composites, the agglomeration of nanofillers started to take place and it is exactly when the filler loading exceeds certain threshold.

After reaching the filler loading threshold, the nanofiller start to stack onto each other and the homogenous dispersion cannot be achieved. As a result, the light trapping capability is reduced and lowered the solar reflectance especially at higher wavelength region (2.5 µm to 14 µm). As the effect on higher wavelength region happened-causing higher emmitance values, the spectral selectivity is reduced and thus showing that Al with 5wt.% of funct. Nanofillers as the best samples according to the spectral selectivity ratio calculated from this study.

The usage of black color nanofillers together with carboxylic attachment through chemical modification help to improve the spectral selectivity ratio of the Al nanocomposites. Even though the agglomeration still noticeable on the Al that use functionalize nanofillers especially at the highest filler loading of 15 wt.%, the agglomeration is not severe as compared to those that using non-functionalize nanofillers. The evidence can be seen from the micrograph from figures 4.12 to 4.15.

In general, the values of ξ obtained in this study are higher than those reported by other researchers for the same category of sintered materials. The highest ξ obtained by Sani *et al*. (Elisa Sani, Mercatelli, Meucci, et al., 2016) was 4.0 for the TaB_2 pellet sintered through spark plasma sintering. The highest ξ obtained by Dan *et al*. (Dan et al., 2016) was 11.97 for W/WAIN/WAION/Al_2O_3 coatings produced using electrodeposition process. Dudita *et al*. (Dudita et al., 2012) synthesized copper(II) oxide (CuO) and nickel (II) oxide (NiO) mixed films where 40 wt. % of ethanol was deposited onto the copper substrate by spray pyrolysis. They obtained ξ of 36.4, which is 0.75 times higher than the highest ξ obtained in this study.

Table 4.1: Light absorbance, thermal emittance, and spectral selectivity ratio of pure Al sample, Al-MWCNT-GNP nanocomposites, and Al-MWCNTCOOH-GNPCOOH nanocomposites

Sample	Light Absorbance α	Thermal Emittance ε	Spectral Selectivity Ratio ξ
100 wt. % Al	0.56	0.23	2.43
95 wt. % Al + 2.5 wt. % MWCNT + 2.5 wt. % GNP	0.80	0.15	5.33
95 wt. % Al + 2.5 wt. % MWCNTCOOH + 2.5 wt. % GNPCOOH	0.73	0.03	27.41
95 wt. % Al + 5 wt. % MWCNT	0.67	0.26	2.58
95 wt. % Al + 5 wt. % GNP	0.84	0.18	4.67
90 wt. % Al + 5 wt. % MWCNT + 5 wt. % GNP	0.84	0.21	4.00
90 wt. % Al + 5 wt. % MWCNTCOOH + 5 wt. % GNPCOOH	0.79	0.11	7.18
90 wt. % Al + 10 wt. % MWCNT	0.73	0.35	2.09
90 wt. % Al + 10 wt. % GNP	0.85	0.29	2.93
85 wt. % Al + 7.5 wt. % MWCNT + 7.5 wt. % GNP	0.86	0.38	2.26
85 wt. % Al + 7.5 wt. % MWCNTCOOH + 7.5wt. % GNPCOOH	0.82	0.15	5.47
85 wt. % Al + 15 wt. % MWCNT	0.84	0.41	2.05
85 wt. % Al + 15 wt. % GNP	0.83	0.40	2.08

CHAPTER 5: CONCLUSIONS AND RECOMMENDATIONS

5.1 Conclusions

In this work, surface morphology, composition, hardness, and optical and spectral selectivity properties of four types of aluminum (Al) nanocomposites have been successfully fabricated and investigated, which cover Al with the addition of pristine multi-walled carbon nanotube (MWCNT), pristine graphene nanoplatelet (GNP), combination of both pristine GNP-MWCNT, and also the combination of both MWCNTCOOH-GNPCOOH. The study on four different types of nanofillers is conducted to evaluate suitable nanofillers to be used with Al for solar absorber applications.

The additional chemical functionalization process applied to pristine MWCNT and GNP nanofillers help to enhance the distribution of nanofillers and significantly improve the hardness value of the samples. The highest hardness value recorded is 44.9 Hv for Al with the addition of 10 wt. % functionalized MWCNT and GNP, whereas the lowest hardness recorded is 21.033 Hv, which belongs to Al with the addition of 5 wt. % pristine MWCNT. The compositional analysis conducted using both Fourier transform infrared spectroscopy (FTIR) and X-ray diffraction (XRD) shows the presence of carboxylic group attachment (-COOH) on MWCNT/GNP nanofillers after chemical modification process and confirms the non-existence of contamination such as aluminum oxide (Al_2O_3) during the sintering process, respectively.

The morphological evaluation conducted through scanning electron microscopy (SEM) analysis shows that homogenized dispersion of nanofillers can be obtained through the introduction of MWCNTCOOH-GNPCOOH nanofillers. The usage of MWCNTCOOH-GNPCOOH nanofillers overcomes the dispersion issues existed for pristine MWCNT and GNP and greatly helps in obtaining homogenous nanofiller distribution in Al nanocomposites.

Homogeneous dispersion of MWCNTCOOH and GNPCOOH in the Al matrix increases the light absorbance (α) within a wavelength range of 200–2,500 nm and decreases the thermal emittance (ε) within a wavelength range of 3,000–14,000 nm. The spectral selectivity for a solar absorber was evaluated based on absorbance-over-emittance ratio (α/ε). The spectral selectivity ratios (ξ) of Al-MWCNTCOOH-GNPCOOH nanocomposites are higher compared to Al-MWCNT-GNP nanocomposites and pure Al sample. The highest ξ (27.41) was observed for the Al nanocomposite with 2.5 wt. % MWCNTCOOH and 2.5 wt. % GNPCOOH. The lowest ξ (2.05) was recorded for Al nanocomposite with 15 wt. % MWCNT. The high ξ obtained for Al with the addition of MWCNTCOOH and GNPCOOH nanofillers indicates the great potential of being used as a solar absorber material for energy applications.

5.2 Recommendations for future work

There are still some works that need to be done in order to assess and improve these materials in the future, which include:

1. Measurement of thermal conductivity

   Thermal conductivity analysis should be conducted in the future in order to obtain more detail of the performance of actual Al nanocomposites with the presence of thermal/heat. Thermal conductivity analysis based on heat/thermal simulates the actual working environment and the potential of Al nanocomposites as solar absorber materials in concentrated solar power applications.

2. Implementation of nanotextured pattern

   The implementation of nanotextured pattern on the surface of existing Al nanocomposites is required to foresee if there is any improvement that can be achieved after applying nanotextured pattern. The addition of uniform texture may help toward the enhancement of light absorption.

3. Conducting corrosion test

   Potentiodynamic/potentiostat corrosion test should be conducted to simulate the effect of temperature, humidity, and existence of water on Al nanocomposites. Through corrosion test, the ability of Al nanocomposites with nanofillers to withstand the real working environment can be assessed and improved.

REFERENCES

Abdel Hamid, Z., et al. (2008). Nanostructured black cobalt coatings for solar absorbers. *Surface and Interface Analysis, 40*(11), 1493-1499.

Agarwal, A., et al. (2016). *Carbon Nanotubes: Reinforced Metal Matrix Composites*: CRC Press.

Akpinar, E. K., & Koçyiğit, F. (2010). Energy and exergy analysis of a new flat-plate solar air heater having different obstacles on absorber plates. *Applied Energy, 87*(11), 3438-3450.

Alvarez, G., et al. (2004). Thermal performance of an air solar collector with an absorber plate made of recyclable aluminum cans. *Solar Energy, 77*(1), 107-113.

Amiri, A., et al. (2013). Influence of different amino acid groups on the free radical scavenging capability of multi walled carbon nanotubes. *Journal of Biomedical Materials Research Part A, 101*(8), 2219-2228.

Anandan, C., et al. (2002). Investigation of surface composition of electrodeposited black chrome coatings by X-ray photoelectron spectroscopy. *Applied Surface Science, 191*(1), 254-260.

Ando, Y., et al. (2004). Growing carbon nanotubes. *Materials Today, 7*(10), 22-29.

Aréna, H., et al. (2019). SiC-TiC nanocomposite for bulk solar absorbers applications: Effect of density and surface roughness on the optical properties. *Solar Energy Materials and Solar Cells, 191*, 199-208.

Atieh, M. A., et al. (2010). Effect of Carboxylic Functional Group Functionalized on Carbon Nanotubes Surface on the Removal of Lead from Water. *Bioinorganic Chemistry and Applications, 2010*, 603978. doi:10.1155/2010/603978

Axelbaum, R., & Brandt, H. (1987). The effect of substrate surface preparation on the optical properties of a black chrome solar absorber coating. *Solar Energy, 39*(3), 233-241.

Bakshi, S. R., et al. (2010). Carbon nanotube reinforced metal matrix composites - a review. *International Materials Reviews, 55*(1), 41-64. doi:10.1179/095066009x12572530170543

Balandin, A. A., et al. (2008). Superior thermal conductivity of single-layer graphene. *Nano Letters, 8*(3), 902-907.

Barrera, E., et al. (1996). Preparation of selective surfaces of black cobalt by the sol-gel process. *Renewable Energy, 9*(1-4), 733-736.

Barshilia, H. C., et al. (2008a). Optical properties and thermal stability of TiAlN/AlON tandem absorber prepared by reactive DC/RF magnetron sputtering. *Solar Energy Materials and Solar Cells, 92*(11), 1425-1433.

Barshilia, H. C., et al. (2008b). Spectrally selective NbAlN/NbAlON/Si 3 N 4 tandem absorber for high-temperature solar applications. *Solar Energy Materials and Solar Cells, 92*(4), 495-504.

Barshilia, H. C., et al. (2008). Deposition and characterization of TiAlN/TiAlON/Si3N4 tandem absorbers prepared using reactive direct current magnetron sputtering. *Thin Solid Films, 516*(18), 6071-6078.

Barshilia, H. C., et al. (2006). TiAlN/TiAlON/Si3N4 tandem absorber for high temperature solar selective applications. *Applied Physics Letters, 89*(19), 191909-191909.

Bartolucci, S. F., et al. (2011). Graphene–aluminum nanocomposites. *Materials Science and Engineering: A, 528*(27), 7933-7937. doi:http://dx.doi.org/10.1016/j.msea.2011.07.043

Behar, O., et al. (2013). A review of studies on central receiver solar thermal power plants. *Renewable and Sustainable Energy Reviews, 23*, 12-39. doi:https://doi.org/10.1016/j.rser.2013.02.017

Berber, S., et al. (2000). Unusually high thermal conductivity of carbon nanotubes. *Physical Review Letters, 84*(20), 4613.

Bogaerts, W. F., & Lampert, C. M. (1983). Materials for photothermal solar energy conversion. *Journal of Materials Science, 18*(10), 2847-2875.

Borkar, T., & Harimkar, S. (2011). Microstructure and wear behaviour of pulse electrodeposited Ni-CNT composite coatings. *Surface Engineering, 27*(7), 524-530. doi:10.1179/1743294410y.0000000001

Borkar, T., & Harimkar, S. P. (2011). Effect of electrodeposition conditions and reinforcement content on microstructure and tribological properties of nickel composite coatings. *Surface and Coatings Technology, 205*(17), 4124-4134.

Borkar, T., et al. (2015). Excellent strength-ductility combination in nickel-graphite nanoplatelet (GNP/Ni) nanocomposites. *Journal of Alloys and Compounds, 646*, 135-144. doi:10.1016/j.jallcom.2015.06.013

Boström, T., et al. (2003). Solution-chemical derived nickel–alumina coatings for thermal solar absorbers. *Solar Energy, 74*(6), 497-503.

Bouadila, S., et al. (2013). Performance of a new solar air heater with packed-bed latent storage energy for nocturnal use. *Applied Energy, 110*, 267-275.

Boubault, A., et al. (2014). Accelerated aging of a solar absorber material subjected to highly concentrated solar flux. *Energy Procedia, 49*, 1673-1681.

Burlafinger, K., et al. (2015). Maximizing concentrated solar power (CSP) plant overall efficiencies by using spectral selective absorbers at optimal operation temperatures. *Solar Energy, 120*, 428-438.

Cao, A., et al. (2002). Tandem structure of aligned carbon nanotubes on Au and its solar thermal absorption. *Solar Energy Materials and Solar Cells, 70*(4), 481-486.

Cao, Q., et al. (2008). Medium-scale carbon nanotube thin-film integrated circuits on flexible plastic substrates. *Nature, 454*(7203), 495-500.

Chen, J., et al. (2012). Graphene layers produced from carbon nanotubes by friction. *Carbon, 50*(5), 1934-1941.

Chen, Z., & Boström, T. (2016). Accelerated ageing tests of carbon nanotube spectrally selective solar absorbers. *Solar Energy Materials and Solar Cells, 157*, 777-782.

Cho, S., et al. (2010). Multiwalled carbon nanotubes as a contributing reinforcement phase for the improvement of thermal conductivity in copper matrix composites. *Scripta Materialia, 63*(4), 375-378. doi:10.1016/j.scriptamat.2010.04.024

Choudhury, C., & Sehgal, H. (1982). Black cobalt selective coatings by spray pyrolysis for photothermal conversion of solar energy. *Solar Energy, 28*(1), 25-31.

Chu, K., et al. (2013). Improvement of interface and mechanical properties in carbon nanotube reinforced Cu-Cr matrix composites. *Materials & Design, 45*, 407-411. doi:10.1016/j.matdes.2012.09.027

Coventry, J., & Burge, P. (2017). *Optical properties of Pyromark 2500 coatings of variable thicknesses on a range of materials for concentrating solar thermal applications.* Paper presented at the AIP Conference Proceedings.

Cuevas, A., et al. (2016). Spectrally selective CuS solar absorber coatings on stainless steel and aluminum. *Surface and Interface Analysis*, *48*(7), 649-653. doi:10.1002/sia.5971

Dan, A., et al. (2016). Spectrally selective absorber coating of WAlN/WAlON/Al 2 O 3 for solar thermal applications. *Solar Energy Materials and Solar Cells, 157,* 716-726.

Dasgupta, K., et al. (2008). Novel catalytic route to bulk production of high purity carbon nanotube. *Journal of Nanoparticle Research, 10*(1), 69-76.

Davis, J. R. (1999). *Corrosion of aluminum and aluminum alloys*: Asm International.

Dudita, M., et al. (2012). Influence of solvents on properties of solar selective coatings obtained by spray pyrolysis. *Bulletin of Materials Science, 35*(6), 997-1002.

Eizenberg, M., & Blakely, J. (1979). Carbon monolayer phase condensation on Ni (111). *Surface Science, 82*(1), 228-236.

El Nady, J., et al. (2016). Nanoparticles Ni electroplating and black paint for solar collector applications. *Alexandria Engineering Journal, 55*(2), 723-729.

Esawi, A., et al. (2010). Effect of carbon nanotube (CNT) content on the mechanical properties of CNT-reinforced aluminium composites. *Composites Science and Technology, 70*(16), 2237-2241.

Esawi, A. M. K., et al. (2009). Fabrication and properties of dispersed carbon nanotube-aluminum composites. *Materials Science and Engineering a-Structural Materials Properties Microstructure and Processing, 508*(1-2), 167-173. doi:10.1016/j.msea.2009.01.002

Eugénio, S., et al. (2011). Electrodeposition of black chromium spectrally selective coatings from a Cr (III)–ionic liquid solution. *Thin Solid Films, 519*(6), 1845-1850.

Exley, C. (2013). Aluminum in Biological Systems. In R. H. Kretsinger, V. N. Uversky, & E. A. Permyakov (Eds.), *Encyclopedia of Metalloproteins* (pp. 33-34). New York, NY: Springer New York.

Gao, X. H., et al. (2016). Structure, optical properties and thermal stability of SS/TiC-ZrC/Al2O3 spectrally selective solar absorber. *Rsc Advances, 6*(68), 63867-63873. doi:10.1039/c6ra11602g

Gorji, T. B., et al. (2015). Optical properties of carboxyl functionalized carbon nanotube aqueous nanofluids as direct solar thermal energy absorbers. *Solar Energy, 119*, 332-342. doi:10.1016/j.solener.2015.07.012

Guiderdoni, C., et al. (2011). The preparation of double-walled carbon nanotube/Cu composites by spark plasma sintering, and their hardness and friction properties. *Carbon, 49*(13), 4535-4543. doi:10.1016/j.carbon.2011.06.063

Guler, Ö., et al. (2015). Electrical and Optical Properties of Carbon Nanotube Hybrid Zinc Oxide Nanocomposites Prepared by Ball Mill Technique. *Fullerenes, Nanotubes and Carbon Nanostructures, 23*(10), 865-869. doi:10.1080/1536383X.2015.1022256

Han, Z., & Fina, A. (2011). Thermal conductivity of carbon nanotubes and their polymer nanocomposites: a review. *Progress in Polymer Science, 36*(7), 914-944.

Harding, G. (1976). Evaporated chromium black selective solar absorbers. *Thin Solid Films, 38*(1), 109-115.

Harris, P. J. F. (2004). Carbon nanotube composites. *International Materials Reviews, 49*(1), 31-43. doi:10.1179/095066004225010505

Heremans, J., & Beetz Jr, C. (1985). Thermal conductivity and thermopower of vapor-grown graphite fibers. *Physical Review B, 32*(4), 1981.

Hernandez-Pinilla, D., et al. (2016). MoSi2-Si3N4 absorber for high temperature solar selective coating. *Solar Energy Materials and Solar Cells, 152*, 141-146. doi:10.1016/j.solmat.2016.04.001

Higginbotham, A. L., et al. (2010). Lower-defect graphene oxide nanoribbons from multiwalled carbon nanotubes. *Acs Nano, 4*(4), 2059-2069.

Hihara, L., & Latanision, R. (1994). Corrosion of metal matrix composites. *International Materials Reviews, 39*(6), 245-264.

Hollands, K., et al. (2001). Solar energy: the state of the art. *James & James Ltd., London, UK.*

Hone, J., et al. (1999). Thermal conductivity of single-walled carbon nanotubes. *Physical Review B, 59*(4), R2514.

Hwang, J., et al. (2013). Enhanced mechanical properties of graphene/copper nanocomposites using a molecular ‐ level mixing process. *Advanced Materials, 25*(46), 6724-6729.

Ienei, E., et al. (2010). Characterization of Al/Al2O3/NiOx solar absorber obtained by spray pyrolysis. *Solid State Sciences, 12*(11), 1894-1897.

Islam, M., et al. (2003). High weight fraction surfactant solubilization of single-wall carbon nanotubes in water. *Nano Letters, 3*(2), 269-273.

Jafari, M., et al. (2012). Mechanical properties of nanostructured Al2024–MWCNT composite prepared by optimized mechanical milling and hot pressing methods. *Advanced Powder Technology, 23*(2), 205-210.

Jeon, C. H., et al. (2014). Material Properties of Graphene/Aluminum Metal Matrix Composites Fabricated by Friction Stir Processing. *International Journal of Precision Engineering and Manufacturing, 15*(6), 1235-1239. doi:10.1007/s12541-014-0462-2

Jeong, Y. J., et al. (2007). Synergistic Strengthening Effect of Ultrafine ‐ Grained Metals Reinforced with Carbon Nanotubes. *Small, 3*(5), 840-844.

Jiang, L., et al. (2012). The use of flake powder metallurgy to produce carbon nanotube (CNT)/aluminum composites with a homogenous CNT distribution. *Carbon, 50*(5), 1993-1998. doi:10.1016/j.carbon.2011.12.057

Jiao, L., et al. (2009). Narrow graphene nanoribbons from carbon nanotubes. *Nature, 458*(7240), 877-880.

John, S. (1997). Electrodeposition of nickel black solar absorber coatings. *Metal Finishing, 95*(6), 84-86.

Kaczmar, J., et al. (2000). The production and application of metal matrix composite materials. *Journal of Materials Processing Technology, 106*(1-3), 58-67.

KalužA, L., et al. (2001). Structural and IR spectroscopic analysis of sol-gel processed CuFeMnO4 spinel and CuFeMnO4/silica films for solar absorbers. *Journal of Sol-Gel Science and Technology, 20*(1), 61-83.

Karlsson, T., & Roos, A. (1984). Optical properties and spectral selectivity of copper oxide on stainless steel. *Solar Energy Materials, 10*(1), 105-119.

Katumba, G., et al. (2008). Optical, thermal and structural characteristics of carbon nanoparticles embedded in ZnO and NiO as selective solar absorbers. *Solar*

Energy Materials and Solar Cells, 92(10), 1285-1292. doi:10.1016/j.solmat.2008.04.023

Kennedy, C., & Price, H. (2005). *Progress in development of high-temperature solar-selective coating.* Paper presented at the ASME 2005 International Solar Energy Conference.

Kennedy, C. E. (2002). *Review of mid-to high-temperature solar selective absorber materials* (Vol. 1617): National Renewable Energy Laboratory Golden, Colo, USA.

Kim, K., et al. (2008). Grain refinement assisted strengthening of carbon nanotube reinforced copper matrix nanocomposites. *Applied Physics Letters, 92*(12), 121901.

Kim, K. T., et al. (2011). Influence of embedded-carbon nanotubes on the thermal properties of copper matrix nanocomposites processed by molecular-level mixing. *Scripta Materialia, 64*(2), 181-184.

Koli, D. K., et al. (2013). Properties and characterization of Al-Al2O3 composites processed by casting and powder metallurgy routes. *International Journal of Latest Trends in Engineering and Technology (IJLTET), 2*(4), 486-496.

Kondoh, K., et al. (2009). Characteristics of powder metallurgy pure titanium matrix composite reinforced with multi-wall carbon nanotubes. *Composites Science and Technology, 69*(7-8), 1077-1081. doi:10.1016/j.compscitech.2009.01.026

Konttinen, P., et al. (2005). Degradation of unglazed rough graphite-aluminium solar absorber surfaces in simulated acid and neutral rain. *Solar Energy, 78*(1), 41-48.

Kosynkin, D. V., et al. (2009). Longitudinal unzipping of carbon nanotubes to form graphene nanoribbons. *Nature, 458*(7240), 872-876.

Kumar, H. G. P., & Xavior, M. A. (2014). Graphene Reinforced Metal Matrix Composite (GRMMC): A Review. *12th Global Congress on Manufacturing and Management (Gcmm - 2014), 97,* 1033-1040. doi:10.1016/j.proeng.2014.12.381

Kumar, S., et al. (1983). Nickel pigmented anodized aluminium as solar selective absorbers. *Solar Energy Materials, 7*(4), 439-452.

Kumar, S. K., et al. (2013). CuO thin films made of nanofibers for solar selective absorber applications. *Solar Energy, 94*, 299-304.

Kunič, R., et al. (2009). Adhesion and thermal stability of thickness insensitive spectrally selective (TISS) polyurethane-based paint coatings on copper substrates. *Solar Energy Materials and Solar Cells, 93*(5), 630-640.

Kuzumaki, T., et al. (1998). Processing of carbon nanotube reinforced aluminum composite. *Journal of Materials Research, 13*(09), 2445-2449.

Kwon, H., et al. (2009). Combination of hot extrusion and spark plasma sintering for producing carbon nanotube reinforced aluminum matrix composites. *Carbon, 47*(3), 570-577.

Laha, T., et al. (2004). Synthesis and characterization of plasma spray formed carbon nanotube reinforced aluminum composite. *Materials Science and Engineering: A, 381*(1), 249-258.

Lampert, C. M. (1987). Advanced Optical Materials for Energy Efficiency and Solar Conversion *Physics and Technology of Solar Energy: Volume 2: Photovoltaic and Solar Energy Materials Proceedings of the International Workshop on Physics of Solar Energy, New Delhi, India, November 24 – December 6, 1986* (pp. 277-346). Dordrecht: Springer Netherlands.

Landry, K., et al. (1998). Wettability of carbon by aluminum and aluminum alloys. *Materials Science and Engineering a-Structural Materials Properties Microstructure and Processing, 254*(1-2), 99-111. doi:Doi 10.1016/S0921-5093(98)00759-X

Latief, F., & Sherif, E.-S. M. (2012). Effects of sintering temperature and graphite addition on the mechanical properties of aluminum. *Journal of Industrial and Engineering Chemistry, 18*(6), 2129-2134.

Lee, C., et al. (2008). Measurement of the elastic properties and intrinsic strength of monolayer graphene. *Science, 321*(5887), 385-388.

Li, D., & Kaner, R. B. (2008). Graphene-based materials. *Nat Nanotechnol, 3*, 101.

Li, Q. Q., et al. (2009). Improved processing of carbon nanotube/magnesium alloy composites. *Composites Science and Technology, 69*(7-8), 1193-1199. doi:10.1016/j.compscitech.2009.02.020

Li, S. F., et al. (2013). Powder metallurgy titanium metal matrix composites reinforced with carbon nanotubes and graphite. *Composites Part a-Applied Science and Manufacturing, 48*, 57-66. doi:10.1016/j.compositesa.2012.12.005

Li, S. H., & Chao, C. G. (2004). Effects of carbon fiber/Al interface on mechanical properties of carbon-fiber-reinforced aluminum-matrix composites. *Metallurgical and Materials Transactions a-Physical Metallurgy and Materials Science, 35a*(7), 2153-2160. doi:DOI 10.1007/s11661-004-0163-z

Li, Z., et al. (2015). Synergistic strengthening effect of graphene-carbon nanotube hybrid structure in aluminum matrix composites. *Carbon, 95*, 419-427. doi:ARTN 325601

10.1016/j.carbon.2015.08.014

Lira-Cantu, M., et al. (2005). Electrochemical deposition of black nickel solar absorber coatings on stainless steel AISI316L for thermal solar cells. *Solar Energy Materials and Solar Cells, 87*(1-4), 685-694.

Liu, W. W., et al. (2014). Synthesis and characterization of graphene and carbon nanotubes: A review on the past and recent developments. *Journal of Industrial and Engineering Chemistry, 20*(4), 1171-1185. doi:10.1016/j.jiec.2013.08.028

Liu, Y. F., et al. (2013). Graphene and Metal Oxide Composites for Supercapacitors. *Progress in Renewable and Sustainable Energy, Pts 1 and 2, 608-609*, 1074-1077. doi:10.4028/www.scientific.net/AMR.608-609.1074

Liu, Z., et al. (2012). Effect of ball-milling time on mechanical properties of carbon nanotubes reinforced aluminum matrix composites. *Composites Part A: Applied Science and Manufacturing, 43*(12), 2161-2168.

Mallikarjuna, H., et al. (2016). Microstructure and Microhardness of Carbon Nanotube-Silicon Carbide/Copper Hybrid Nanocomposite Developed by Powder Metallurgy. *Indian Journal of Science and Technology, 9*(14).

Maruyama, T. (1998). Copper oxide thin films prepared by chemical vapor deposition from copper dipivaloylmethanate. *Solar Energy Materials and Solar Cells, 56*(1), 85-92.

Maruyama, T., & Nakai, T. (1991). Cobalt oxide thin films prepared by chemical vapor deposition from cobalt (II) acetate. *Solar Energy Materials, 23*(1), 25-29.

Mizuno, K., et al. (2009). A black body absorber from vertically aligned single-walled carbon nanotubes. *Proceedings of the National Academy of Sciences, 106*(15), 6044-6047.

Munir, K. S., et al. (2015). Carbon Nanotube Reinforced Titanium Metal Matrix Composites Prepared by Powder Metallurgy-A Review. *Critical Reviews in Solid State and Materials Sciences, 40*(1), 38-55. doi:10.1080/10408436.2014.929521

Munir, K. S., et al. (2016). Identifying and understanding the effect of milling energy on the synthesis of carbon nanotubes reinforced titanium metal matrix composites. *Carbon, 99*, 384-397. doi:10.1016/j.carbon.2015.12.041

Nair, R. R., et al. (2008). Fine structure constant defines visual transparency of graphene. *Science, 320*(5881), 1308-1308.

Nam, D. H., Cha, S. I., Lim, B. K., Park, H. M., Han, D. S., & Hong, S. H. . (2012). Synergistic strengthening by load transfer mechanism and grain refinement of CNT/Al–Cu composites. *Carbon, 50*(7), 2417-2423.

Nandamuri, G., et al. (2010). Remote plasma assisted growth of graphene films. *Applied Physics Letters, 96*(15), 154101.

Nardone, V. C., & Prewo, K. M. (1986). On the Strength of Discontinuous Silicon-Carbide Reinforced Aluminum Composites. *Scripta Metallurgica, 20*(1), 43-48. doi:Doi 10.1016/0036-9748(86)90210-3

Novak, P., et al. (2014). Powder metallurgy preparation of Al-Cu-Fe quasicrystals using mechanical alloying and Spark Plasma Sintering. *Intermetallics, 52*, 131-137. doi:10.1016/j.intermet.2014.04.003

Novoselov, K. S., et al. (2004). Electric field effect in atomically thin carbon films. *Science, 306*(5696), 666-669.

Olek, M. (2006). Carbon nanotube composites–mechanical, electrical, and optical properties. *Dr. Rer. Nat Rheinischen Friedrich-Wilhelms-Universität Bonn. Bonn*.

Orel, B., et al. (1990). Coil-coating paints for solar collector panels—II. FT-IR spectroscopic investigations. *Solar & Wind Technology, 7*(6), 713-717.

Ostovan, F., et al. (2016). Nanomechanical behavior of multi-walled carbon nanotubes particulate reinforced aluminum nanocomposites prepared by ball milling. *Materials, 9*(3), 140.

Poirier, D., et al. (2009). Structural characterization of a mechanically milled carbon nanotube/aluminum mixture. *Composites Part A: Applied Science and Manufacturing, 40*(9), 1482-1489.

Raccurt, O., et al. (2015). Study of the Stability of a Selective Solar Absorber Coating under Air and High Temperature Conditions. *Energy Procedia, 69*, 1551-1557. doi:https://doi.org/10.1016/j.egypro.2015.03.107

Rana, R., et al. (2012). Reviews on the influences of alloying elements on the microstructure and mechanical properties of aluminum alloys and aluminum alloy composites. *International Journal of Scientific and Research Publications, 2*(6), 1-7.

Rashad, M., et al. (2015). Enhanced ductility of Mg-3Al-1Zn alloy reinforced with short length multi-walled carbon nanotubes using a powder metallurgy method. *Progress in Natural Science-Materials International, 25*(4), 276-281. doi:10.1016/j.pnsc.2015.08.002

Rashad, M., et al. (2015). Improved strength and ductility of magnesium with addition of aluminum and graphene nanoplatelets (Al plus GNPs) using semi powder metallurgy method. *Journal of Industrial and Engineering Chemistry, 23*, 243-250. doi:10.1016/j.jiec.2014.08.024

Rawal, S. P. (2001). Metal-matrix composites for space applications. *Jom, 53*(4), 14-17.

Razak, A. A., et al. (2016). Review on matrix thermal absorber designs for solar air collector. *Renewable & Sustainable Energy Reviews, 64*, 682-693. doi:10.1016/j.rser.2016.06.015

Rebouta, L., et al. (2015). Solar selective absorbers based on Al2O3: W cermets and AlSiN/AlSiON layers. *Solar Energy Materials and Solar Cells, 137*, 93-100.

Reina, A., et al. (2008). Large area, few-layer graphene films on arbitrary substrates by chemical vapor deposition. *Nano Letters, 9*(1), 30-35.

Richharia, P. (1996). Microstructural investigations of a textured black brass selective surface. *Thin Solid Films, 272*(1), 7-9.

Richharia, P., et al. (1991). Surface analysis of a black copper selective coating. *Solar Energy Materials, 23*(1), 93-109.

Sani, E., et al. (2016). Compositional dependence of optical properties of zirconium, hafnium and tantalum carbides for solar absorber applications. *Solar Energy, 131*, 199-207. doi:http://dx.doi.org/10.1016/j.solener.2016.02.045

Sani, E., et al. (2016). Optical properties of dense zirconium and tantalum diborides for solar thermal absorbers. *Renewable Energy, 91*, 340-346. doi:http://dx.doi.org/10.1016/j.renene.2016.01.068

Sani, E., et al. (2014). Optical properties of boride ultrahigh-temperature ceramics for solar thermal absorbers. *Journal of Photonics for Energy, 4*. doi:Artn 045599

10.1117/1.Jpe.4.045599

Sathiaraj, T. S., et al. (1991). Optical properties of selectively absorbing rf sputtered Ni ・ Al2O3 composite films. *Thin Solid Films, 195*(1-2), 33-42.

Sciti, D., et al. (2013). Suitability of ultra-refractory diboride ceramics as absorbers for solar energy applications. *Solar Energy Materials and Solar Cells, 109*, 8-16.

Selvakumar, N., et al. (2010). Structure, optical properties and thermal stability of pulsed sputter deposited high temperature HfO x/Mo/HfO 2 solar selective absorbers. *Solar Energy Materials and Solar Cells, 94*(8), 1412-1420.

Selvakumar, N., et al. (2014). Carbon Nanotube- Based Tandem Absorber with Tunable Spectral Selectivity: Transition from Near- Perfect Blackbody Absorber to Solar Selective Absorber. *Advanced Materials, 26*(16), 2552-2557. doi:10.1002/adma.201305070

Shanker, K., & Holloway, P. H. (1985). Electrodeposition of black chrome selective solar absorber coatings with improved thermal stability. *Thin Solid Films, 127*(3-4), 181-189.

Shariah, A., et al. (1999). Effect of thermal conductivity of absorber plate on the performance of a solar water heater. *Applied Thermal Engineering, 19*(7), 733-741.

Shelton, J., et al. (1974). Equilibrium segregation of carbon to a nickel (111) surface: A surface phase transition. *Surface Science, 43*(2), 493-520.

Singhal, S., et al. (2012). Carbon nanotubes: amino functionalization and its application in the fabrication of Al-matrix composites. *Powder Technology, 215*, 254-263.

Solangi, K., et al. (2016). Experimental investigation of heat transfer performance and frictional loss of functionalized GNP-based water coolant in a closed conduit flow. *Rsc Advances, 6*(6), 4552-4563.

Somani, P. R., et al. (2006). Planer nano-graphenes from camphor by CVD. *Chemical Physics Letters, 430*(1–3), 56-59. doi:http://dx.doi.org/10.1016/j.cplett.2006.06.081

Srinivasan, K., et al. (1984). Nickel-black solar absorber coatings. *Energy Conversion and Management, 24*(4), 255-258.

Stein, J., et al. (2012). Mechanical reinforcement of a high-performance aluminium alloy AA5083 with homogeneously dispersed multi-walled carbon nanotubes. *Carbon, 50*(6), 2264-2272.

Sun, D.-M., et al. (2013). Mouldable all-carbon integrated circuits. *Nature Communications, 4*.

Survilienė, S., et al. (2014). The use of trivalent chromium bath to obtain a solar selective black chromium coating. *Applied Surface Science, 305*, 492-497.

Szabó, A., et al. (2010). Synthesis methods of carbon nanotubes and related materials. *Materials, 3*(5), 3092-3140.

Tan, J. M., et al. (2015). Release behaviour and toxicity evaluation of levodopa from carboxylated single-walled carbon nanotubes. *Beilstein Journal of Nanotechnology, 6*, 243-253. doi:10.3762/bjnano.6.23

Tesfamichael, T., & Roos, A. (1998). Treatment of antireflection on tin oxide coated anodized aluminum selective absorber surface. *Solar Energy Materials and Solar Cells, 54*(1), 213-221.

Tharamani, C., & Mayanna, S. (2007). Low-cost black Cu–Ni alloy coatings for solar selective applications. *Solar Energy Materials and Solar Cells, 91*(8), 664-669.

Tinchev, S., et al. (2010). *Thermal solar absorber made of diamond-like carbon thin films.* Paper presented at the Journal of Physics: Conference Series.

Tjong, S. C. (2009). *Carbon nanotube reinforced composites: metal and ceramic matrices*: John Wiley & Sons.

Tjong, S. C. (2013). Recent progress in the development and properties of novel metal matrix nanocomposites reinforced with carbon nanotubes and graphene nanosheets. *Materials Science and Engineering: R: Reports, 74*(10), 281-350. doi:http://dx.doi.org/10.1016/j.mser.2013.08.001

Tjong, S. C., & Lau, K. C. (1999). Properties and abrasive wear of TiB2/Al-4%Cu composites produced by hot isostatic pressing. *Composites Science and Technology, 59*(13), 2005-2013. doi:Doi 10.1016/S0266-3538(99)00056-1

Tjong, S. C., & Ma, Z. Y. (2000). Microstructural and mechanical characteristics of in situ metal matrix composites. *Materials Science & Engineering R-Reports, 29*(3-4), 49-113. doi:Doi 10.1016/S0927-796x(00)00024-3

Toozandehjani, M., et al. (2017). Effect of Milling Time on the Microstructure, Physical and Mechanical Properties of Al-Al2O3 Nanocomposite Synthesized by Ball Milling and Powder Metallurgy. *Materials, 10*(11), 1232.

Uddin, S. M., et al. (2010). Effect of size and shape of metal particles to improve hardness and electrical properties of carbon nanotube reinforced copper and copper alloy composites. *Composites Science and Technology, 70*(16), 2253-2257. doi:10.1016/j.compscitech.2010.07.012

Vince, J., et al. (2003). Solar absorber coatings based on CoCuMnO x spinels prepared via the sol–gel process: structural and optical properties. *Solar Energy Materials and Solar Cells, 79*(3), 313-330.

Wang, C., et al. (2013). User-interactive electronic skin for instantaneous pressure visualization. *Nature materials, 12*(10), 899-904.

Wang, C., et al. (2009). Wafer-scale fabrication of separated carbon nanotube thin-film transistors for display applications. *Nano Letters, 9*(12), 4285-4291.

Wang, H., et al. (2009). Solvothermal reduction of chemically exfoliated graphene sheets. *Journal of the American Chemical Society, 131*(29), 9910-9911.

Wang, J., et al. (2012). Reinforcement with graphene nanosheets in aluminum matrix composites. *Scripta Materialia, 66*(8), 594-597.

Wang, J., et al. (2004). Free-standing subnanometer graphite sheets. *Applied Physics Letters, 85*(7), 1265-1267.

Wang, X., et al. (2014). The degradation of solar thermal absorption coatings. *Energy Procedia, 49*, 1747-1755.

Wang, X., et al. (2004). Contact-damage-resistant ceramic/single-wall carbon nanotubes and ceramic/graphite composites. *Nature materials, 3*(8), 539-544.

Wang, X. J., et al. (2014). The Degradation of Solar Thermal Absorption Coatings. *Energy Procedia, 49*, 1747-1755. doi:10.1016/j.egypro.2014.03.185

Wejrzanowski, T., et al. (2016). Thermal conductivity of metal-graphene composites. *Materials & Design, 99*, 163-173. doi:10.1016/j.matdes.2016.03.069

Wu, Z. S., et al. (2012). Graphene/metal oxide composite electrode materials for energy storage. *Nano Energy, 1*(1), 107-131. doi:10.1016/j.nanoen.2011.11.001

Xiao, X., et al. (2011). A facile process to prepare copper oxide thin films as solar selective absorbers. *Applied Surface Science, 257*(24), 10729-10736.

Yadav, T. P., et al. (2012). Mechanical milling: a top down approach for the synthesis of nanomaterials and nanocomposites. *Nanoscience and Nanotechnology, 2*(3), 22-48.

Yan, H., & Qiu, H. (2016). Fabrication of carbon nanotube reinforced A356 nanocomposites. *Journal of Materials Research, 31*(15), 2277-2283.

Yang, J., & Schaller, R. (2004). Mechanical spectroscopy of Mg reinforced with Al 2 O 3 short fibers and C nanotubes. *Materials Science and Engineering: A, 370*(1), 512-515.

Yianoulis, P., et al. (2012). Solar selective coatings: Elsevier Ltd.

Zehn, L., et al. (1997). Effect of natural aging and preaging on subsequent precipitation process of an Al-Mg-Si alloy with high excess silicon. *Materials Science and Technology*, *13*, 905.

Zhang, J., et al. (2011). Separated carbon nanotube macroelectronics for active matrix organic light-emitting diode displays. *Nano Letters*, *11*(11), 4852-4858.

Zhang, Z., et al. (2009). Transforming carbon nanotube devices into nanoribbon devices. *Journal of the American Chemical Society*, *131*(37), 13460-13463.

Zheng, L., et al. (2015). Angular solar absorptance and thermal stability of Mo–SiO2 double cermet solar selective absorber coating. *Solar Energy*, *115*, 341-346.

Zhu, M., et al. (2007). A mechanism for carbon nanosheet formation. *Carbon*, *45*(11), 2229-2234.